

This is to certify that the thesis entitled

SYNTHESIS AND CHARACTERIZATION OF TETRAHYDROFURFURYL SUBSTITUTED POLYLACTIDES

presented by

Thomas L. Jurek II

has been accepted towards fulfillment of the requirements for the

M.S. degree in Chemistry

Major Professor's Signature

August 31, 2010

Date

MSU is an Affirmative Action/Equal Opportunity Employer

LIBRARY Michigan State University

PLACE IN RETURN BOX to remove this checkout from your record. TO AVOID FINES return on or before date due. MAY BE RECALLED with earlier due date if requested.

DATE DUE	DATE DUE	DATE DUE
	`	

5/08 K:/Proj/Acc&Pres/CIRC/DateDue.indd

SYNTHESIS AND CHARACTERIZATION OF TETRAHYDROFURFURYL SUBSTITUTED POLYLACTIDES

Ву

Thomas L. Jurek II

A THESIS

Submitted to
Michigan State University
in partial fulfillments of the requirements
for the degree of

MASTER OF SCIENCE

Chemistry

2010

ABSTRACT

SYNTHESIS AND CHARACTERIZATION OF TETRAHYDROFURFURAL SUBSTITUTED POLYLACTIDES

Ву

Thomas L. Jurek II

Polylactides are widely used in biomedical applications due to their degradability, and their value as commodity plastics is increasing due to their attractiveness as "green materials." However, the use of polylactide in biomedical applications is limited by its hydrophobicity, which reduces the degradation rate. In structural applications, dimensional stability depends on polymer crystallinity since the polylactide glass transition temperature is low ($T_g \approx 50\text{-}60$ °C). Modifying the polylactide structure while retaining the polyester backbone, provides polylactide derivatives that retain desired attributes such as biodegradability. The goal of this research was to synthesize a polylactide derivative with an increased T_g and hydrophilicity.

We synthesized two new polylactide derivatives with pendant THF rings. The stereochemical systems of poly(THFglycolide1) and poly(THFglycolide2) were different, and the polymers had glass transition temperatures (T_g 's) of ~64 °C and 44 °C, respectively. No changes in T_g were observed when LiCl was added to poly(THFglycolide1), but the T_g of poly(THFglycolide2) increased from ~44 °C to 64 °C. Static contact angle measurements showed that both polymers were relatively hydrophilic compared to poly(rac-lactide).

ACKNOWLEDEMENTS

The journey I took in coming to graduate school seemed to be my true American Dream Hunter S. Thompson so lavishly described in his literature. It was the wave of life which brought me to this place with many people to thank along the way. I would especially like to acknowledge my high school and undergraduate professors for feeding that swell and providing an environment conducive to the furthering of my education. However, no calm sea stays that way forever. Once the wave broke and I woke up on the shores of the chemistry building of Michigan State University, I realized I had washed up on the beaches of some uncharted land of which I had always been afraid to explore and take head on. I had grown many ways in my life but in this place I was still a child. Growing up is one of the hardest things to do and if it weren't for my wonderful parents, loving brother, best friend(s), the Spirit and those within, and all of my friends and family in Arenac county and everywhere else, I would have died a well fed but beaten child on that rocky shore.

I faltered and fell many times along the path through graduate school, more than most people would believe, and my boss Greg and all the members of the Baker group along with some other scattered souls throughout the building helped pick me back up many times and encouraged me to keep going. I thank you all for the care and compassion. I especially want to thank Greg for allowing me to be successful in my own way.

And so as I sit here I realize the child has come a long way in the past few years. He may not have grown up, but he has survived. So, to the eternal child within me, thank you. I know you will never leave, for that would mean the death of me.

TABLE OF CONTENTS

LIST OF TABLES	v i
LIST OF FIGURES	vii
LIST SCHEMES	x
LIST OF ABBREVIATIONS	xi
Chapter 1 Introduction	
1.1 The synthesis of polylactides	
1.2 Glass transition temperatures of polylactides	
1.4 Furfural-based polymers	22
Chapter 2 Poly(tetrahydrofurfuryl glycolide)s	32
2.1 Monomer synthesis	33
2.2 Synthesis of poly(THFglycolide)s	
2.3 Physical properties of poly(THFglycolide)s2.4 Glass transitions of poly(THFglycolide)s	
Chapter 3 Experimental	58
3.1 General details	
3.2 Materials synthesis	59
Appendix	67
References	Q _Z

LIST OF TABLES

Table 1 . Composition and T_g s of poly(MMD- co -glycolide)	21
Table 2 . Composition and T_9 s of poly(IPMD- co -lactide)	21
Table 3. Water contact angle at 20°C for various packaging materials	26
Table 4 . Glass transition temperature of poly(2-furyloxirane) as a fund of M_n	
Table 5. Polymer data before precipitation with the polymerizations in bu 160°C with monomer to initiator ratios ([M]/[I]) of 200	
Table 6. Polymer data after precipitation with [M]/[I] = 200	46
Table 7. T _g data for poly(THFglycolides)	49
Table 8. Results from computational study performed on model poly(THF glycolide) systems in Figure 30	50
Table 9 . Contact angle measurements for poly(THFglycolides) and polylactic where θ_{adv} - θ_{rec} is the contact angle hysteresis	

LIST OF FIGURES

Figure 1. Structure of polylactide1
Figure 2. Isomers of lactide
Figure 3. Common lactide polymerization catalysts and initiators6
Figure 4. Representative organocatalysts developed for the ROP of lactide7
Figure 5 . For n-alkyl substituted polylactides, $T_{\rm g}$ decreases as the alkyl chain increases
Figure 6. Polylactides further illustrating the effects of dipole-dipole screening or T_9 11
Figure 7 . T_g 's of aryl and cylcohexyl substituted polylactides13
Figure 8. Isotactic, syndiotactic, and heterotactic polylactides14
Figure 9 . Star shaped poly(L-lactide) (M_n ≈ 16,000-96,000 g/mol) and poly(D,L-lactide) (M_n ≈ 1,500-9,500 g/mol)15
Figure 10. Branched copolymer with mevalonolactone/L-lactide 10:90 M _n ≈ 23,00015
Figure 11 . Examples of comb-like polylactides including poly(glycidol)- g -poly(L-lactide) ($M_n \approx 25,000\text{-}287,000 \text{ g/mol}$), poly(vinyl alcohol)- g -PLLA ($M_n \approx 76000\text{-}274,000 \text{ g/mol}$) and poly(vinyl alcohol)- g -PDLA ($M_n \approx 125,000\text{-}260,000 \text{ g/mol}$), and dextrin- g -PLLA($M_n \approx 110,000\text{-}350,000 \text{ g/mol}$)16
Figure 12 . Examples of functional polymers with pendent ring or rings in the polymer backbone structures: poly(L-lactide-co-benzylIPPTC) and poly(L-lactide-co-IPPTC), poly(PAGYL) and poly(L-lactide-co-PAGYL), poly(N-acetyl-4-hydroxyproline-co-mandelic acid), and poly(L-lactide-co-IPXTC)18
Figure 13. T_g trends in homopolymers from AB monomers
Figure 14. Copolymerization of morpholine-2,5-dione derivatives with glycolide and lactide)20

Figure 15. Removal of the protective benzyl groups from poly(lactic acid-alt-Asp(OBn)) and poly((lactic acid-alt-Asp(OBn))-co-lactic acid) increase their $T_{\rm g}$ s by 53 and 17 °C, respectively
Figure 16. Contact angle of a liquid drop on a solid surface and representation of surface tensions at the three-phase contact point23
Figure 17. PEO-grafted polylactide structures25
Figure 18. Hydrophilic polylactide derivative with pendant hydroxyl groups26
Figure 19. Structures of common packaging materials27
Figure 20. Furfural self-condensation products isolated from furfural heated under neutral conditions
Figure 21. Well defined polymers containing furfuryl groups31
Figure 22. Furfural to poly(di-tetrahydrofurfuryl glycolide)32
Figure 23 . ¹ H NMR spectra showing (top) coupling between the α-hydroxy proton and the methine proton on the adjacent carbon36
Figure 24 . Actual ¹ H NMR (top) and gNMR simulated ¹ H NMR (bottom) spectra of the methylene protons of ethyl 2-(furan-2-yl)-2-hydroxyacetate. For the simulation, the chemical shifts were 4.25 ppm and 4.28 ppm for H_a and H_b and coupling constants of ¹ J _{HH} = 12 Hz and ³ J _{HH} = 7.2 Hz37
Figure 25. ¹ H NMR spectra of RR/SS (top) and RS/SR (bottom) THFAHA39
Figure 26. X-ray crystal structure of RS/SR THFAHA (provided by Erin Vogel)41
Figure 27. X-ray crystal structure of RR/SS THFAHA (provided by ErinVogel).41
Figure 28. TGA analysis results for the different stereoisomers of poly(THFglycolide)s. Samples were run in air at a heating rate of 10 °C/min
Figure 29. TGA analysis results for substituted poly(glycolide)s run in air. Heating rate: 10 °C/min48
Figure 30. Stereoisomers of poly(dicyclohexylalycolide)s and their T ₂ s49

Figure 31. Model poly(THFglycolide) system used in computational study of rotational barriers with stereocenters 1, 2, 3, and 4 (*defines the bonds involved in the backbone rotation)
Figure 32 . DSC analysis of poly(<i>rac</i> -lactide) with varying Lithium ior concentrations. Heating rate: 10 °C/min under nitrogen. The data are from the second heating scan
Figure 33. DSC analysis of poly(RRRR/SSSS, RRSS-THFglycolide) (M3) with varying Lithium ion concentrations. Heating rate: 10 °C/min under nitrogen The data are from the second heating scan
Figure 34 . DSC analysis of poly(RSSR/SRRS, RSRS-THFglycolide) (M1M2 with varying Lithium ion concentrations ($M_n \approx 7800$). Heating rate 10 °C/min under nitrogen. The data are from the second heating scan55
Figure 35 . DSC analysis of poly(RSSR/SRRS,RSRS-THFglycolide) (M1M2 with varying Lithium ion concentrations ($M_n \approx 20200$). Heating rate 10 °C/min under nitrogen. The data are from the second heating scan56
Figure A-1. ¹ H NMR spectrum of 2-(furan-2-yl)-2-hydroxyacetonitrile68
Figure A-2. ¹³ C NMR spectrum of 2-(furan-2-yl)-2-hydroxyacetonitrile69
Figure A-3. ¹ H NMR spectrum of ethyl 2-(furan-2-yl)-2-hydroxyacetate70
Figure A-4. ¹³ C NMR spectrum of ethyl 2-(furan-2-yl)-2-hydroxyacetate71
Figure A-5. ¹ H NMR spectrum of 2-(furan-2-yl)-2-hydroxyacetic acid72
Figure A-6. ¹³ C NMR spectrum of 2-(furan-2-yl)-2-hydroxyacetic acid73
Figure A-7. ¹ H NMR spectrum of R,S/S,R-2-hydroxy-2-(tetrahydrofuran-2-yl)-acetic acid
Figure A-8. ¹³ C NMR spectrum spectrum of R,S/S,R-2-hydroxy-2(tetrahydrofuran-2-yl)-acetic acid
Figure A-9. IR spectrum of R,S/S,R-2-hydroxy-2-(tetrahydrofuran-2-yl)-acetic acid
Figure A-10. ¹ H NMR spectrum of R,R/S,S-2-hydroxy-2-(tetrahydrofuran-2-yl)-acetic acid
Figure A-11. ¹³ C NMR of R,R/S,S-2-hydroxy-2-(tetrahydrofuran-2-yl)-acetic acid

	IR spectrum of R,R/S,S-2-hydroxy-2-(tetrahydrofuran-2-yl)-acetic79
	¹ H NMR spectrum of RSSR/SRRS, RSRS-3,6-bis(tetrahydrofuran-dioxane-2,5-dione (monomer 1)80
	¹³ C NMR spectrum of RSSR/SRRS,RSRS-3,6-bis(tetrahydrofuran-dioxane-2,5-dione (monomer 1)81
	IR spectrum RSSR/SRRS/RSRS-3,6-bis(tetrahydrofuran-2-yl)-1,4-2,5-dione (monomer 1)82
	¹ H NMR spectrum of RSSR/SRRS, RSRS-3,6-bis(tetrahydrofuran-dioxane-2,5-dione (monomer 2)83
Figure A-17. bis(tetral	¹³ C NMR spectrum of RSSR/SRRS, RSRS-3,6- nydrofuran-2-yl)-1,4-dioxane-2,5-dione (monomer 2)84
	IR spectrum RSSR/SRRS/RSRS-3,6-bis(tetrahydrofuran-2-yl)-1,4-2,5-dione (monomer 2)8
	¹ H NMR spectrum of RRRR/SSSS,RRSS-3,6-bis(tetrahydrofuran-dioxane-2,5-dione (monomer 3)86
	¹³ C NMR spectrum of RRRR/SSSS, RRSS-3,6- nydrofuran-2-yl)-1,4-dioxane-2,5-dione (monomer 3)87
	IR spectrum RRRR/SSSS/RRSS-3,6-bis(tetrahydrofuran-2-yl)-1,4- 2,5-dione (monomer 3)88
	¹ H NMR spectrum of poly(RSSR/SRRS, RSRS- drofurfurylglycolide) (poly((M1M2))89
	¹³ C NMR spectrum of poly(RSSR/SRRS,RSRS-drofurfurylglycolide) (poly(M1M2))90
	¹ H NMR spectrum of poly(RRRR/SSSS,RRSS-drofurfurylglycolide) (poly(M3))91
	¹³ C NMR spectrum of poly(RRRR/SSSS, RRSS- drofurfurylglycolide) (poly(M3))92

LIST OF SCHEMES

Scheme 1. Pathways to polylactide from lactic acid	4
Scheme 2. The synthetic equivalent route to polylactide	4
Scheme 3. Mechanism of the DMAP-catalyzed ROP of lactide as proposed b	
Scheme 4. DMAP-catalyzed ROP of lactide proposed from intermediates calculated by Bonduelle and co-workers	9
Scheme 5. Formation of furfural from D-xylose	28
Scheme 6. Synthetic route 1 to di-tetrahydrofurfuryl glycolide	.33
Scheme 7. Vogel's synthetic route to di-tetrahydrofurfuryl glycolide	.34
Scheme 8. Formation of the furfural cyanohydrins	35
Scheme 9. Equilibrium between furfural and its cyanohydrins	.35
Scheme 10. Synthetic routes to ethyl 2-(furan-2-yl)-2-hydroxyacetate	.35
Scheme 11. Basic hydrolysis of ethyl 2-(furan-2-yl)-2-hydroxyacetate	.38
Scheme 12. Hydrogenation of 2-(furan-2-yl)-2-hydroxyacetic acid	.38
Scheme 13. Synthesis of di-tetrahydrofurfuryl glycolides	.42
Scheme 14. Synthesis of poly(THFqlycolide)s	.45

LIST OF ABBREVIATIONS

Al(O- <i>i</i> -pr) ₃	aluminum triisopropoxide
BBA	4-tert-butylbenzyl alcohol
ВЕМР	2- <i>tert</i> -butylimino-2-diethylamino-1,3-dimethylperhydro-1,3,2-diazaphosphorine
br	broad
d	doublet
dd	doublet of doublets
DMAP	4-(dimethylamino)-pyridine
DP	degree of polymerization
DSC	differential scanning calorimetry
dt	doublet of triplets
EC	ethylcellulose
El	electron impact
g	gram
GPC	gel permeation chromatography
HEC	hydroxyethyl cellulose
HOTf	trifluoromethanesulfonic acid
HPC	hydroxypropyl cellulose
НРМС	hydroxypropyl methylcellulose
Hz	hertz
IPMD	3(S)-isopropylmorpholine-2,5-dione
IR	infrared
J	coupling constant
LDPE	low density polyethylene
LLDPE	linear low density polyethylene
M	molar
m	multiplet
m/z	mass of ion(atomic units)/charge of ion
M1	monomer 1
M2	monomer 2
M3	monomer 3
MC	methylcellulose
MMD	6-methylmorpholine-2,4-dione

mp melting point mS mass spectrometry Mw weight average molecular weight NHC N-heterocyclic carbenes NMR nuclear magnetic resonance OCAs O-carboxyanhydrides PDI poly dispersity index PEC polyethylene oxide PET poly(ethylene terephthalate) PPMMA poly(methyl methacrylate) PP poly(propylene) ppm parts per million PPY 4-pyrrolidinopyridine PS polystyrene psi pound per square inch PTFE poly(terifluoroethylene) PVC poly(vinyl chloride) rac racemic ROP ring opening polymerization s singlet Sn(Oct) ₂ tin(II)-2-ethylhexanoate terit tertiary T _g glass transition temperature TGA thermal gravimetric analysis THF tetrahydrofuran THFAHA tetrahydrofuran alpha hydroxy acid THFglycolide wt weight δ chemical shift θ contact angle μm micrometer v wavenumber	<i>M</i> _n	number average molecular weight
Mw weight average molecular weight NHC N-heterocyclic carbenes NMR nuclear magnetic resonance OCAs O-carboxyanhydrides PDI poly dispersity index PEO polyethylene oxide PET poly(ethylene terephthalate) PMMA poly(methyl methacrylate) PP poly(propylene) ppm parts per million PPY 4-pyrrolidinopyridine PS polystyrene psi pound per square inch PTFE poly(itetrafluoroethylene) PVC poly(vinyl chloride) rac racemic ROP ring opening polymerization s singlet Sn(Oct)2 tin(II)-2-ethylhexanoate t triplet TBD triazabicyclodecene tert tertiary Tg glass transition temperature TGA thermal gravimetric analysis THF tetrahydrofuran THFAHA tetrahydrofuran alpha hydroxy acid tetrahydrofuran glycolide wt wt	mp	melting point
NHC N-heterocyclic carbenes NMR nuclear magnetic resonance OCAs O-carboxyanhydrides PDI poly dispersity index PEO polyethylene oxide PET poly(ethylene terephthalate) PMMA poly(methyl methacrylate) PP poly(propylene) ppm parts per million PPY 4-pyrrolidinopyridine PS polystyrene psi pound per square inch PTFE poly(tetrafluoroethylene) PVC poly(vinyl chloride) rac racemic ROP ring opening polymerization s singlet Sn(Oct) ₂ tin(II)-2-ethylhexanoate t triplet TBD triazabicyclodecene tert tertiary T _g glass transition temperature TGA thermal gravimetric analysis THF THFAHA tetrahydrofuran alpha hydroxy acid THFGIPOLOGICA Verification N-heterocyclic carbenes POCastoxyanhydrides POLOGICA Verification PET (Verification) Verification N-heterocyclic carbenes PDI (Verification) N-heterocyclic carbenes PDI (Verification) N-heterocyclic carbenes PDI (Verification) N-heterocyclic carbenes PDI (Verification) N-heterocyclic carbenes N-Heterocyclic carbonace N-He	MS	mass spectrometry
NMR OCAS O-carboxyanhydrides PDI poly dispersity index PEO polyethylene oxide PET poly(ethylene terephthalate) PMMA poly(methyl methacrylate) PP poly(propylene) ppm parts per million PPY 4-pyrrolidinopyridine PS poly(tetrafluoroethylene) PVC poly(vinyl chloride) rac rac ROP ring opening polymerization s singlet Sn(Oct) ₂ tin(II)-2-ethylhexanoate tert TBD triazabicyclodecene tert TGA thermal gravimetric analysis THF THFAHA tetrahydrofuran THFAHA tetrahydrofuran alpha hydroxy acid THFglycolide wt weight δ chemical shift θ contact angle μm	M _w	weight average molecular weight
OCAS O-carboxyanhydrides PDI poly dispersity index PEO polyethylene oxide PET poly(ethylene terephthalate) PMMA poly(methyl methacrylate) PP poly(propylene) ppm parts per million PPY 4-pyrrolidinopyridine PS polystyrene psi pound per square inch PTFE poly(tetrafluoroethylene) PVC poly(vinyl chloride) rac racemic ROP ring opening polymerization s singlet Sn(Oct) ₂ tin(II)-2-ethylhexanoate tert TBD triazabicyclodecene tert tertiary T _g glass transition temperature TGA thermal gravimetric analysis THF tetrahydrofuran THFAHA tetrahydrofuran alpha hydroxy acid THFglycolide wt weight δ chemical shift θ contact angle μm	NHC	N-heterocyclic carbenes
PDI poly dispersity index PEO polyethylene oxide PET poly(ethylene terephthalate) PMMA poly(methyl methacrylate) PP poly(propylene) ppm parts per million PPY 4-pyrrolidinopyridine PS polystyrene psi pound per square inch PTFE poly(tetrafluoroethylene) PVC poly(vinyl chloride) rac racemic ROP ring opening polymerization s singlet Sn(Oct) ₂ tin(II)-2-ethylhexanoate t triplet TBD triazabicyclodecene tert tertiary T _g glass transition temperature TGA thermal gravimetric analysis THF tetrahydrofuran THFAHA tetrahydrofuran alpha hydroxy acid THFglycolide wt weight δ chemical shift θ contact angle μm micrometer	NMR	nuclear magnetic resonance
PEO polyethylene oxide PET poly(ethylene terephthalate) PMMA poly(methyl methacrylate) PP poly(propylene) ppm parts per million PPY 4-pyrrolidinopyridine PS polystyrene psi pound per square inch PTFE poly(tetrafluoroethylene) PVC poly(vinyl chloride) rac racemic ROP ring opening polymerization s singlet Sn(Oct) ₂ tin(II)-2-ethylhexanoate t triplet TBD triazabicyclodecene tert tertiary T _g glass transition temperature TGA thermal gravimetric analysis THF THFAHA tetrahydrofuran THFAHA tetrahydrofuran alpha hydroxy acid THFglycolide wt weight δ chemical shift θ contact angle μm micrometer	OCAs	O-carboxyanhydrides
PET poly(ethylene terephthalate) PMMA poly(methyl methacrylate) PP poly(propylene) ppm parts per million PPY 4-pyrrolidinopyridine PS polystyrene psi pound per square inch PTFE poly(tetrafluoroethylene) PVC poly(vinyl chloride) rac racemic ROP ring opening polymerization s singlet Sn(Oct) ₂ tin(II)-2-ethylhexanoate t triplet TBD triazabicyclodecene tert tertiary T _g glass transition temperature TGA thermal gravimetric analysis THF tetrahydrofuran THFAHA tetrahydrofuran alpha hydroxy acid THFglycolide wt weight δ chemical shift θ contact angle μm micrometer	PDI	poly dispersity index
PMMA poly(methyl methacrylate) PP poly(propylene) ppm parts per million PPY 4-pyrrolidinopyridine PS polystyrene psi pound per square inch PTFE poly(tetrafluoroethylene) PVC poly(vinyl chloride) rac racemic ROP ring opening polymerization s singlet Sn(Oct) ₂ tin(II)-2-ethylhexanoate t triplet TBD triazabicyclodecene tert tertiary T _g glass transition temperature TGA thermal gravimetric analysis THF tetrahydrofuran THFAHA tetrahydrofuran alpha hydroxy acid THFglycolide wt weight δ chemical shift θ contact angle μm micrometer	PEO	polyethylene oxide
PP poly(propylene) ppm parts per million PPY 4-pyrrolidinopyridine PS polystyrene psi pound per square inch PTFE poly(tetrafluoroethylene) PVC poly(vinyl chloride) rac racemic ROP ring opening polymerization s singlet triplet TBD triazabicyclodecene tert tertiary Tg glass transition temperature TGA thermal gravimetric analysis THF tetrahydrofuran THFAHA tetrahydrofuran alpha hydroxy acid THFglycolide wt weight δ chemical shift θ contact angle μm micrometer	PET	poly(ethylene terephthalate)
ppm parts per million PPY 4-pyrrolidinopyridine PS polystyrene psi pound per square inch PTFE poly(tetrafluoroethylene) PVC poly(vinyl chloride) rac racemic ROP ring opening polymerization s singlet tin(II)-2-ethylhexanoate t triplet TBD triazabicyclodecene tert tertiary Tg glass transition temperature TGA thermal gravimetric analysis THF tetrahydrofuran THFAHA tetrahydrofuran alpha hydroxy acid THFglycolide tetrahydrofuran glycolide wt weight δ chemical shift θ contact angle μm micrometer	PMMA	poly(methyl methacrylate)
PPY 4-pyrrolidinopyridine PS polystyrene psi pound per square inch PTFE poly(tetrafluoroethylene) PVC poly(vinyl chloride) rac racemic ROP ring opening polymerization s singlet Sn(Oct) ₂ tin(II)-2-ethylhexanoate t triplet TBD triazabicyclodecene tert tertiary T _g glass transition temperature TGA thermal gravimetric analysis THF tetrahydrofuran THFAHA tetrahydrofuran alpha hydroxy acid THFglycolide wt weight δ chemical shift θ contact angle μm micrometer	PP	poly(propylene)
PS polystyrene psi pound per square inch PTFE poly(tetrafluoroethylene) PVC poly(vinyl chloride) rac racemic ROP ring opening polymerization s singlet Sn(Oct) ₂ tin(II)-2-ethylhexanoate t triplet TBD triazabicyclodecene tert tertiary T _g glass transition temperature TGA thermal gravimetric analysis THF tetrahydrofuran THFAHA tetrahydrofuran alpha hydroxy acid THFglycolide wt weight δ chemical shift θ contact angle μm micrometer	ppm	parts per million
psi pound per square inch PTFE poly(tetrafluoroethylene) PVC poly(vinyl chloride) rac racemic ROP ring opening polymerization s singlet Sn(Oct) ₂ tin(II)-2-ethylhexanoate t triplet TBD triazabicyclodecene tert tertiary T _g glass transition temperature TGA thermal gravimetric analysis THF tetrahydrofuran THFAHA tetrahydrofuran alpha hydroxy acid THFglycolide tetrahydrofuran glycolide wt weight δ chemical shift θ contact angle μm micrometer	PPY	4-pyrrolidinopyridine
PTFE poly(tetrafluoroethylene) PVC poly(vinyl chloride) rac racemic ROP ring opening polymerization s singlet Sn(Oct) ₂ tin(II)-2-ethylhexanoate t triplet TBD triazabicyclodecene tert tertiary T _g glass transition temperature TGA thermal gravimetric analysis THF tetrahydrofuran THFAHA tetrahydrofuran alpha hydroxy acid THFglycolide tetrahydrofuran glycolide wt weight δ chemical shift θ contact angle μm micrometer	PS	polystyrene
PVC poly(vinyl chloride) rac racemic ROP ring opening polymerization s singlet Sn(Oct) ₂ tin(II)-2-ethylhexanoate t triplet TBD triazabicyclodecene tert tertiary T _g glass transition temperature TGA thermal gravimetric analysis THF tetrahydrofuran THFAHA tetrahydrofuran alpha hydroxy acid THFglycolide tetrahydrofuran glycolide wt weight δ chemical shift θ contact angle μm micrometer	psi	pound per square inch
rac racemicROPring opening polymerizationssinglet $Sn(Oct)_2$ $tin(II)$ -2-ethylhexanoatettripletTBDtriazabicyclodecene $tert$ tertiary T_g glass transition temperatureTGAthermal gravimetric analysisTHFtetrahydrofuranTHFAHAtetrahydrofuran alpha hydroxy acidTHFglycolidetetrahydrofuran glycolidewtweight δ chemical shift θ contact angle μm micrometer	PTFE	poly(tetrafluoroethylene)
ROPring opening polymerizationssingletSn(Oct)2tin(II)-2-ethylhexanoatettripletTBDtriazabicyclodeceneterttertiary T_g glass transition temperatureTGAthermal gravimetric analysisTHFtetrahydrofuranTHFAHAtetrahydrofuran alpha hydroxy acidTHFglycolidetetrahydrofuran glycolidewtweight δ chemical shift θ contact angle μm micrometer	PVC	poly(vinyl chloride)
$\begin{array}{cccccccccccccccccccccccccccccccccccc$	rac	racemic
$\begin{array}{cccccccccccccccccccccccccccccccccccc$	ROP	ring opening polymerization
triplet TBD triazabicyclodecene tert tertiary T_g glass transition temperature TGA thermal gravimetric analysis THF tetrahydrofuran THFAHA tetrahydrofuran alpha hydroxy acid THFglycolide tetrahydrofuran glycolide wt weight δ chemical shift θ contact angle μ m micrometer	s	singlet
TBD triazabicyclodecene tert tertiary T_g glass transition temperature TGA thermal gravimetric analysis THF tetrahydrofuran THFAHA tetrahydrofuran alpha hydroxy acid THFglycolide tetrahydrofuran glycolide wt weight δ chemical shift θ contact angle μm micrometer	Sn(Oct) ₂	tin(II)-2-ethylhexanoate
$ \begin{array}{cccccccccccccccccccccccccccccccccccc$	t	triplet
$T_{\rm g}$ glass transition temperature TGA thermal gravimetric analysis THF tetrahydrofuran THFAHA tetrahydrofuran alpha hydroxy acid THFglycolide tetrahydrofuran glycolide wt weight δ chemical shift θ contact angle μm micrometer	TBD	triazabicyclodecene
TGA thermal gravimetric analysis THF tetrahydrofuran THFAHA tetrahydrofuran alpha hydroxy acid THFglycolide tetrahydrofuran glycolide wt weight δ chemical shift θ contact angle μ m micrometer	tert	tertiary
THF tetrahydrofuran THFAHA tetrahydrofuran alpha hydroxy acid tetrahydrofuran glycolide wt weight δ chemical shift σ contact angle μm micrometer	T_{g}	glass transition temperature
THFAHA tetrahydrofuran alpha hydroxy acid THFglycolide tetrahydrofuran glycolide wt weight δ chemical shift θ contact angle μm micrometer	TGA	thermal gravimetric analysis
THFglycolide tetrahydrofuran glycolide wt weight δ chemical shift θ contact angle μm micrometer	THF	tetrahydrofuran
$\begin{array}{ccc} wt & & weight \\ \delta & & chemical shift \\ \theta & & contact angle \\ \mu m & & micrometer \end{array}$	THFAHA	tetrahydrofuran alpha hydroxy acid
δchemical shiftθcontact angleμmmicrometer	THFglycolide	tetrahydrofuran glycolide
θ contact angle μm micrometer	wt	weight
μm micrometer	δ	chemical shift
	θ	contact angle
v wavenumber	μm	micrometer
	V	wavenumber

CHAPTER 1

Introduction

1.1 Poly(lactide)s

Most commodity plastics are derived from petroleum, a limited resource. However, biodegradable polyesters derived from renewable resources may be viable replacements for petroleum based plastics. Polylactide (**Figure 1**), which is emerging as a high volume "green material", is biodegradable, bioassimible, and can be recycled and composted. Unlike its petrochemical counterparts, polylactides sequester carbon dioxide from the atmosphere through its production through photosynthesis. Polylactide also can mimic poly(vinyl chloride) (PVC), linear low density polyethylene (LLDPE), polypropylene (PP), and polystyrene (PS)³ because a wide range of physical properties can be obtained through manipulating polylactide's stereochemistry, crystallinity, and architecture.

Figure 1. Structure of polylactide

Initially, polylactides were limited to biomedical applications such as bioassimable sutures, biodegradable implants and orthopedic devices such as ligating clips and bone pins.⁵ Production costs for polylactides were greater than \$2/lb in 2000,⁶ much higher than commodity plastics such as polystyrene, which ranged between \$0.40 - \$1.00/lb from 2007-2009.⁷ Polylactide costs have

steadily declined since 2000, and polylactides offer benefits (from renewable sources, degradable, ...) that petrochemical-based polymers do not.

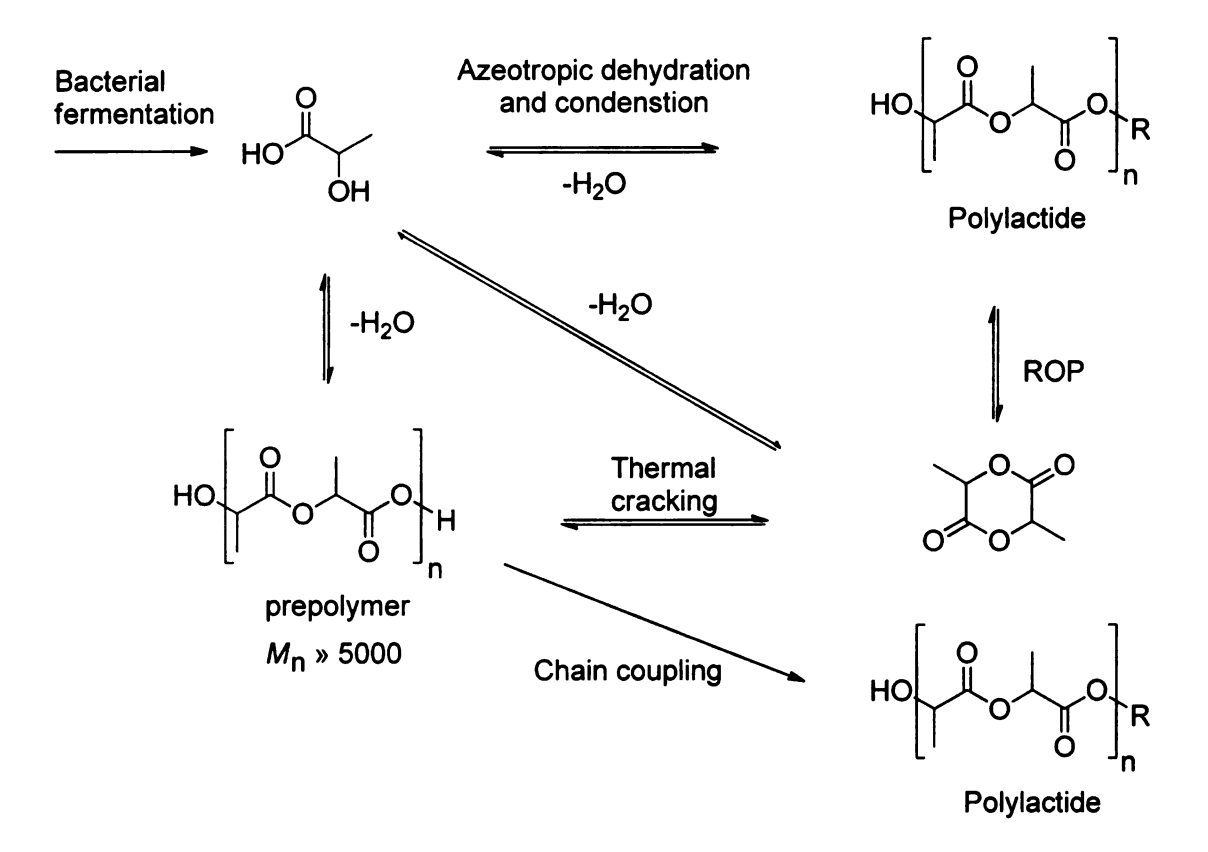
Polylactide is commonly described as biodegradable, but the word must be defined. The use of the word "biodegradable" should only be applied to living cell-mediated degradation and not abiotic enzymatic degradation. In the case of polylactides, simple chemical hydrolysis breaks down the polymer backbone into oligomeric degradation byproducts. Once small enough, microorganisms may then biochemically process the polylactide byproducts, or the partially degraded polymer may enter the food chain and be processed indirectly by animals such as earthworms. However, certain enzymes such as proteinase K have been shown to cleave the main chain.⁸ Polylactides eventually degrade to carbon dioxide, water, and humus.⁶ The bioassimibility of polylactides stems from the lactic acid's presence in nearly every form of life. In humans and animals its primary function is related to the supply of energy to muscle tissue. In the average adult male the turnover of lactic acid, the Cori cycle, has been estimated at 120-150 g per day.⁹

Lactic acid and therefore polylactide can be derived from many renewable resources such as cornstarch, cassava starch, cottonseed hulls, Jerusalem artichokes, corn cobs, corn stalks, beet molasses, wheat bran, rye flour, sugarcane press mud, barley starch, cellulose, carrot processing waste, spent molasses wash, and potato starch. There has been increased interest in the fermentive production of lactic acid from these feedstocks owing to their low cost and environmental friendliness. Two microorganisms valuable in the fermentation

of biomass to lactic acid are the amylolytic bacteria *Lactobacillus amylovorus* ATCC 33622 and *Lactobacillus helveticus*. *L. amylovorus* has been reported to effect full conversion of liquefied cornstarch to lactic acid with a productivity of 20 g L⁻¹ h⁻¹ while high cell density *L. helveticus* (27 g L⁻¹) has a maximum productivity of 35 g L⁻¹ h⁻¹ and complete conversion of 55-60 g L⁻¹ lactose present in whey.

1.2 The synthesis of polylactides

As shown in **Scheme 1**, there are multiple pathways to high molecular weight polylactide. Polycondensation of lactic acid, with concomitant removal of water to drive the polymerization reaction towards completion, usually provides low molecular weight oligomers and with forcing, higher molecular weight polymer with polydispersities near 2.0.¹¹ Since driving the equilibrium to high molecular weight is slow, low molecular weight polylactide oligomers may be converted to high molecular weight polymer by using chain coupling reagents. Alternatively, oligomers may be thermally cracked to lactide, the lactic acid dimer, using a catalyst such as zinc oxide, and then ring opening polymerization (ROP) of lactide can provide high molecular weight polymers with excellent control over the molecular weight. Lactide also can be obtained directly from dimerization of lactic acid.



Scheme 1. Pathways to polylactide from lactic acid⁶

Another route to polylactides is the polymerization of activated lactide equivalents such as the decarboxylation polymerization of 1,3-dioxolane-2,4-diones, or *O*-carboxyanhydrides (OCAs). The organo-catalyzed ROP of carboxyanhydrides derived from lactic acid (lacOCA), provides high molecular weight polymers with controlled molecular weights and narrow polydispersities under mild conditions.¹² Molecular weights up to 60,000 g/mol have been achieved using the methodology illustrated in **Scheme 2**.¹²

Scheme 2. The synthetic equivalent route to polylactide

The thermodynamics for the polymerization of lacOCA was predicted to be more favorable than the ROP of lactide for both enthalpic and entropic reasons, the liberation of CO₂ being a considerable driving force.¹²

Lactic acid is one of the smallest chiral organic molecules. Naturally occurring lactic acid is mainly L(+), while the D(-) isomer is uncommon.⁹ Dimerization of *rac*-lactic acid leads to three lactides, L-lactide, D-lactide, and *meso*-lactide (**Figure 2**). D and L lactide are optically active while the meso lactide is inactive. A 1:1 mixture of L and D lactide is called D,L-lactide, or racemic or *rac*-lactide

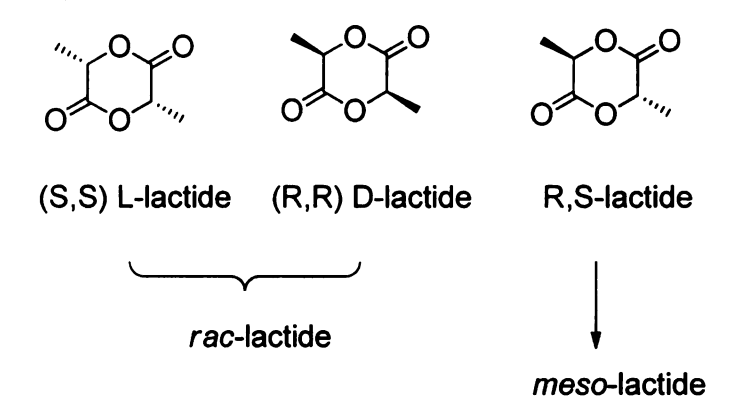


Figure 2. Isomers of lactide

Polymerization of the different stereochemical forms of lactide provides polymers with different properties. For example, rac-lactide polymerizes to an amorphous polymer with a glass transition temperature, T_g , of 50-60 °C while polylactide synthesized from stereochemically pure D or L lactide generally is highly crystalline with a melting transition T_m around 180 °C.¹³ Common catalysts and/or initiators include Sn(2-ethylhexanoate)₂ (Sn(Oct)₂) paired with an alcohol

initiator such as benzyl alcohol or *p-tert*-butylbenzyl alcohol (BBA), and aluminum triisopropoxide (Al(O-*i*-Pr)₃) which acts as both a catalyst and initiator **Figure 3**. Recently, organocatalysts such as 4-(dimethylamino)pyridine (DMAP) have been developed which yield high molecular weight polymers under mild conditions⁵ and eliminate the use of toxic metal catalysts.

Figure 3. Common lactide polymerization catalysts and initiators

It is widely accepted that these catalyst and initiator systems operate by a coordination-insertion mechanism.¹⁴ With Sn(Oct)₂, at least one of the 2-ethylhexanoate ligands is exchanged with the initiating alcohol to form a tin alkoxide initiator. Ring opening of the monomer forms an ester from the initiating alcohol, and a new metal alkoxide derived from the ring-opened lactide. Propagation proceeds through successive steps of ring opening and formation of tin alkoxides.¹⁵⁻¹⁷ The catalyst/initiator systems utilized in this work were Sn(Oct)₂/BBA as well as DMAP/BBA. As described below, ROP of alkyl-substituted monomers using the DMAP/BBA system¹⁵ may follow a different mechanism.

Since Hedrick and co-workers reported the first organocatalytic ROP of lactide with DMAP and PPY (4-pyrrolidinopyridine),¹⁸ new organocatalysts have been developed including N-heterocyclic carbenes (NHC's), trifluoromethanesulfonic acid (HOTf), thiourea/amine combinations, guanidines, and phosphazenes (**Figure 4**).¹⁹

Figure 4. Representative organocatalysts developed for the ROP of lactide 19

The mechanism by which DMAP effects ROP of lactides is only superficially understood. Two proposed mechanisms, illustrated in **Schemes 3** and **4**, were evaluated via computational studies at the B3LYP/6-31G(d) level, with solvent effects (dichloromethane) taken into account through PCM/SCRF single-point calculations at the B3LYP/6-31G(d) level of theory.

Scheme 3. Mechanism of the DMAP-catalyzed ROP of lactide as proposed by Hedrick^{18,19}

Hedrick *et al.* proposed that DMAP acts as a nucleophile, attacking the carbonyl carbon and forming a zwitterionic acylpyridinium intermediate (**Scheme 3**). Addition of alcohol to the acylpyridinium carbonyl carbon forms an ester, regenerates DMAP, and generates a new alcohol species to propagate the polymerization. This route was found to be less favorable than DMAP acting as a base that activates nucleophilic attack by an alcohol as proposed in **Scheme 4**.¹⁹ In this mechanism, the optimized intermediates and transition states, found through theoretical calculations, invoke a central role for multiple hydrogen bonding, and the possibility of DMAP acting as a bifunctional catalyst through its basic nitrogen center and the acidic *ortho*-hydrogen via non-classical hydrogen bonding.¹⁹

Scheme 4. DMAP-catalyzed ROP of lactide proposed from intermediates calculated by Bonduelle and co-workers¹⁹

1.3 Glass transition temperatures of polylactides

The $T_{\rm g}$ is a physical property that depends tacticity, crystallinity, molecular weight, polymer architecture, and the presence of plasticizers. At $T_{\rm g}$ a polymer transforms from a rigid amorphous solid state to a melt state. The reptation model is often used to describe the movement of polymer chains entangled in networks such as polymer gels, melts, and concentrated polymer solutions. In the melt state, the movement of a single chain can be described as a snakelike motion constrained in a tube defined by entangled neighboring polymer

molecules.²⁰ Using the reptation model, qualitative conclusions can be drawn about the relationship between polymer structure and T_g in polymers such as polylactides.

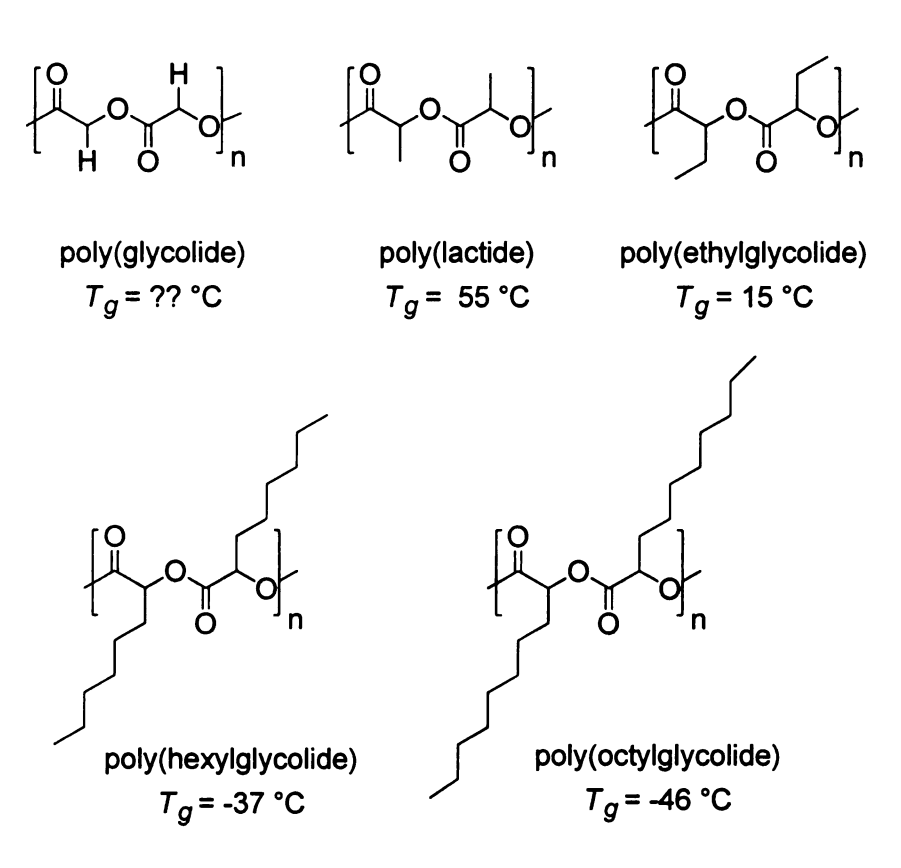


Figure 5. For n-alkyl substituted polylactides, $T_{\rm g}$ decreases as the alkyl chain increases. ²¹

A homologous series of n-alkylpolyglycolides was synthesized and the measured $T_{\rm g}$ decreased with increasing alkyl length. Simple considerations of the rotational barriers would predict that $T_{\rm g}$ should increase as the alkyl chain length increases. However, the observed decrease in $T_{\rm g}$ suggests that the dominant effect is to screen dipole-dipole interactions between ester groups on adjacent

chains. Another possibility is that alkyl groups are acting as internal plasticizers and lower $T_{\rm q}$.²¹

Another series of polylactides supports dipole-dipole screening as the mechanism for lowering T_g . These polyglycolides are substituted with isopropyl and isobutyl groups as shown in **Figure 6**. For isopropyl glycolide, one would expect that the increased the steric bulk of the isopropyl groups will increase rotational barriers about the polymer backbone and increase T_g , but the the T_g of

Figure 6. Polylactides further illustrating the effects of dipole-dipole screening²¹

poly(isopropylglycolide) is almost identical to poly(lactide). Dipole-dipole screening apparently compensates for any chain stiffening caused by the increased rotational barriers. Similar effects are seen in poly(isobutyl glycolide).

Extending the isopropyl groups one more carbon from the polymer backbone increases screening effects and markedly lowers the $T_{\rm g}$ to 23° C.²¹

Screening effects are also observed in aryl-substituted polylactides. Two aromatic polylactide systems, poly(phenyllactide) and poly(mandelide), were synthesized from naturally occurring α -hydroxyacids. These aryl analogues of polylactide were expected to have high glass transition temperatures due to the steric bulkiness of aromatic rings, as well as the possibility of π - π interactions. However, the T_g s of high molecular weight poly(phenyllactide) and poly(mandelide) were 50 and 100 °C, respectively. The low T_g of poly(phenyllactide), comparable to poly(lactide), mirrors the poly(isobutyl glycolide) system. In both cases, moving the sterically demanding group one carbon from the polymer backbone decreased the rotational barriers and increased screening effects.⁴

Poly(mandelide) would seem to be an ideal high $T_{\rm g}$ biodegradable material with polystyrene-like polymers, however each repeat unit has a labile methine proton, α to a carbonyl and an aromatic ring, making it relatively acidic. Consequently, the poly(mandelide) epimerizes, discolors, and is prone to thermal and photochemical degradation. Replacing the aromatic ring of mandelide with a cyclohexyl group stabilized the methine proton in both the monomer and the corresponding polymer while maintaining chain rigidity. As shown in **Figure 7**, the $T_{\rm g}$ s of the resulting poly(dicyclohexylglycolide)s are 98 °C, for *rac*-poly(dicyclohexylglycolide) and 104 °C and no signs of crystallization for

poly(R,R-dicyclohexylglycolide) (greater than 98% stereochemical purity, determined by integration of ¹³C NMR).²²

Figure 7. T_g s of aryl and cylcohexyl substituted polylactides

Tacticity can have an affect the preferred chain conformations of a polymer and therefore the polymer $T_{\rm g}$.¹³ Isotactic polylactide synthesized from stereochemically pure D or L-lactide is generally crystalline with $T_{\rm g}$ s of ~60 °C and $T_{\rm m}$ s around 180 °C.^{23,24} Through the use of selective catalysts, heterotactic as well as syndiotactic polylactides have been prepared (**Figure 8**). Syndiotactic polylactide synthesized from *meso*-lactide and annealed at 95 °C for 60 minutes exhibits a $T_{\rm g}$ of 34 °C and a $T_{\rm m}$ at 152 °C.²⁵ Heterotactic polylactide made from *rac*-lactide polymerizes to an amorphous polymer ($T_{\rm g}$ = 49 °C) despite its stereoregularity.²⁶

Although not all stereoregular polymers form crystalline phases, stereoregularity generally enables polymer chains to pack in a regular fashion and crystallize. As the degree of crystallinity increases, the chain mobility in the

amorphous phase becomes restricted, thereby increasing $T_{\rm g}$.¹³ The effects of crystallinity on polylactide $T_{\rm g}$ s have been explored by Gupta *et al.* using oriented fibers with draw ratios from 1-12. As the draw ratio increased, the degree of crystallinity increased, the melting transition increased from 176 to 180 °C, and the $T_{\rm g}$ increased from 61 to 72 °C.²⁷ Uryama *et al.* examined the effects of crystallinity on the polylactide $T_{\rm g}$ by deliberately adding defects to poly(L-lactide). In a series of poly(L-lactide-co-D,L-lactide) copolymers with the L-lactide content ranging from 75-100%, the polymer $T_{\rm g}$ s decreased from 61 °C for poly(L-lactide) to 53 °C for a copolymer 75% poly(L-lactide). In addition, polymers with \leq 85% poly(L-lactide) content were amorphous.²⁸

H
$$\left(\begin{array}{c} 0 \\ 0 \\ 0 \end{array} \right)$$
 $\left(\begin{array}{c} 0 \\ 0 \end{array} \right)$ \left

Figure 8. Isotactic, 23,24 syndiotactic25 and heterotactic26 polylactides

Heterotactic polylactide T_q = 49 °C

Linear polylactides joined to form different polymer architectures have varying T_g s. Figures 10-12 show examples of star-shaped, branched, and comblike polymers, all exhibiting differing properties. For each architecture, increasing

the composition of L-lactide in the polymer increases both $T_{\rm g}$ and $T_{\rm m}$, as expected.

Figure 9. Star shaped poly(L-lactide) $(M_n \approx 16,000-96,000 \text{ g/mol})^{29}$ and poly(D,L-lactide) $(M_n \approx 1,500-9,500 \text{ g/mol})^{30}$

Branched poly(L-lactide-co-mevalonolactone) $T_{\rm g} \approx$ 47 °C $T_{\rm m} \approx$ 161 °C

Figure 10. Branched copolymer with mevalonolactone/L-lactide 10:90 $M_{\rm n} \approx 23{,}000^{31}$

Dex-g-PLLA
$$T_g \sim 46-57 \,^{\circ}\text{C} \, T_m \sim 130-174 \,^{\circ}\text{C}$$
PVA-g-PDLA $T_g \sim 38-44 \,^{\circ}\text{C}$

Figure 11. Examples of comb-like polylactides including poly(glycidol)-g-poly(L-lactide) ($M_n \approx 25,000\text{-}287,000 \text{ g/mol}$), 32 poly(vinyl alcohol)-g-PLLA ($M_n \approx 76000\text{-}274,000 \text{ g/mol}$) and poly(vinyl alcohol)-g-PDLA ($M_n \approx 125,000\text{-}260,000 \text{ g/mol}$), 33 and dextrin-g-PLLA($M_n \approx 110,000\text{-}350,000 \text{ g/mol}$). 34,35

Copolymerization is commonly used to alter the polylactide and achieve higher T_g materials. Copolymer T_g s vary with composition and fall between the

 $T_{\rm g}$ s of the two homopolymers. For homogeneous copolymers, the $T_{\rm g}$ can be described empirically by the Fox equation³⁶ as:

$$1/T_g = w_1/T_g^1 + w_2/T_g^2$$
 Equation 1

where w_1 and w_2 are the mass fractions of components 1 and 2, respectively. To obtain a high polylactide T_g , lactide must be copolymerized with a monomer that yields a higher T_g polymer. Accordingly to the guidelines outlined earlier, the required monomers are those that provide polymers with restricted rotational barriers or a stiff backbone. The examples shown in **Figure 12** incorporate pendant rings that restrict backbone flexibility and stiffen the polymer chain.

$$\left\{ \left(\begin{array}{c} \\ \\ \\ \\ \end{array} \right) \left(\begin{array}{c} \\ \\ \\ \end{array} \right) \left(\begin{array}{$$

poly(L-lactide-co-benzyIIPPTC) T_g = 60-69 °C poly(L-lactide-co-IPPTC) T_g = 58 °C

poly(L-lactide-co-IPPTC) $T_g = 52 \, ^{\circ}\text{C}$

poly(DIPAGYL) $T_g = 95 \,^{\circ}\text{C}$

poly(L-lactide-co-PAGYL) T_g = 73 °C

$$\begin{bmatrix} \begin{pmatrix} 0 & & \\ & 0 & \\ &$$

poly(N-acetyl-4-hydroxyproline-co-mandelic acid) R=CH₃, $T_{\rm g}$ = 53-119 °C; R=OCH₂Ph, $T_{\rm g}$ = 54 ° C

poly(L-lactide-co-IPXTC) T_g = 60-89 °C

Figure 12. Examples of functional polymers with pendent ring or rings in the polymer backbone structures: poly(L-lactide-co-benzylIPPTC) and poly(L-lactide-co-IPPTC), ³⁷ poly(PAGYL) and poly(L-lactide-co-PAGYL), ³⁸ poly(N-acetyl-4-hydroxyproline-co-mandelic acid), ³⁹ and poly(L-lactide-co-IPXTC). ⁴⁰

A class of polylactides analogous to copolymers is homopolymers derived from AB monomers. AB monomers are unsymmetrical lactides synthesized from two different glycolic acid units. The $T_{\rm g}$ s of polymers synthesized from AB monomers are roughly the average of the $T_{\rm g}$ s of the two homopolymers. The examples shown in **Figure 13** were synthesized in the Baker lab with the exception of the *n*-hexyl derivative reported by Trimaille *et al.*⁴¹

$$T_{g} = ?? ^{\circ}C$$

$$T_{g} = -11 ^{\circ}C$$

$$T_{g} = 50 ^{\circ}C$$

$$T_{g} = 73 ^{\circ}C$$

Figure 13. T_g trends in homopolymers from AB monomers²¹

Cross-linking increases the $T_{\rm g}$ of polymer systems, and is usually attributed to a decrease in configurational entropy as the distance between cross-links decreases. In polylactide systems, cross-linking is accomplished by a number of methods including post-synthesis addition of polymerizable cross-linking agents, end-capping polylactides with cross-linkable acrylates or other polymerizable groups, and the synthesis of lactide-based cross-linking agents that can be copolymerized with lactide. When the cross-linking is less

than 10 mol%, T_g usually increases less than 10 °C. Most examples reported in the literature involving high molecular weight polylactide fall into this category. Larger increases in T_g usually require cross-linking low molecular weight oligomers to high molecular weight polymer.¹³

Inter and intrachain hydrogen bonding can also increase polymer T_g s. Hydrogen bonding makes the polymer chains "sticky", restricting their movement through the tube described in the reptation model. Morpholine-2,5-dione derivatives, glycolides where an α -hydroxyacid group has been replaced by an α -amino acid, place amides in the polymer backbone (**Figure 14**). As expected, the data in **Tables 1** and **2** show that the copolymer T_g increases with the amide concentration, illustrating the effects of hydrogen bonding and the higher rotational barrier of the amide bonds.

Figure 14. Copolymerization of morpholine-2,5-dione derivatives with glycolide⁴⁴ and lactide).⁴⁵

Table 1. Composition and T_g s of poly(MMD-co-glycolide)

Mole fraction of MMD in copolymer (%)	T _g (°C)
0	43
9	54
20	63
26	68
35	72
45	75
66	75
85	86
100	91

Table 2. Composition and T_g s of poly(IPMD-co-lactide)

Mole fraction of IPMD in copolymer (%)	Τ _g (°C)
0	40
7	41
9	42
29	45
46	48
70	56
100	74

When pendant carboxylic acid groups are added to polylactides, T_g increases significantly due to hydrogen bonding (**Figure 15**). Feng *et al.* polymerizated benzyl-protected morpholine-2,5-diones (poly(lactic acid-*alt*-Asp(OBn)) and their copolymers with D,L-lactide (poly((lactic acid-*alt*-Asp(OBn lactic acid)-*co*-lactic acid) 30 mol % aspartic acid, as determined by ¹H NMR). The T_g s were 34 °C

and 47 °C, respectively. 46 Removal of the protective benzyl groups provides poly(lactic acid-alt-Asp(OBn)) and poly((lactic acid-alt-Asp(OBn))-co-lactic acid) with $T_{\rm q}$ s of 87 °C and 64 °C, respectively.

poly(Lactic acid-alt-Asp(OBn)) poly(Lactic acid-alt-Asp)

$$T_g = 34 \,^{\circ}\text{C}$$
 $T_g = 87 \,^{\circ}\text{C}$

poly(Lactic acid-co-Asp(OBn)) poly(Lactic acid-co-Asp)

 $T_g = 47 \,^{\circ}\text{C}$

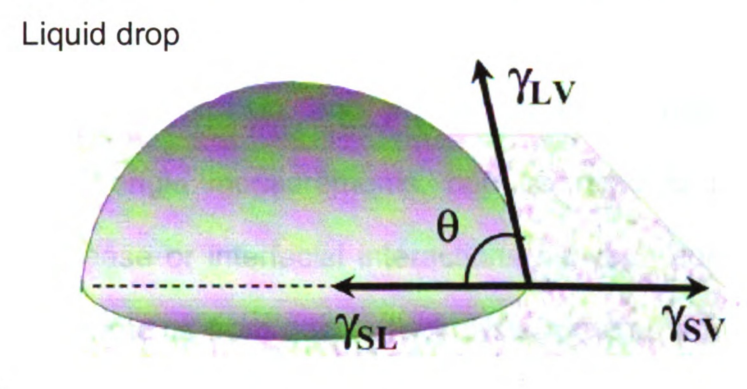
Figure 15 Removal of the protective benzyl groups from poly(lactic acid-*alt*-Asp(OBn)) and poly((lactic acid-*alt*-Asp(OBn))-co-lactic acid) increase their T_g s by 53 and 17 °C, respectively.

1.4 Hydrophilic polylactides

Adding hydrogen bonding to polymers increases their $T_{\rm g}$ s, and can impart other properties such has hydrophilicity. Polylactides are typically hydrophobic, but hydrophilic polylactides may exhibit useful properties such as the ability to form micelles, lower critical solution temperature (LCST) behavior, and water solubility. These properties could prove useful in medical applications such as in

drug delivery, where a hydrophilic polylactide may have accelerated degradation rates *in vivo* or resist protein fouling.⁴⁷

The usual method for evaluating the hydrophobicity/hydrophilicity of materials is contact angle measurements. In 1805, Young described the relationship between the surface tension at the three-phase contact line between a smooth, rigid, solid phase S, a liquid L, and its vapor V (**Figure 16**).



Solid surface

Figure 16. Contact angle of a liquid drop on a solid surface and representation of surface tensions at the three-phase contact point.⁴⁸

The contact angle, θ , is defined by the equation:

$$\gamma_{LV} \cdot \cos\theta = \gamma_{SV} - \gamma_{SL}$$
 Equation 2

where γ_{LV} , γ_{SV} and γ_{SL} are the surface tensions (or free energy per unit area) of the liquid-vapor, solid-vapor and solid-liquid interfaces.⁴⁹

The value of θ indicates the hydrophobicity of a surface. A large θ corresponds to a hydrophobic surface while a small θ implies a hydrophilic surface. The range of contact angle measurements are from 0-180°. Materials that are completely wetted have a contact angle of 0°, while the other extreme, 180°, is not possible because it would imply a total lack of interaction between

the liquid and the solid. Vogler differentiated "hydrophilic" and "hydrophobic" surfaces by their water contact angle. Materials with contact angles > 65° were considered to be hydrophobic, and a contact angle < 65° indicated a hydrophilic material.⁵⁰

The usefulness of contact angle measurements is quite apparent in drug delivery systems where they can be used to determine the behavior of a substance in a particular environment, to improve processability and bioavailability, and to control process and product quality. The wettability, determined from contact angle measurements, can be used to predict and determine the rate of release or interfacial interactions between components.⁵¹ For example, protecting proteins from gastric hydrolysis requires a hydrophobic polymer.

Polylactides are hydrophobic by nature. The reported contact angles for poly(D,L-lactide) range from 87° to 69°,⁵² while a contact angle of 100° for poly(hexylglycolide) was attributed to the added hydrophobicity of the hexyl groups.⁴⁷ If a hydrophobic group increases the contact angle of polylactides, then adding a hydrophilic side group should have the opposite effect. Hydrophilic polylactides have been synthesized by grafting polyethylene oxide (PEO) segments to the polymer backbone via a hexyl spacer as shown in **Figure 17**. The polymers contain n = 1,2,3, and 4 PEO units, and all had weak T_g values at ~-25 °C.⁴⁷ When n = 1 and 2, the contact angles were between 50-75°. Although hydration of the hydrophilic side chains prevented precise measurements, the increased hydrophilicity was obvious compared to more hydrophobic polylactide

examples. When n = 3 or 4 the polymers were water-soluble and formed clear solutions below their LCST.⁴⁷

Figure 17. PEO-grafted polylactide structure⁴⁷

Other examples of hydrophilic polylactides include polymers with pendant alcohol groups. Poly(DIPAGYL) (**Figure 18**) is derived from glycolic acid and D-gluconic acid with its alcohol functional groups protected with propylidene groups. The protected polymer is insoluble in hydrophilic solvents such as methanol, ethanol, and water. After deprotection, (maximum deprotection achieved was 60%) the polymer was soluble in methanol and ethanol and partially soluble in water.³⁸ Poly(3-benzyloxymethyl-1,4-dioxane-2,5-dione) (PBMG), synthesized by Yang *et al.*, shows similar behavior. Removing the benzyl group revealed the hydroxyl group (poly(3-hydroxymethyl-1,4-dioxane-2,5-dione, PHMG)) and greatly increased the polymer hydrophilicity, as confirmed by a decrease in the water contact angle from 90° to 20°. The polymer remained insoluble in water, but the polymer absorbed approximately 58 wt% water after only 8 hours.

Adding pendant carboxylic acid groups to polylactides have similar affects. The hydrophilicity of poly(Lac-alt-Asp) and poly((Lac-alt-Asp)-co-Lac)) (**Figure 15**) were soluble in methylene chloride before deprotection, but insoluble in water or methanol. However, after deprotection, poly(Lac-alt-Asp) was soluble in water

and methanol, but not in methylene chloride, while poly((Lac-alt-Asp)Lac-co-Lac)) (30 mol % aspartic acid) is insoluble in water and methanol but soluble in methylene chloride. The results clearly show the correlation between higher hydrophilicity and the carboxylic acid content in poly(Lac-alt-Asp).⁴⁶

Figure 18. Hydrophilic polylactides with pendant hydroxyl groups^{38,53}

Table 3. Water contact angle at 20°C for various packaging materials

material	θ_{static}	material	$\theta_{ ext{static}}$
LDPE	94	Filter paper	15
LDPE	97	Starch	32
PET	81	Starch + 20% glycerol	53
PMMA	80	HPMC	70
PMMA	74	MC	54
PMMA	65	HPC	70
PP	100	HEC	38
PS	91	EC	85
Parrafin	108		

(LDPE: Low density polyethylene; PET: poly(ethylene terephthalate); PMMA: poly(methyl methacrylate); PP: polypropylene; PS: polystyrene; HPMC: hydroxypropyl methylcellulose; MC: methylcellulose; HPC: hydroxypropyl cellulose; HEC: hydroxyethyl cellulose; EC: ethylcellulose

Figure 19. Structures of common packaging materials

 $R = CH_2CH_3 = ethylcellulose$

 $R = CH_2CH_2OH = hydroxyethylcellulose$

The contact angles of most synthetic polymers are greater than 65°, classifying them as hydrophobic materials. The contact angles of common packaging materials are listed in **Table 3**. The measured contact angles can be rationalized from their structures, as shown in **Figure 20**. Aliphatic polymers such as polypropylene and polyethylene have large contact angles owing to their hydrophobic nature. The cellulosic materials have contact angles ranging from 38° to 85° depending on the hydrophobicity or hydrophilicity of the ether group which directly corresponds to the presence of hydroxyl groups.

1.5 Furfural-based polymers

Furfural has been a commodity chemical for many decades due to its easy access from corn cobs, oat and rice hulls, sugar-cane bagasse, cotton seeds, olive husks, wood chips, and a vast array of other pentose-containing materials.⁵⁴ Furfural is formed from aldopentoses when exposed to aqueous acid and elevated temperatures, as shown in **Scheme 5** for its formation from D-xylose.⁵⁵ The worldwide production of furfural in 2005 was ~250,000 tons/year with a market price around \$1000/ton (USD).⁵⁶

Scheme 5. Formation of furfural from D-xylose⁵⁵

The full scope of furfural and furfural-containing polymers is too large to summarize in this work. Instead, examples of well-defined polymers containing furan rings will be discussed due to their inherent link to the tetrahydrofurfuryl substituted polylactides described in Chapter 2. Homopolymerization of the furfural carbonyl is thermodynamically unfavorable, but furfural can be a comonomer in polymerizations.⁵⁴ However, modifying the furfural structure provides polymerizable monomers. Of these, only a handful of well-defined homopolymers have been synthesized as the reactivity of the furan ring often leads to crosslinking.

Furfural's tendency to form cross-linked products has been known for decades, induced by acids, bases (including zeolites⁵⁷), and to a much lesser extent under neutral conditions at high temperatures.⁵⁴ The classical product of these processes is a black, insoluble mass. When highly purified anhydrous furfural was sealed in an evacuated ampoule and subjected to prolonged heating (100-250 °C) in the dark, a difuryl ketonic aldehyde and a trifurylic dialdehyde were formed (**Figure 20**).

Figure 20. Furfural self-condensation products isolated from furfural heated under neutral conditions

Further condensation of these products undoubtedly led to the formation of the both soluble oligomers and insoluble resins, in which the net result was the slow but progressive accumulation of a black crosslinked product.^{58,59} The significance of isolating structures such as the trifurylic dialdehyde is that it shows the formation of a labile tertiary hydrogen atom attached to a carbon bearing three furyl moieties. This hydrogen atom can be abstracted as a free radical, as a hydride in acidic media, or as a proton in basic media, which would lead to further resinification of the material.⁵⁴

Several well-defined furfuryl polymers are shown in **Figure 21**. Their T_g s depend on the details of their structure. The T_g of poly(furfuryl acrylate) is reported to be 48 °C, but there was no mention of the polymer molecular weight. Poly(2-furyloxirane) has a T_g which varies greatly with molecular weight (**Table 4**). The relationship between T_g and M_n has been confirmed for many polymers and is often described by the Fox-Flory relationship:

$$T_{\rm q} = T_{\rm q} - {\rm K}/M_{\rm n}$$
 Equation 3

Where $T_{\rm g}\infty$ is the glass transition temperature at infinite number average molecular weight ($M_{\rm n}$) and K is a constant that depends on the polymer structure.

Figure 21. Well defined polymers containing furfuryl groups. 60,61,63-65

Table 4. Glass transition temperature of poly(2-furyloxirane) as a function of $M_{\rm n}^{61}$

$M_{\rm n} \times 10^{-3} (g/{\rm mol})$	Tg(°C)
1.0	-52
2.0	-31
3.2	-14
4.0	-3
5.0	5
8.2	11
10.1	14

Chapter 2 Poly(tetrahydrofurfuryl glycolide)s

As petroleum reserves are depleted, analogues of materials derived from petroleum must be devised from renewable resources. Polylactide is one such material, but it has its limitations. Its low $T_{\rm g}$ (50-60 °C) limits its use as rigid, clear replacement for large-volume thermoplastics such as polystyrene ($T_{\rm g} \sim 100$ °C). In drug delivery systems, its hydrophobicity slows *in vivo* degradation rates. New materials must be synthesized which address these issues.

The abundance and low cost of furfural makes it an attractive building block for new materials. However, the high reactivity of the furan ring limits its use in the synthesis of well-defined materials, and it must be modified, usually by hydrogenation. The goal of this work was to synthesize and characterize a polylactide derivative based on furfural (**Figure 22**). Our motivation for the synthesis was that a furan-based polylactide might have unique physical properties. In particular, the T_g trends seen in polylactides with differing pendant alkyl and aryl groups suggest that a pendant THF ring should stiffen the polymer backbone, increase the T_g , increase polymer hydrophilicity, and increase the degradation rate.

Figure 22. Furfural to poly(di-tetrahydrofurfuryl glycolide).

2.1 Monomer synthesis

Di-tetrahydrofurfuryl glycolide was synthesized by the dimerization of 2-hydroxy-2-(tetrahydrofuran-2-yl)acetic acid. Two approaches were explored for the synthesis of the hydroxyacid from furfural. (**Schemes 6** and **7**).

Scheme 6. Synthetic route 1 to ditetrahydrofurfuryl glycolide

Scheme 6 was based on reducing the furan ring early in the synthesis to avoid furan's tendency to form undesired condensation products. Hydrogenation of furfural was uneventful, but oxidation of the tetrahydrofurfuryl alcohol to tetrahydrofurfural proved difficult, and the desired aldehyde was obtained in low yields. In addition, it was difficult to scale-up the oxidation methodology to provide sufficient quantities of the aldehyde. Therefore, Scheme 6 was abandoned in favor of the protocol shown in Scheme 7, developed by Dr. Erin Vogel.

Scheme 7. Vogel's synthetic route to ditetrahydrofurfuryl glycolide

The initial step of the synthesis is the formation of the furfural cyanohydrin, as shown in **Scheme 8**. The intermediate bisulfite addition complex provides a desirable sodium sulfate leaving group while protonating the oxyanion. In acidic conditions, the furfural cyanohydrin is in equilibrium with furfural as shown in **Scheme 9**. Since evolution of HCN drives the equilibrium toward furfural, a large amount of 12.1 M HCl was carefully added to the reaction mixture just prior to isolating the cyanohydrins by extraction. Since 5 equivalents of KCN are used in this step, copious amounts of HCN is produced and extreme caution must be used.

Scheme 8. Formation of furfural cyanohydrins

$$\begin{array}{c|c}
O & OH & -H^{+} \\
C & +H^{+}
\end{array}$$

$$\begin{array}{c|c}
O & O \\
+HCN$$

Scheme 9. Equilibrium between furfural and its cyanohydrins

The furfural cyanohydrin was recovered as a slightly unstable black oil and was used without purification. Direct hydrolysis of the nitrile to the acid under acidic and basic conditions proved unsuccessful. Boatright and Degering encountered similar problems in their attempts to synthesize 2-(furan-2-yl)-2-hydroxyacetic acid, ⁶⁶ but they successfully converted the nitrile to the ortho ester, and then isolated ethyl 2-(furan-2-yl)-2-hydroxyacetate. A modified version of their synthesis was used (**Scheme 10**).

Isolated yield 58%

Scheme 10. Synthetic routes to ethyl 2-(furan-2-yl)-2-hydroxyacetate

Ethyl 2-(furan-2-yl)-2-hydroxyacetate was recovered as a highly viscous brown/black oil which solidified upon standing. While recrystallization failed to provide the pure ester, sublimation gave white powdery crystals with a melting point (mp 40-41 °C), comparable to the literature value (39 °C). 66 H NMR spectra taken before and after sublimation show only minor differences (**Figure 23**). Prior to sublimation, the signal for the α -hydroxy proton appeared as a singlet due to proton exchange, but after sublimation and loss of water, the signal evolved into broad doublet (J = 5.5 Hz) from coupling with the adjacent methine.

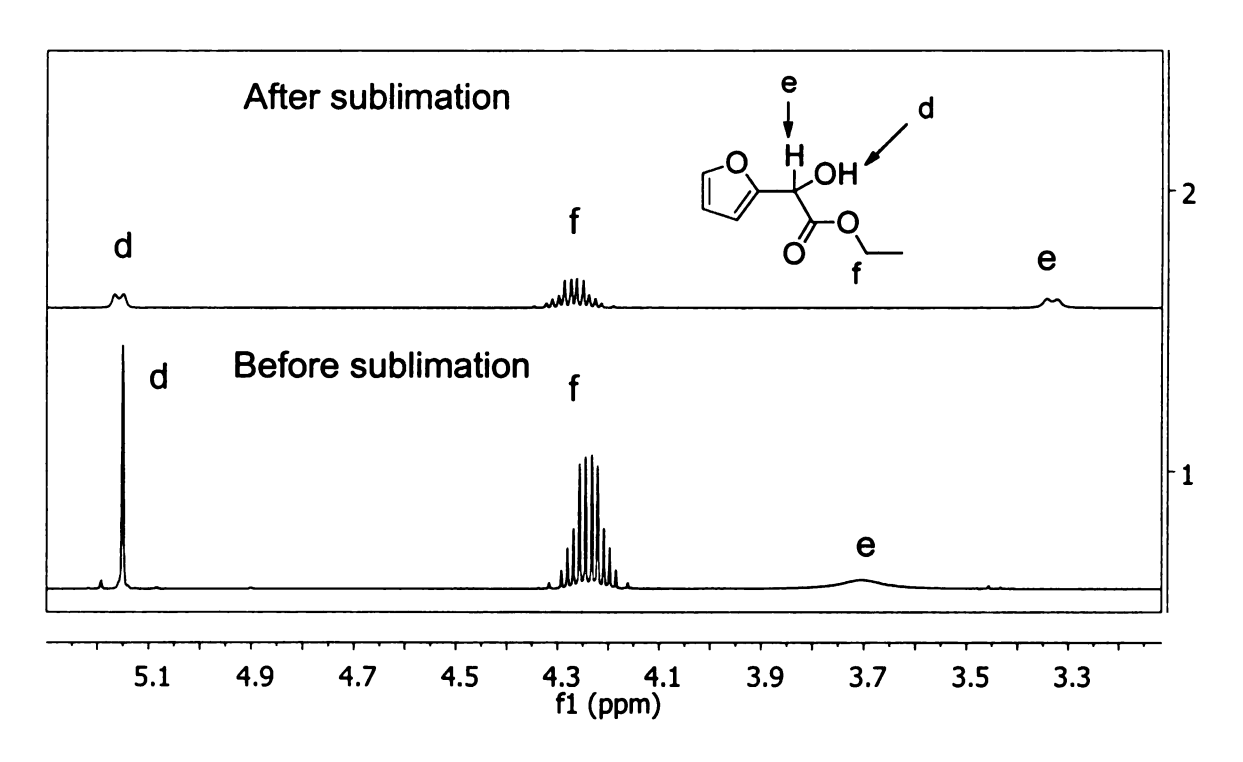


Figure 23. ¹H NMR spectra showing (top) coupling between the α-hydroxy proton and the methine proton on the adjacent carbon.

The methylene protons of the ethyl ester show an interesting splitting pattern. The difference in the chemical shifts of the diastereotopic methylene protons (≈ 0.03 ppm or 9 Hz) is comparable to their coupling constants ($^1J_{HH} \approx 12$ Hz) leading to a higher order pattern, as shown at the top of **Figure 24**. The chemical shift and coupling constant values were determined by gNMR simulations performed by Dr. Daniel Holmes of the Max T. Rogers NMR facility. The simulated spectrum is shown at the bottom of **Figure 24**

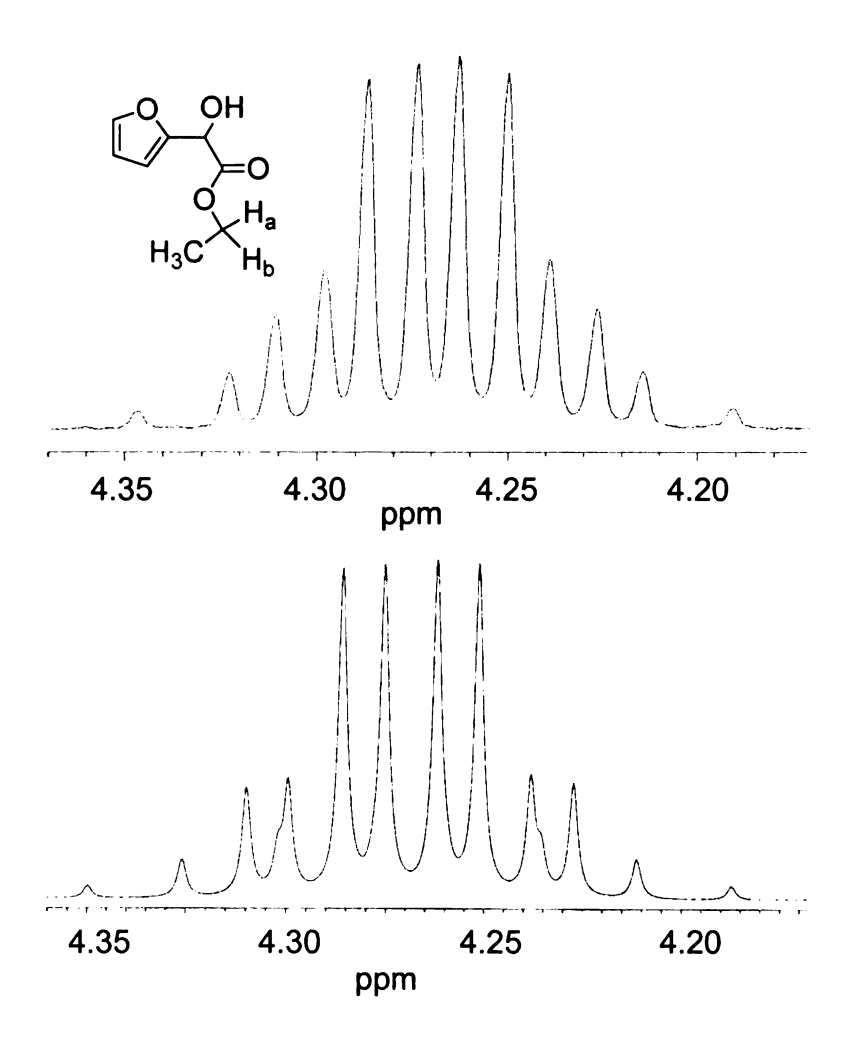


Figure 24. Actual ¹H NMR (top) and gNMR simulated ¹H NMR (bottom) spectra of the methylene protons of ethyl 2-(furan-2-yl)-2-hydroxyacetate. For the

simulation, the chemical shifts were 4.25 ppm and 4.28 ppm for H_a and H_b and coupling constants of $^1J_{HH}$ = 12 Hz and $^3J_{HH}$ = 7.2 Hz

Ethyl 2-(furan-2-yl)-2-hydroxyacetate was hydrolyzed in aqueous sodium hydroxide (**Scheme 11**). The reaction proceeded cleanly and no purification was necessary.

Scheme 11. Basic hydrolysis of ethyl 2-(furan-2-yl)-2-hydroxyacetate

Hydrogenation of the furan ring, as shown in **Scheme 12**, resulted in two sets of diastereomers, R,R/S,S and R,S/S,R 2-hydroxy-2-(tetrahydrofuran-2-yl)acetic acid (THFAHA).

Scheme 12. Hydrogenation of 2-(furan-2-yl)-2-hydroxyacetic acid

The diastereomers were separated by recrystallization from EtOAc/hexanes; the RR/SS isomers had a melting point of 76-77 °C while the RS/SR diastereomers melted at 126.5-127.5 °C (lit. 129 °C).⁶⁷ The ¹H NMR spectra of the compounds

were different, as expected (**Figure 25**). Proton H_a is shielded in the RR/SS stereoisomer while proton H_b is deshielded and its signal is located farther downfield. The opposite was true for the RS/SR stereoisomers; H_a proton was downfield and the H_b proton upfield.

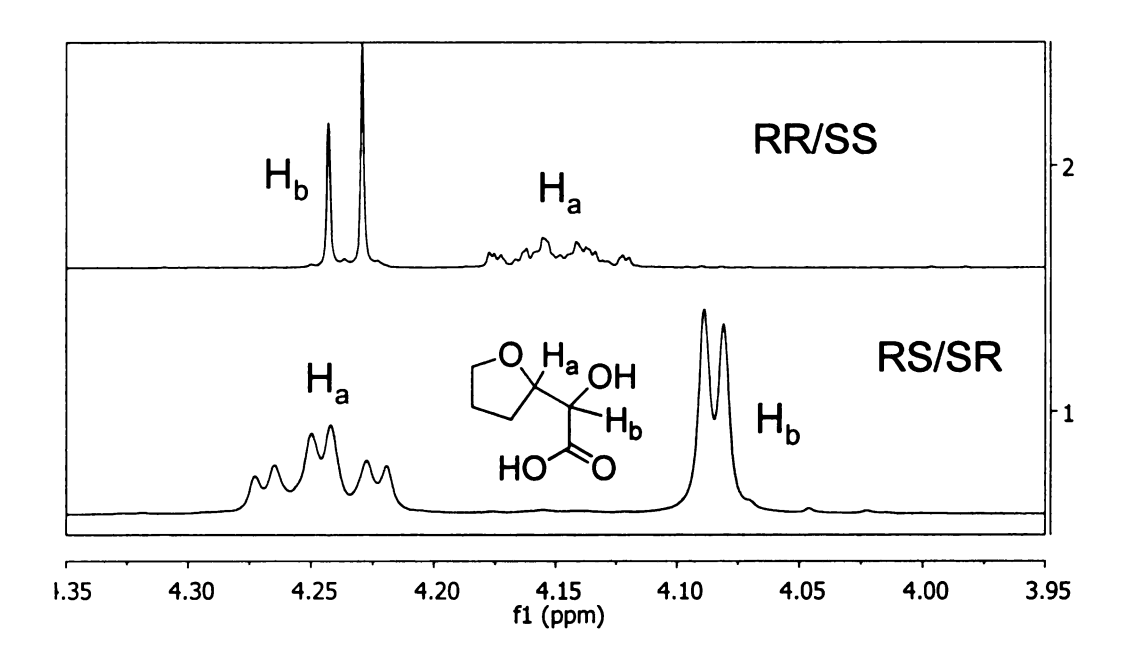


Figure 25. ¹H NMR spectra of RR/SS (top) and RS/SR (bottom) THFAHA

An examination of the crystal structures of the diastereomers explains the chemical shift difference for protons H_a and H_b . Dr. Erin Vogel obtained single crystal X-ray diffraction data and determined the stereochemistry of the diastereomers. In the RS/SR THFAHA structure (**Figure 26**), proton H_a is attached to C(5) and oriented toward O(1) of the THF ring, while proton H_b , attached to C(6), points down and away from O(1) of the THF ring. In RR/SS THFAHA (**Figure 27**), H_b is attached to C(6) and oriented toward O(1) in the THF ring while H_a , attached to C(5), points away from O(1) of the THF ring. As

observed in the ¹H NMR spectra of the various stereoisomers, protons oriented toward the O(1) of THF ring are shifted farther downfield (increased deshielding by oxygen) while protons oriented away from O(1) are less deshielded and their chemical shifts are upfield.

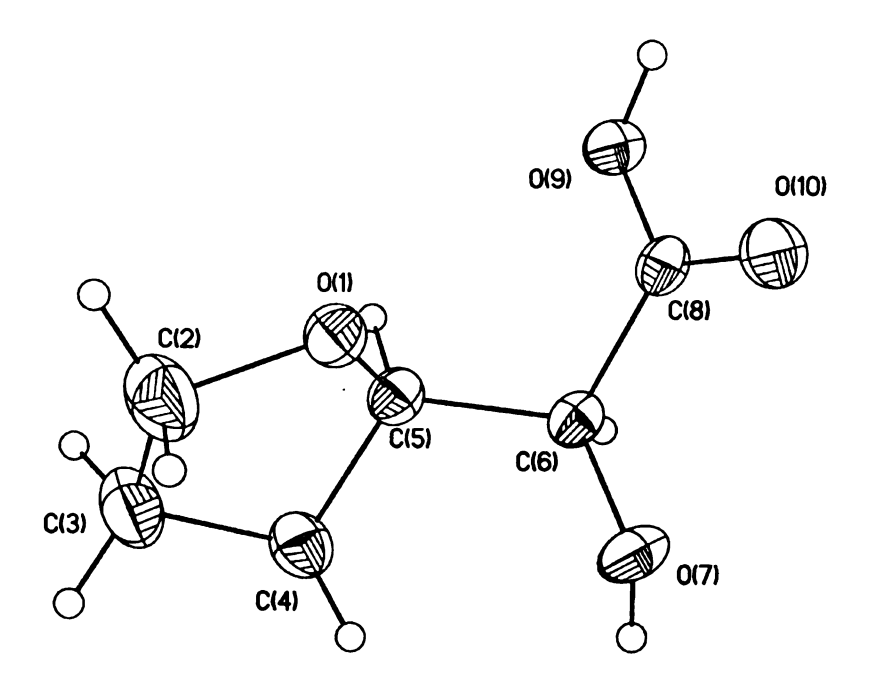


Figure 26. X-ray crystal structure of RS/SR THFAHA (provided by Erin Vogel)

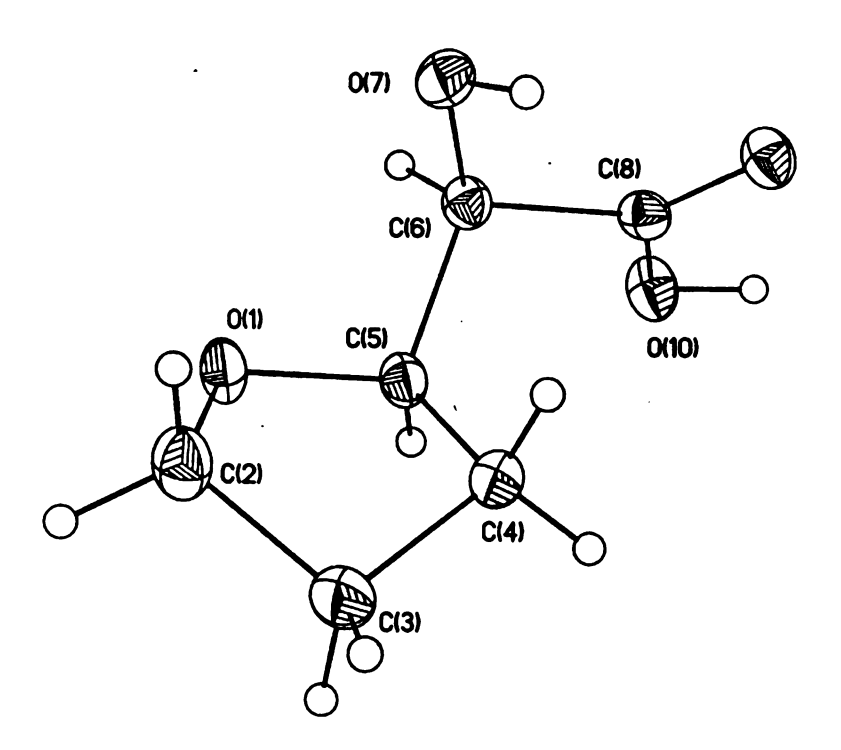


Figure 27. X-ray crystal structure of RR/SS THFAHA (provided by Erin Vogel)

After separating the α -hydroxyacid diastereomers, they were dimerized separately in refluxing toluene with p-TsOH as a catalyst. The reaction was driven to completion by azeotropic removal of water via a Dean-Stark trap (Scheme 13).²²

Scheme 13. Synthesis of di-tetrahydrofurfuryl glycolides

Dimerization of RS/SR acids provided ditetrahydrofurfuryl glycolide (THFglycolide) stereoisomers (*meso* and *rac*) in low yields, likely due to the harsh reaction conditions and the competing formation of low molecular weight oligomers. Recrystallization from acetone gave products enriched in the *meso* or *rac* isomers, but neither pure *meso* or *rac* products were obtained. These results

and the characterization data are summarized in the experimental section of this thesis. The stereochemistry of the separated monomers was not determined, but *rac*-glycolides usually have higher melting points than *meso*-glycolides. The higher melting monomer, denoted as M1, was a stereochemically pure racemic mixture of either RSSR/SRRS or RSRS and melted at 200-201°C. The lower melting monomer, M2, (mp 146-150°C) could not be fully purified by recrystallization, and ¹H NMR showed that it was contaminated with ~ 6% of the higher melting M1. For melt polymerizations, the monomers were combined to obtain a lower melting point. A ~2:1 mixture of RRRR/SSSS and RRSS (denoted as M3) melted at 144-154°C while a M1/M2 mixture melted at 145-147°C.

2.2 Synthesis of poly(THFglycolide)s

The polymerization of the monomers posed problems. Both THFglycolide mixtures, RRRR/SSSS RRSS and RSSR/SRRS RSRS, were insoluble in toluene, partially soluble in THF, and fully soluble in dichloromethane. Attempts to polymerize them in THF and dichloromethane, as solutions or slurries, resulted in no conversion to polymer. However, bulk polymerizations of both mixtures were successful at 160°C using different catalyst/ initiator systems (**Scheme 14**).

Polymerization of RRRR/SSSS RRSS THFglycolide (M3) proceeded nicely using the Sn(Oct)₂/BBA methodology, however, ¹H NMR showed that the conversion to polymer was only 80 % at 30 minutes. Longer reaction times may have provided higher conversions. The RSSR/SRRS RSRS THG glycolide M1 (mp 200-201 °C) was heated at an oil bath temperature of 215 °C for 30 minutes but failed to provide polymer. ¹H NMR analysis showed signs of degradation.

Mixtures of M1 and M2 (mp of M1/M2 was 145-147°C), were polymerized at 160 °C with the Sn(Oct)₂/BBA system several times, but reached only 10-15% conversion for reaction times up to 1.5 hrs. We speculated that the RSSR/SRRS RSRS THF-substituted glycolide might be more sterically demanding than its stereoisomeric counterpart, and therefore, we used DMAP as the catalyst since it is known to polymerize sterically hindered glycolides.¹⁵ With the DMAP/BBA system, conversions of monomer to polymer 97-100% were attained after 2.5 hrs at 160 °C.

Both polymers were light brown. Prior to precipitation, their polydispersities (PDIs) ranged from 1.47-2.15 (**Table 5**), and the number average molecular weights (M_n) were lower than predicted by the monomer to initiator ratios ([M]/[I]). The target degree of polymerization (DP) was 200 for all entries except for the last entry (([M]/[I] = 500). The highest DP achieved was 65, which suggests intramolecular chain transfer or a low molecular weight impurity, likely water, that acts as a competing initiator in the system.

RRRR/SSSS RRSS

RSSR/SRRS RSRS

Scheme 14. Synthesis of poly(THFglycolide)s

Table 5. Polymer data before precipitation with the polymerizations in bulk at 160°C with monomer to initiator ratios ([M]/[I]) of 200

sample	catalyst	rxn	0/ 0001/***	$M_{\rm n} \times 10^{-3}$	$M_{\rm w} \times 10^{-3}$	$M_{\rm w}/M_{\rm n}$	DP
Sample	Catalyst	time (min)	76 COTTV	(g/mol)	(g/mol)	W/W n	from M_n
poly(lactide)*	Sn(Oct) ₂	37	97	5.1	8.2	1.63	35
poly(M3)	Sn(Oct) ₂	30	75	16.8	25.9	1.54	65
poly(M3)	Sn(Oct) ₂	31	82	15.2	25.8	1.63	59
poly(M1M2)	DMAP	150	97	6.3	13.3	2.11	24
poly(M1M2)	DMAP	150	100	7.9	16.9	2.15	30
poly(M1M2)**	DMAP	361	97	3.4	5	1.47	13

^{*} Polymerization carried out at 130°C

After precipitation, the polymer molecular weights increased significantly but the PDIs improved only modestly. In contrast, the PDI of lactide improved from 1.63 to 1.13 after two precipitations (**Table 6**.). The increase in molecular

^{** [}M]/[I] = 500

^{***} Determined by ¹H NMR spectroscopy

weight was expected since the more soluble lower molecular weight species are preferentially removed during re-preciptation. Two poly(THFglycolide)s, poly(RRRR/SSSS RRSS THFglycolide) (poly(M3)) were precipitated twice to remove the catalyst and residual monomer (less than 1% by ¹H NMR) while poly(RSSR/SRRS RSRS THFglycolide) (poly(M1M2)) required one precipitation to remove all residual monomer and catalyst.

Table 6. Polymer data after precipitation with [M]/[I] = 200

sample	M _n x 10 ⁻³ (g/mol)	M _w x 10 ⁻³ (g/mol)	$M_{\rm w}/M_{\rm n}$	DP from M _n
poly(lactide)	22.0	24.8	1.13	152
poly(M3)	22.4	30.9	1.54	87
poly(M3)	22.5	32.6	1.63	87
poly(M1M2)	11.0	17.1	1.73	42
poly(M1M2)	7.8	11.9	1.51	30
poly(M1M2)*	20.2	25.4	1.25	78

^{* [}M]/[I] = 500

2.3 Physical properties of poly(THFglycolide)s

The poly(THFglycolide)s were characterized by thermal gravimetric analysis (TGA), differential scanning calorimetry (DSC), and contact angle measurements. The TGA data for poly(RRRR/SSSS, RRSS-THFglycolide), shown in **Figure 28**, show an onset for weight loss at ~250 °C followed by rapid degradation. Compared to data from alkyl lactides (**Figure 29**), the degradation profile has a plateau that persists to >500 °C. Decomposition of poly(RSSR/SRRS, RSRS-THFglycolide) shows a similar trend to its stereoisomer counterpart, but over a larger temperature range. Shoulders in TGA curves in other polymer systems are attributed to slow degradation of thermostable cross-linked products, formed by oxidative reactions at elevated temperatures.⁶⁸

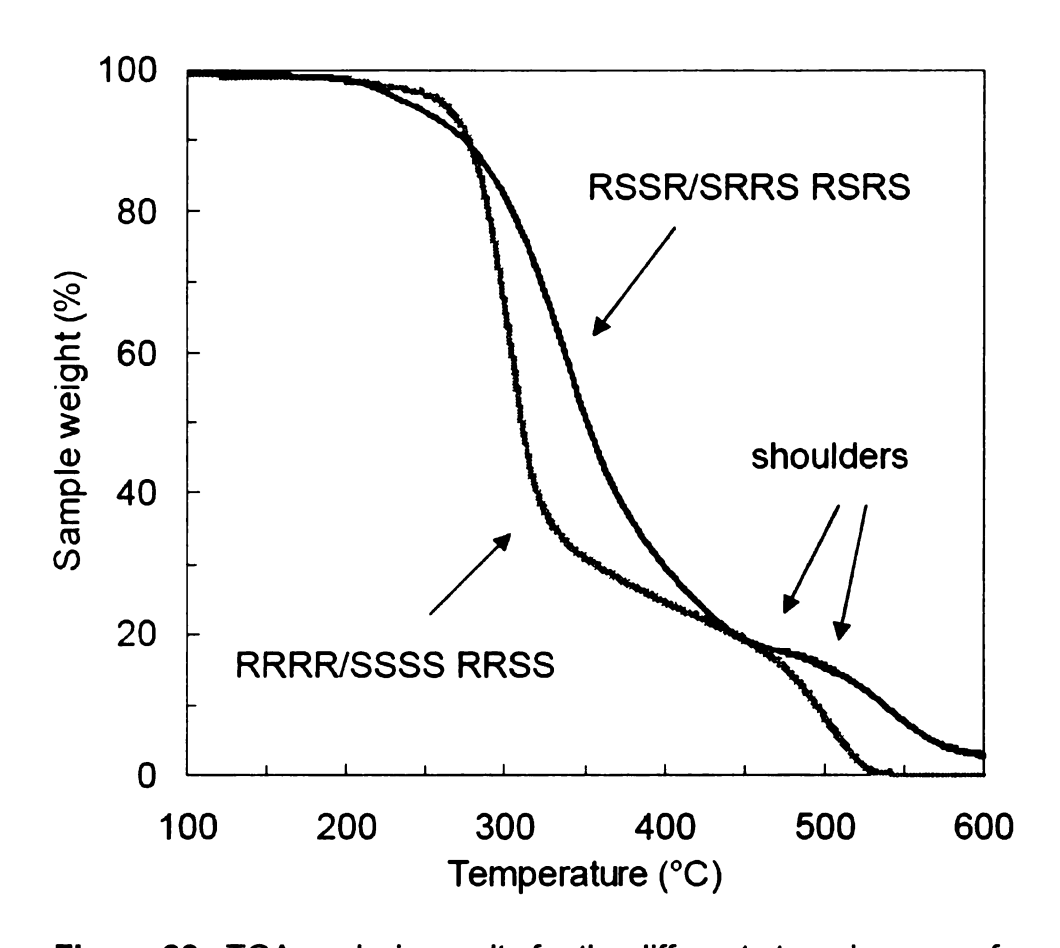


Figure 28. TGA analysis results for the different stereoisomers of poly(THFglycolide)s. Samples were run in air at a heating rate of 10 °C/min

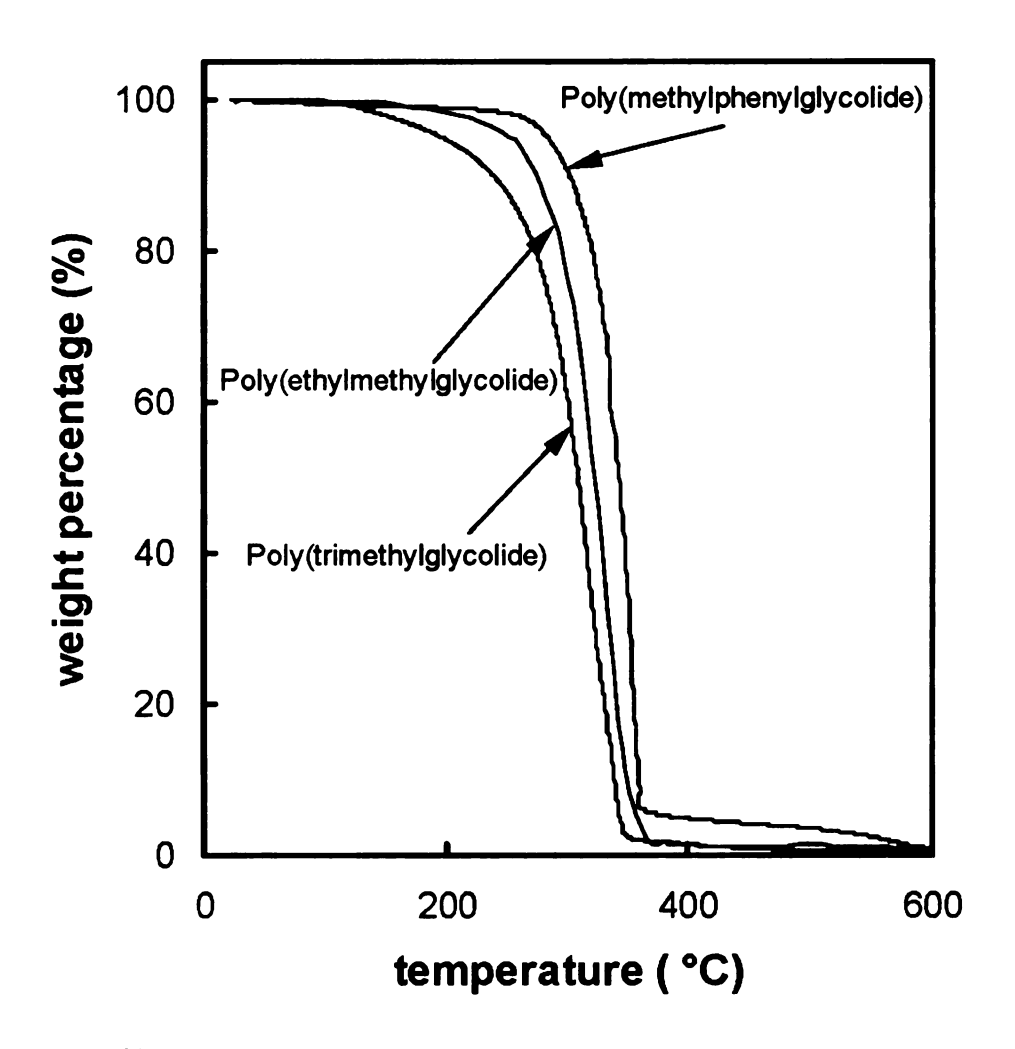


Figure 29.²¹ TGA analysis results for substituted poly(glycolide)s run in air.

Heating rate: 10 °C/min.

2.4 Glass transitions of poly(THFglycolide)s

The $T_{\rm g}$ s of the different poly(THFglycolide)s were determined by DSC and are summarized in **Table 7**. Interestingly, the $T_{\rm g}$ values for the different poly(THFglycolide) stereoisomers differ by 20 °C, suggesting that stereochemistry plays a role. As previously reported for amorphous poly(cyclohexylglycolide) systems (**Figure 30**), the stereochemistry of the main chain made little difference in the $T_{\rm g}$ of the polymers.²²

Table 7. T_g data for poly(THFglycolides)

sample	$M_{\rm n} \times 10^{-3}$ (g/mol)	M _w x 10 ⁻³ (g/mol)	<i>M</i> _w / <i>M</i> _n	T _g (°C)
poly(rac-lactide)	22.0	24.8	1.13	50
poly(M3)	22.5	32.6	1.63	64
poly(M1M2)	7.8	11.9	1.51	43
poly(M1M2)	20.2	25.4	1.25	44

poly(meso-dicyclohexylglycolide)

$$T_g = 96 \, ^{\circ}C$$

 $poly(rac\mbox{-dicylohexylglycolide}) \quad poly(R,R\mbox{-dicyclohexylglycolide}) \\ T_g = 98 \mbox{ °C} \qquad \qquad T_g = 104 \mbox{ °C}$

Figure 30. Stereoisomers of poly(dicyclohexylglycolide)s and their T_g s

Theoretical calculations performed on the poly(THFglycolide)s do not seem to support the experimental T_g data obtained. The maximum rotational barriers were calculated for the model system shown in (**Figure 31**). Methyl groups were used as "end caps" for the model system with the assumption they would contribute little or no interaction.

1234 = RRRR, RRSS, RSSR, RSRS

Figure 31. Model poly(THFglycolide) system used in computational study of rotational barriers with stereocenters 1, 2, 3, and 4 (*defines the bonds involved in the backbone rotation)

Table 8. Results from computational study performed on model poly(THF glycolide) systems in Figure 30

Stereocenters 1234	rotational barrier (kcal/mol)	
RRRR	~0	
RRSS	~0	
RSSR	~14	
RSRS	~13	

As shown in **Table 8** the rotational barrier for the RRRR and RRSS systems was approximately zero. These results are interesting, especially since the T_g of

poly(RRRR/SSSS, RRSS-THFglycolide) is ~20° higher than poly(RSSR/SRRS, RSRS-THFglycolide). The expectation was that the higher rotational barrier would correspond to the higher T_g , but the exact opposite was observed.

Li⁺ ions and T_q

An interesting experiment was performed in order to alter the T_g of the polymers. Since the pendant group of the new polyester is a THF ring and it is known Li $^+$ coordinates to the oxygen of the THF ring⁶⁹, Li $^+$ was added to the polymer to see if it would have any effect on T_g due to Li $^+$ coordination. The general procedure for the experiment was carried out as follows. Approximately 3-5 mg of polylactide (the control experiment) or poly(THFglycolide) was added to a sample vial flushed with N₂. The number of oxygen atoms in each sample (including ester oxygens) was calculated based on the mass of the sample. Then anhydrous LiCl in a 0.5 M THF solution was added in an inert N₂ atmosphere corresponding to the desired Li $^+$:O ratio desired for the sample. The THF was removed under vacuum and the DSC samples were prepared in air. The Li $^+$:O ratios used for this experiment were 1:1, 2:1, 3:1, and 4:1. The results are summarized in the following **Figures 32-35**.

As can be observed in **Figure 32**. The T_g of poly(rac-lactide) is not altered at all by the addition of Li⁺ as is the same case for poly(RRRR/SSSS, RRSS-THFglycolide) (**Figure 33**). However, the T_g of poly(RSSR/SRRS, RSRS-THFglycolide) does change after the addition of LiCl. The lower molecular weight species of M_n of ~7800 with a larger PDI 1.51 shows an increase of T_g with increasing Li⁺ concentration from ~43 °C to ~63 °C (**Figure 34**). The higher

molecular weight species with M_n of ~20,200 with a PDI of 1.25 shows the same increase in T_g from ~44 °C to ~64 °C (**Figure 35**). However, the higher molecular weight species does not show the gradual increase in T_g with increasing concentration of Li⁺. Instead, the T_g increases directly to the higher temperature with a 1:1 ratio of Li⁺ to oxygen. This may be a result of the increased number of chain ends in the lower molecular weight polymer with a higher PDI. The polymer is not fully saturated with Li⁺ at lower ratios while the higher molecular weight polymer is. As to the question why one stereochemical system coordinates to Li⁺ and the other doesn't; we speculate it may be due to the formation of pockets Li⁺ can fit into between the THF ring oxygens and the carbonyls of the ester backbone in one system versus the other.

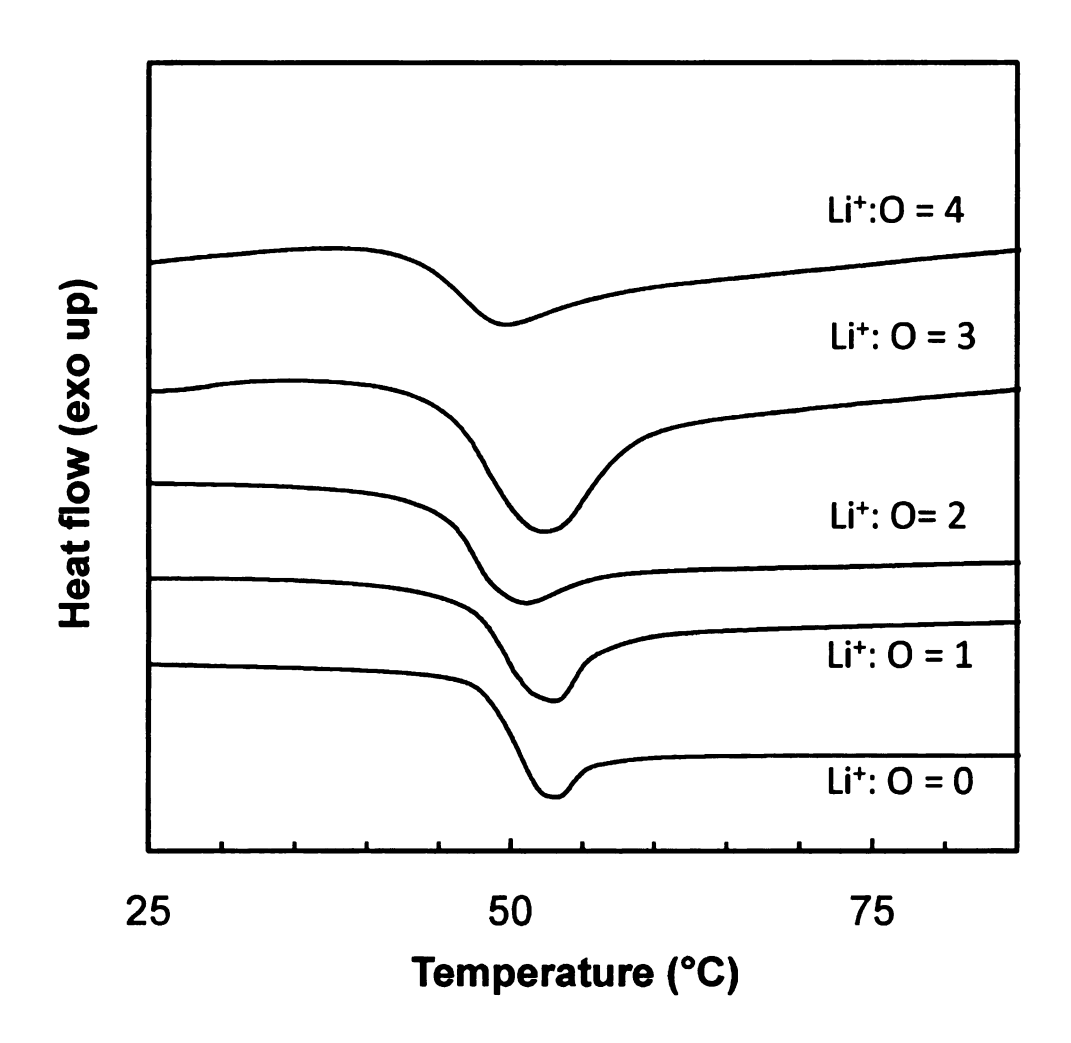


Figure 32. DSC analysis of poly(*rac*-lactide) with varying Lithium ion concentrations. Heating rate: 10 °C/min under nitrogen. The data are from the second heating scan.

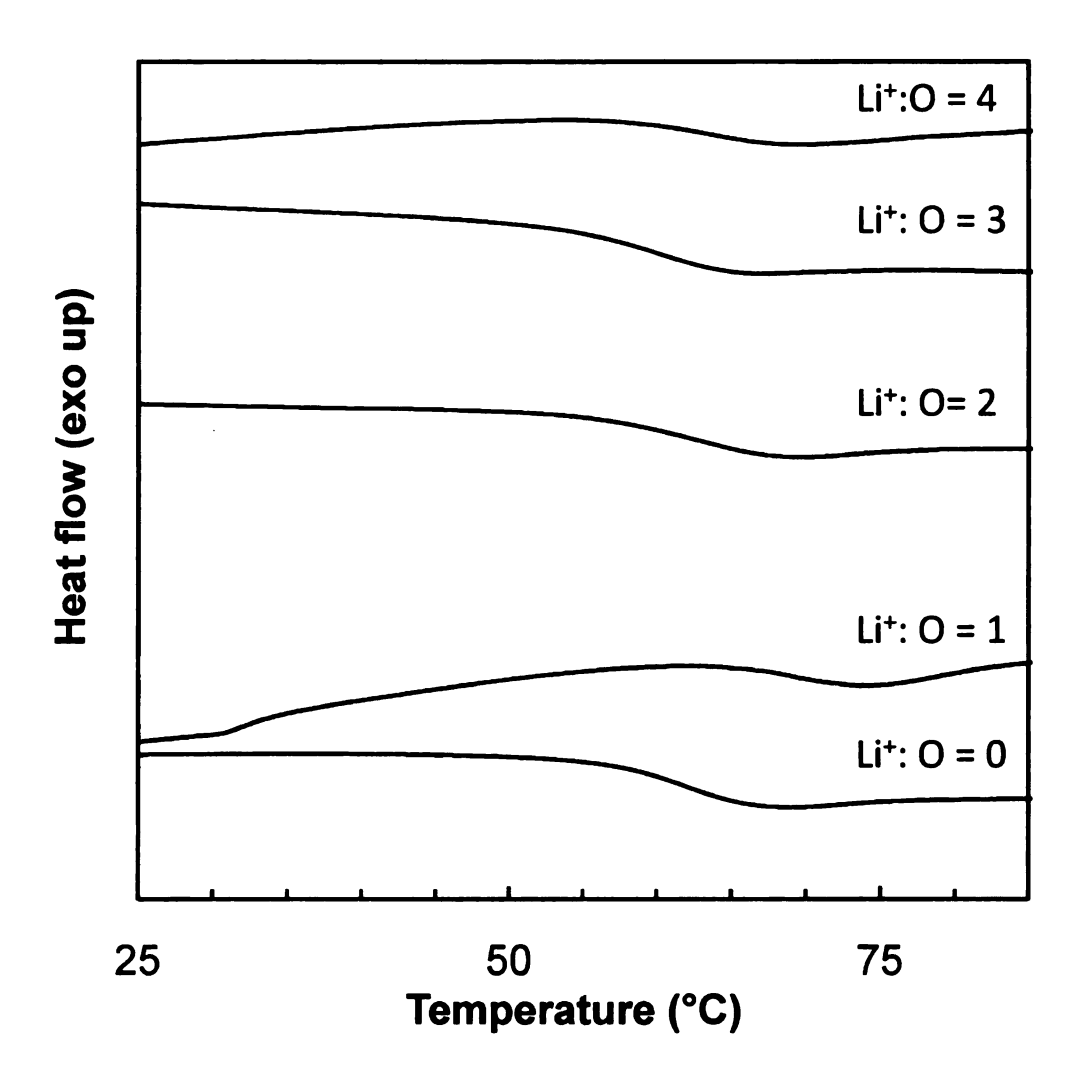


Figure 33. DSC analysis of poly(RRRR/SSSS, RRSS-THFglycolide) (M3) with varying Lithium ion concentrations. Heating rate: 10 °C/min under nitrogen. The data are from the second heating scan.

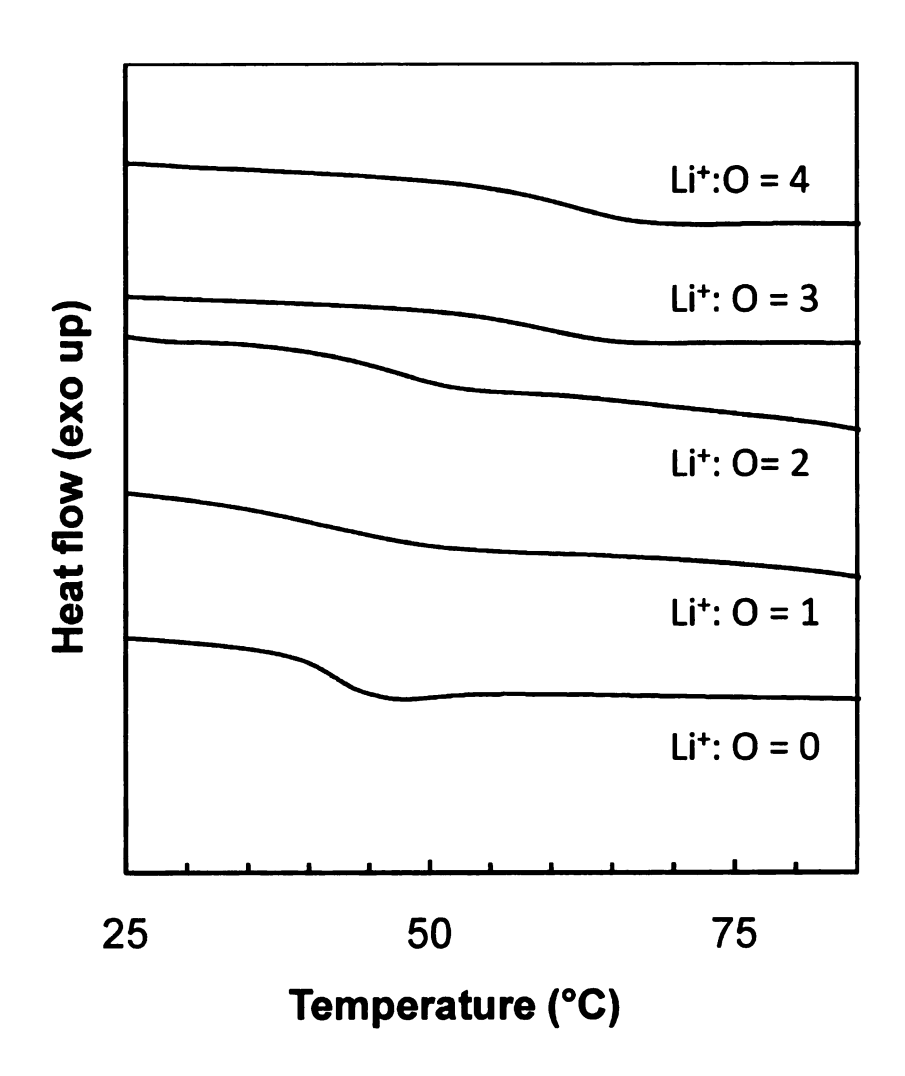


Figure 34. DSC analysis of poly(RSSR/SRRS, RSRS-THFglycolide) (M1M2) with varying Lithium ion concentrations ($M_n \approx 7800$). Heating rate: 10 °C/min under nitrogen. The data are from the second heating scan.

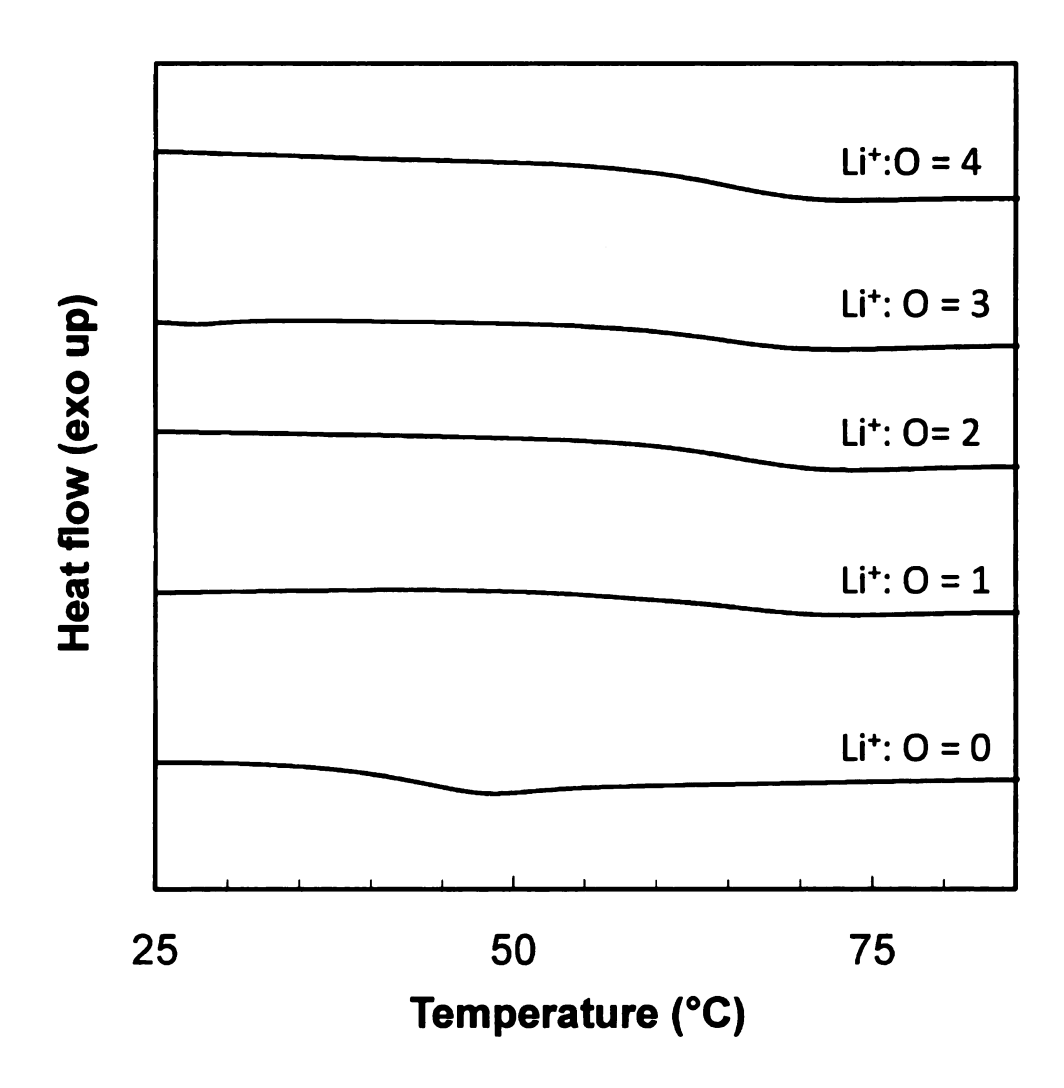


Figure 35. DSC analysis of poly(RSSR/SRRS,RSRS-THFglycolide) (M1M2) with varying Lithium ion concentrations ($M_n \approx 20200$). Heating rate: 10 °C/min under nitrogen. The data are from the second heating scan.

Contact angle measurements were also taken for the different poly(THFglycolide)s and the results are summarized in **Table 9**. As indicated by the contact angles attained both poly(THFglycolide)s are slightly hydrophobic with more hydrophilic character than polylactide.

Table 9. Contact angle measurements for poly(THFglycolides) and polylactide where θ_{adv} - θ_{rec} is the contact angle hysteresis

sample	$\theta_{ ext{static}}$	$ heta_{ ext{advancing}}$	$\theta_{ m receding}$	θ_{adv} - θ_{rec}
poly(rac -lactide)	82	98	74	24
poly(M3)	68	85	53	32
poly(M1M2)	67	86	49	37

Chapter 3

Experimental

3.1 General details

Unless otherwise specified, ACS reagent grade intermediates and solvents were used as received from commercial suppliers without further purification. EtOH was dried by refluxing with Mg⁰ and CCl₄. House nitrogen was used in air and moisture sensitive reactions.

¹H NMR (300 or 500 MHz) and ¹³C NMR (75 or 125 MHz) spectra were acquired using either a Varian Gemini 300 spectrometer or a Varian UnityPlus 500 spectrometer, with the residual proton signal from the CDCl₃ solvent used as the chemical shift standard. IR spectra were taken with a Mattson Galaxy 3000 FT-IR. Elemental analyses were determined using a Perkin-Elmer 2400 CHNS/O Analyzer, and mass spectral analyses were carried out on a VG Masslab Trio-1. Melting points were taken on an Electrothermal capillary melting point apparatus and are uncorrected.

Polymer molecular weights were determined by gel permeation chromatography (GPC) at 35 °C using two PLgel 10 μ mixed-B columns in series (manufacturer-stated linear molecular weight range of 500-10×10⁶ g/mol). The eluting solvent was THF at a flow rate of 1 mL/min, and the concentration of polymer solutions used for GPC was 1 mg/mL. GPC data were obtained using GPC-MALLS (Multi-Angle Laser Light Scattering) at 35 °C using THF as the eluting solvent at a flow rate of 1 mL/min. An Optilab rEX (Wyatt Technology

Co.) and a DAWN EOS 18-angle light scattering detector (Wyatt Technology Co.) with a laser wavelength of 684 nm were used to calculate absolute molecular weights. Differential Scanning Calorimetry (DSC) analyses of polymers were obtained using a TA DSC Q100. Samples were run under a nitrogen atmosphere at a heating rate of 10 °C/min, with the temperature calibrated with an indium standard.

Contact angle measurements were taken by making polymer solutions containing 1-5 wt % of the desired polymer.dissolved in toluene and filtered through Whatman 0.2 µm PTFE filters. The samples were then spin-coated onto silicon wafers and the advancing, static, and receding contact angles were measured using dionized water and reported as an average of 5 measurements.

3.2 Material synthesis

Synthesis of 2-(furan-2-yl)-2-hydroxyacetonitrile. Danger: This preparation generates copious amounts of HCN. All manipulations must be carried out in a fume hood. A 3L, 3 neck flask was charged with 500 mL of de-ionized water and 452 g of KCN. The mixture was stirred for 30 minutes at 0 °C, and then freshly distilled furfural (100 mL, 115.9 g, 1.207 mol) was added drop-wise to the solution over a period of 10 minutes. After the furfural addition was complete, saturated NaHSO₃ (375 mL) and 400 mL of ice-cold water were quickly added, and the mixture was stirred for 15 minutes. Then, 700 mL of concentrated HCl (12.1 M) was added slowly added to the solution. (This step generates copious amounts of HCNI) The solution was extracted with ether (6X600 mL), washed with saturated brine solution (600 mL) and dried overnight

with Na₂SO₄. Gravity filtration and removal of the solvent by rotary evaporation gave a dark brown oil (70.55 g). ¹H NMR analysis showed that the oil was a mixture of the desired furfural cyanohydrin (68.33 g, 0.5554 mol, 46%) and the starting aldehyde (2.22 g.) ¹H NMR (CDCl₃): δ (ppm) 7.41 (s, 1H), 6.5 (dd, ¹J = 3.3 Hz, ²J = 0.9 Hz 1H), 6.35 (dd, ¹J = 2.1 Hz, ²J = 1.8 Hz, 1H), 5.5 (s, 1H), 3.5-4.5 (br s, 1H). ¹³C NMR (CDCl₃): δ (ppm) 147.3, 144.2, 116.9, 110.8, 110.0, 56.7. (Lit.⁷⁰ ¹H NMR: (CDCl₃, 300 MHz): δ (ppm) 7.47 (d, J = 1.9 Hz, 1H), 6.58 (d, J = 3.4 Hz, 1H), 6.41 (d, J = 1.8 Hz, J = 3.4 Hz, 1H), 5.53 (s, 1H), 4.25 (br s, 1H)).

Synthesis of ethyl 2-(furan-2-yl)-2-hydroxyacetate. This procedure was adapted from Boatright and Degering. Dry EtOH (750 mL) was charged into a 3 L, 3 neck flask protected with nitrogen, stirred and cooled to 0 °C. Over 30 minutes, HCl gas, produced by slowly dripping concentrated H₂SO₄ (500 mL, 18 M) over 452 g of NaCl, was bubbled into the EtOH. Then, over 30 minutes, a solution of the furfural cyanohydrin (68.33 g, 0.5554 mol) in 250 mL of dry EtOH was added dropwise to the stirred EtOH/HCl mixture. After the addition of the furfural cyanohydrin was complete, stirring was discontinued, and HCl_(g) was bubbled through the solution for an additional 3.5 hours at 0 °C. The reaction vessel was transferred to a refrigerator at 4 °C. After 4 days, the flask was removed from the refrigerator, and warmed to room temperature. De-ionized water (500 mL) was added to the mixture, and after stirring for 10 minutes, the solution was extracted with ether (5 X 750 mL, and then washed with de-ionized water (3 X 400 mL) until the pH was neutral. The ether was dried with Na₂SO₄

overnight. Gravity filtration and removal of the solvent by rotary evaporation gave the crude product as a dark brown liquid which eventually solidified (72.19 g, 0.4246 mol, 76.46%). Sublimation of the dark brown solid (50 °C, 20 mtorr) over a period of three days gave the desired product as white powdery crystals (55.29 g, 0.3252 mol, 58.56%). 1 H NMR (CDCl₃): δ (ppm) 7.38 (s, 1H), 6.32-6.37 (m, 2H), 5.14-5.18 (d, J = 5.5 Hz, 1H), 4.20-4.33 (m, J = 3.6 Hz, 2H), 3.31-3.35 (d, J = 5.5 Hz, 1H), 1.22-1.29 (t, J = 7.2 Hz, 3H). 13 C NMR (CDCl₃): δ (ppm) 171.5, 150.9, 144.0, 110.5, 106.7, 66.9, 62.6, 14.1. Anal. Cald. for C₈H₁₀O₄: C 56.47; H, 5.92 Found: C, 56.46; H, 5.84. MS (EI) m/z 170, 97 (100), 69. mp 40-41 °C (Lit. 66 mp 39 °C). (Lit. 71 H NMR data: (CDCl₃) δ (ppm), 7.40 (m, 1 H) 6.35 (m, 2 H), 5.20 (s, H), 4.25 (q, J = 7 Hz, 2 H), 3.55 (s, OH, 1 H), 1.20 (t, J = 7 Hz, 3 H))

Synthesis of 2-(furan-2-yl)-2-hydroxyacetic acid. This procedure is adapted from Boatright and Degering.⁶⁶ A 3L 3-neck flask protected with nitrogen was cooled to 0 °C and charged with 2-(furan-2-yl)-2-hydroxyacetate (55.29 g, 0.3252 mol). 2.5 M NaOH (800 mL) was added to the flask, and after the mixture was stirred for 1 hour at 0 °C, the ice bath was removed and the stirred reaction was allowed warm to room temperature over a period of 2 hours. Concentrated HCl (250 mL, 12.1 M) was added to adjust the pH to ~1-2, and then the resulting solution was extracted with EtOAc (4 X 600 mL). After drying the combined EtOAc layers overnight with Na₂SO₄, gravity filtration and removal of the solvent by rotary evaporation gave the desired hydroxyacid as light brown crystals (41.64 g, 0.2932 mol, 90.17%). ¹H NMR (acetone-d₆): δ (ppm) 7.52-7.53 (dd, J = 0.9

Hz 1H), 6.41-6.44 (m, 2H), 5.24 (s, 1H). ¹³C NMR (D₆-acetone): δ (ppm) 171.5, 152.5, 142.6, 110.4, 106.0, 66.5. Anal Calcd. for C₆H₆O₄: C, 50.71; H, 4.26. Found: C, 50.40, H, 4.19. mp 109-111 °C (Lit. mp 108-111 °C⁷², 115 °C⁶⁶). (Lit. NMR data⁷²: ¹H NMR (acetone-d₆): δ (ppm) 7.60 (d, J = 0.8, 1H), 7.50 (d, J = 1.8, 1H), 6.40 (dd, J = 1.8 and 0.8, 1H), 5.25 (s, 1H); ¹³C NMR (acetone-d₆): δ (ppm) 172.6, 153.5, 143.6, 111.4, 109.0, 67.6)

Synthesis of 2-hydroxy-2-(tetrahydrofuran-2-yl) acetic acid. A Parr hydrogenation bomb was charged with a solution 2-(furan-2-yl)-2-hydroxyacetic acid (41.64 g, 0.2932 mol) in 250 mL of anhydrous EtOH, and 1.0 g of 5% Rh on Al₂O₃ (Engelhard Lot # C003081). The bomb was pressurized to 1500 psi H₂ and the reaction stirred for 48 hours. The reaction was monitored by ¹H NMR and when the reaction was complete, the bomb was opened and the reaction mixture was filtered through Celite to remove the catalyst. Removal of the solvent by rotary evaporation gave the desired acid as a light brown solid (35.64 g, 0.2441 mol, 83.25%). Crystallization of the product in a minimal amount of EtOAc provided the R,R/S,S product as white crystals (5.06 g, 0.0347 mol, 23.6%) and R,S/S,R as white crystals (5.30 g, 0.0363 mol, 24.8%) (stereochemistry determined by x-ray crystallography)

R,R/S,S: ¹H NMR (acetone-d₆): δ (ppm) 4.20-4.23 (d, J=4.2 Hz, 1H), 4.09-4.15 (m, 1H), 3.77-3.86 (m, 1H), 3.63-3.72 (m, 1H), 1.76-1.97 (m, 4H). ¹³C NMR (D₆-acetone): δ (ppm) 173.5, 80.5, 73.0, 69.0, 26.3, 26.3. IR (NaCl): v (cm⁻¹) 3710-3068, 2983, 2967, 2900, 2696-2466, 1737, 1218, 1137, 1062. Anal. Calcd. for

 $C_6H_{10}O_4$: C, 49.32; H, 6.90. Found: C, 49.37; H, 6.83. MS (EI) m/z 147.1 (0.11), 128 (0.97), 110.0 (4.86), 101.0 (8.63). mp = 76-77 °C.

R,S/S,R: ¹H NMR (acetone-d₆): δ (ppm) 4.18-4.27 (dt, ¹J = 6.9 Hz, ²J = 2.4 Hz, 1H), 4.03-4.09 (d, J = 2.4 Hz, 1H), 3.75-3.84 (m, 1H), 3.61-3.69 (m, 1H), 1.75-2.08 (m, 4H). ¹³C NMR (acetone-d₆): δ (ppm) 174.0, 80.0, 72.3, 69.2, 22.7, 22.6. IR (NaCl): v (cm⁻¹) 3430, 3397, 2971, 2967, 2935, 2661-2495, 1735, 1215, 1137, 1049. Anal. Calcd. for C₆H₁₀O₄: C, 49.32; H, 6.90. Found: C, 49.38; H, 7.10. MS (EI) m/z 128.1 (0.57), 111.0 (2.65), 110.0 (1.28), 101.1 (24.49). mp = 126.5 – 127.5 °C (Lit.⁶⁷ mp 129 °C).

Synthesis of RSSR/SRRS/RSRS 3,6-bis(tetrahydrofuran-2-yl)-1,4-dioxane-2,5-dione. A 2 L, 2 neck flask protected with N₂ and equipped with a Dean-Stark trap and a jacketed water condenser was charged with R,S/S,R-2-hydroxy-2-(tetrahydrofuran-2-yl)-acetic acid (5.30 g, 0.0363 mol), *p*-TsOH (0.340 g, 1.79 mmol), and 900 mL of toluene. The flask was heated to the reflux temperature, and the reaction was monitored by ¹H NMR. When the oligomeric by-products became noticeable (~5 days), the reaction solution was filtered while hot and then the toluene was removed by rotary evaporation. The resulting solid was dissolved in CH₂Cl₂ and washed with aqueous saturated sodium bicarbonate (3 x 200 mL) followed by saturated brine solution (1 x 200 mL). After drying over Na₂SO₄ and gravity filtration, the solvent was removed by rotary evaporation. Two recrystallizations of the crude product from acetone gave colorless crystals of 3,6-bis(tetrahydrofuran-2-yl)-1,4-dioxane-2,5-dione (1.36 g, 531 mmol, 29.2%) as a statistical mixture of the RSSR/SRRS and RSRS isomers. The monomers

were purified and almost completely separated by crystallization from acetone. The stereochemistry was not determined for the mixtures of monomers. The monomers were labeled M1 and M2. Monomer M1 was isolated in its pure state as flake like colorless crystals. Characterization for M1: ¹H NMR (CDCl₃): δ (ppm) 4.84-4.88 (d, J=3.6 Hz, 1H), 4.48-4.56 (dt, ${}^{1}J=6.9$ Hz, ${}^{2}J=2.4$ Hz, 1H), 3.77-3.91 (m. 2H), 1.82-2.16 (m. 4H), 13 C NMR (CDCl₃); δ (ppm) 164.6, 78.5. 78.3, 69.2, 27.8, 26.0. IR (NaCl): v (cm⁻¹) 2992, 2875, 1766, 1232. Anal. calcd. for C₁₂H₁₆O₆: C, 56.18; H, 6.29. Found C, 56.23; H, 6.00. MS (EI) m/z 256.1 (0.12), 238.1 (0.14), 186.1 (1.79), 128 (3.55). mp 200-201 °C. Characterization for M2: ¹H NMR (CDCl₃): δ (ppm) 4.94-4.97 (d, J=3.0 Hz, 1H), 4.47-4.54 (dt, ^{1}J =9.0, ^{2}J = 3.0, 1H), 3.73-3.89 (m, 2H), 1.81-2.14 (m, 4H). ^{13}C NMR (CDCl₃): δ (ppm) 165.1, 79.1, 77.9, 69.8, 27.1, 26.1. IR (NaCl): v (cm⁻¹) 2989, 2964, 2877. 1754, 1378, 1275, 1058. Anal. calcd. for C₁₂H₁₆O₆: C, 56.18; H, 6.29. Found C, 56.39; H, 6.54. MS (EI) m/z 256.0 (0.03), 238.1 (0.02), 186.1 (0.96), 156.0 (0.23), 129.0 (0.85). mp 146-150 °C.

Synthesis of RRRR/SSSS/RRSS 3,6-bis(tetrahydrofuran-2-yl)-1,4-dioxane-2,5-dione. A 2 L, 2 neck flask, protected with N_2 and equipped with a Dean Stark trap and a jacked water condenser, was charged with R,R/S,S-2-hydroxy-2-(tetrahydrofuran-2-yl)acetic acid (5.06 g, 363 mmol) and p-TsOH (0.340 g, 1.79 mmol) and 900 mL of toluene. The reaction was heat to reflux and the reaction was monitored by 1 H NMR. When the oligomeric by-products became noticeable (~5 days), the reaction solution was filtered while hot and then the toluene was removed by rotary evaporation. The resulting solid was dissolved in CH_2Cl_2 and

washed with saturated aqueous sodium bicarbonate (3 x 200 mL) followed by saturated brine solution (1x200 mL). After drying over Na₂SO₄, and gravity filtration, the solvent was removed by rotary evaporation. Crystallization of the product twice from acetone gave 1.81 g (70.7 mmol, 40.8%) of a statistical mixture of RSSR/SRRS and RSRS stereoisomers of 3,6-bis(tetrahydrofuran-2-yl)-1,4-dioxane-2,5-dione as colorless crystals. ¹H NMR (CDCl₃): δ (ppm) 5.17-5.21 (d, J=3.0 Hz, 1H), 5.04-5.08 (d, J=3.0 Hz, 1H), 4.52-4.59 (dt, 1J =3.0 Hz, 2J =6.0 Hz, 1H), 4.40-4.57 (dt, 1J =3.0 Hz, 2J =6.0 Hz, 1H), 3.73-3.99 (m, 4H), 1.80-2.20 (m, 8H). ¹³C NMR (CDCl₃): δ (ppm) 164.4, 164.2, 79.5, 78.7, 77.0, 76.9, 69.4, 69.4, 26.7, 26.20, 26.0, 25.7. IR (NaCl): v (cm⁻¹) 2971, 2935, 2875, 1751, 1253, 1068. Anal. calcd. for C₁₂H₁₆O₆: C, 56.18; H, 6.29. Found C, 56.54; H, 6.55. MS (EI) m/z 256.3, 213, 186.1, 149.0, 128.0. mp 144-154 °C

Bulk Polymerization of Substituted Glycolides. Solvent-free polymerizations were carried out in sealed ampoules prepared from 3/8 in. diameter glass tubing. Ampoules were charged with monomer and a stir bar and connected via a Cajon fitting to a T-shaped vacuum adapter fitted with a stopcock and an air-free Teflon valve. A septum was attached to the outlet of the stopcock, and the apparatus was connected to a vacuum line and evacuated through the Teflon valve. After 2 h, the ampoule was backfilled with nitrogen, and a syringe was used to add predetermined amounts of Sn-(2-ethylhexanoate)₂ or DMAP solutions, and 4-tert-butylbenzyl alcohol solutions to the ampoules through the stopcock. The solvent was removed *in vacuo* and the ampoule was flame-sealed and immersed in an oil bath. At the end of the polymerization, the ampoule was cooled, opened, and

the polymer was dissolved in CH₂Cl₂. A portion of the solution was evacuated to dryness and analyzed by NMR for conversion. The remaining polymer solution was precipitated 1-2 times into cold methanol until residual monomer and catalysts were removed.

Appendix

Instrument Frequency			Chemical Shift (ppm)	Signal	Int.	J (Hz)	
Temperature	25 °C		7.41	S	H H		
Nucleus		τ	6.50	pp	Ŧ	$^{1}J=3.3, ^{2}J=0.9$	6.0=
Solvent	CDCl ₃	5 —	6.35	pp	Ŧ	$^{1}J=2.1,^{2}J$	-1 .8
			5.50	တ	Ŧ		
			3.50-4.50	br,s	Ŧ		
	æ			[©] I			
		q o		a O e	z		
				، م			
*	¥	*	Φ				
	my r						
-	-		-		-	}	-
9.5 9.0	8.5 8.0 7.5 7.0	6.5 6.0 5.5	5.0 4.5 4.0 3.5 ppm	5 3.0 2.5	2.0	1.5 1.0	0.5

Figure A-1. ¹H NMR spectrum of 2-(furan-2-yl)-2-hydroxyacetonitrile (*furfural starting material, other peaks are oligomeric "junk")

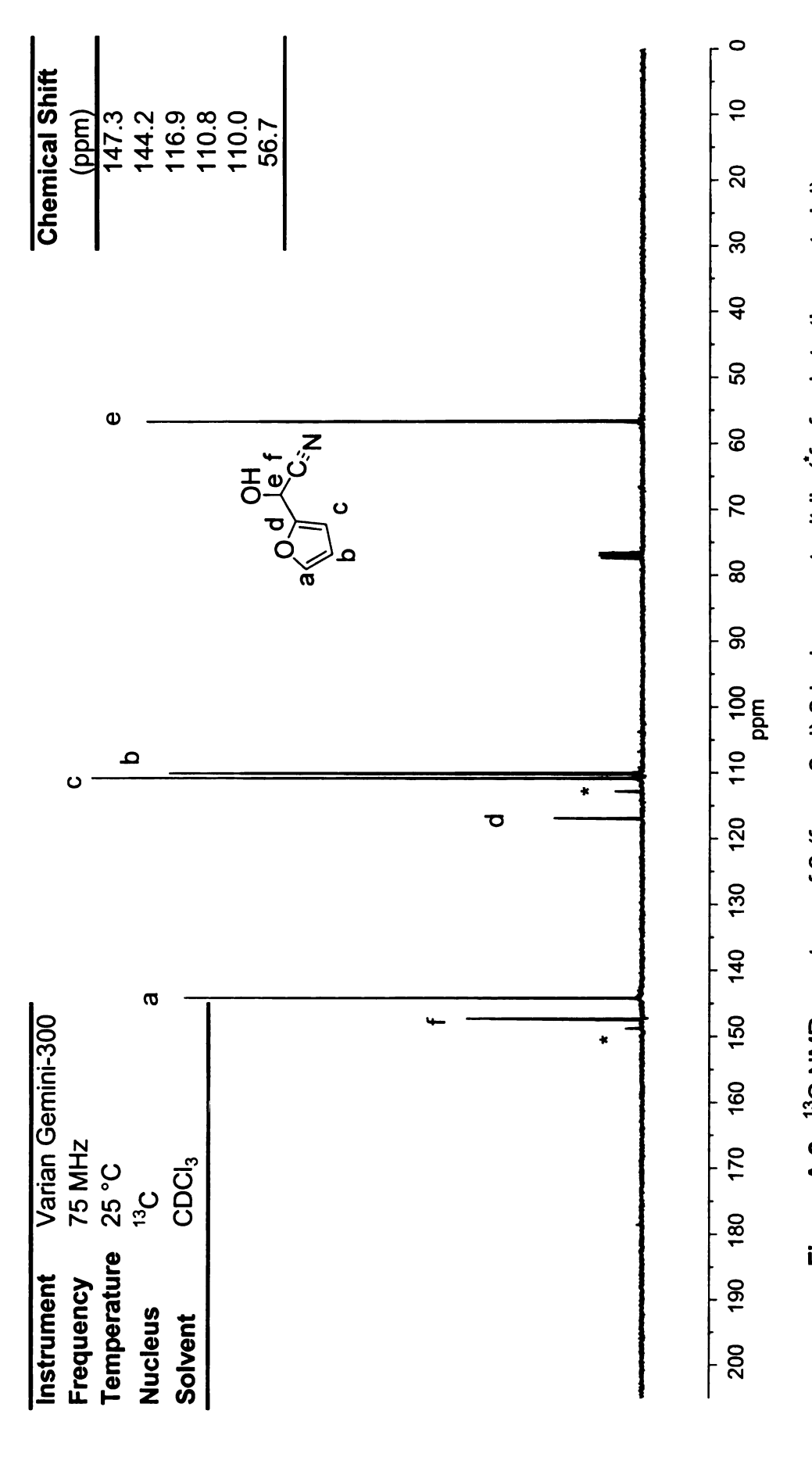


Figure A-2. ¹³C NMR spectrum of 2-(furan-2-yl)-2-hydroxyacetonitrile (furfural starting material)

Chemical Shift Signal Int. J (Hz) g	S	٤	d 1H	4.28^* m $^1J_{HH} = 12, ^3J_{HH} = 7.2$	m H	1.25 t 3H 7.2
Instrument Varian Gemini-300 C	<u> </u>	T, sielsik		Solvent CDC13		!

Figure A-3. ¹H NMR spectrum of ethyl 2-(furan-2-yl)-2-hydroxyacetate (* diastereotopic methylene chemical shifts and coupling constants determined by gNMR simulation)

0.5

2.0

3.0

3.5

4.5

5.0 ppm

6.0

6.5

7.5

8.0

9.0

9.5

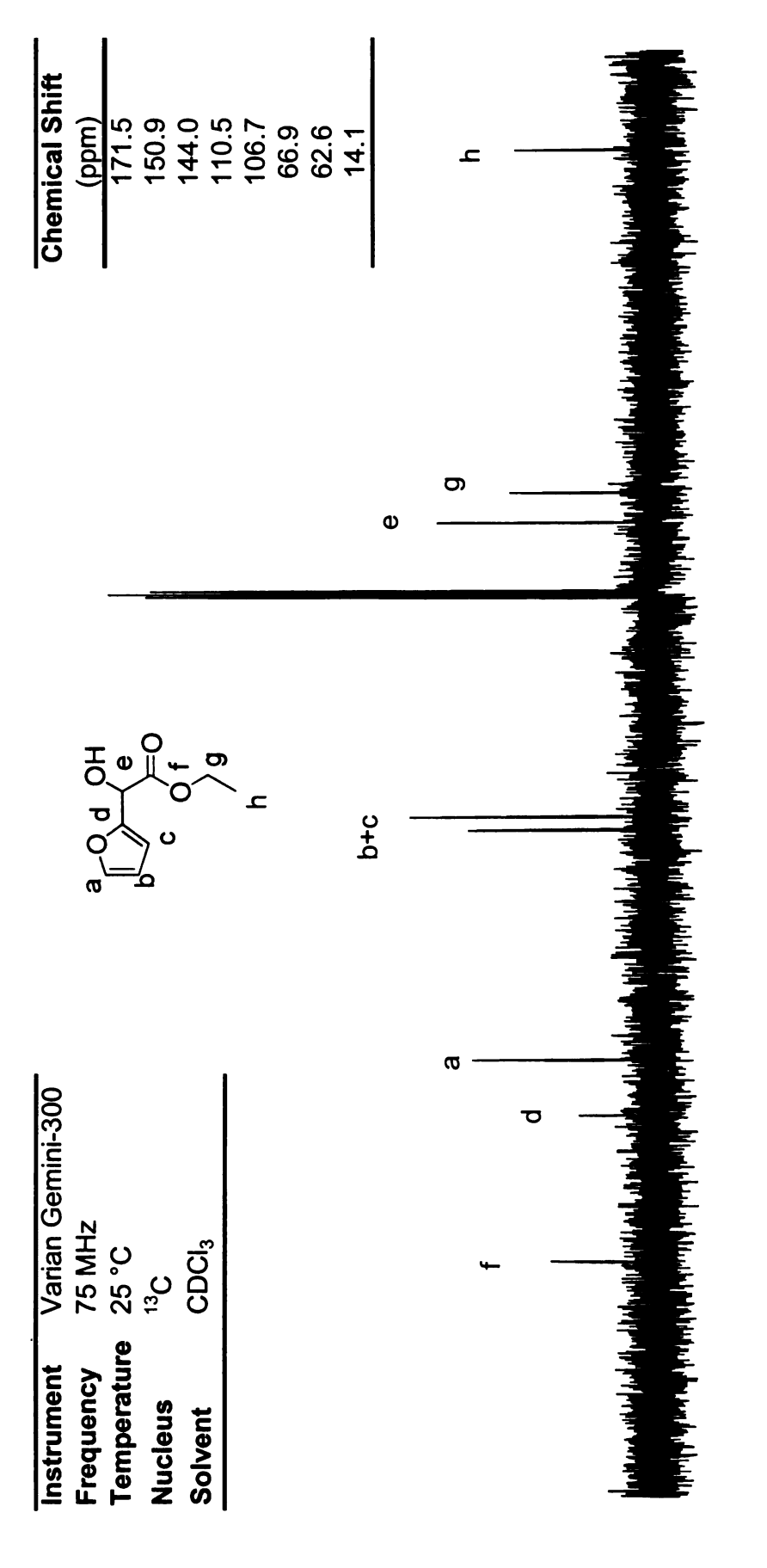


Figure A-4. ¹³C NMR spectrum of ethyl 2-(furan-2-yl)-2-hydroxyacetate

110 100 ppm

200 190

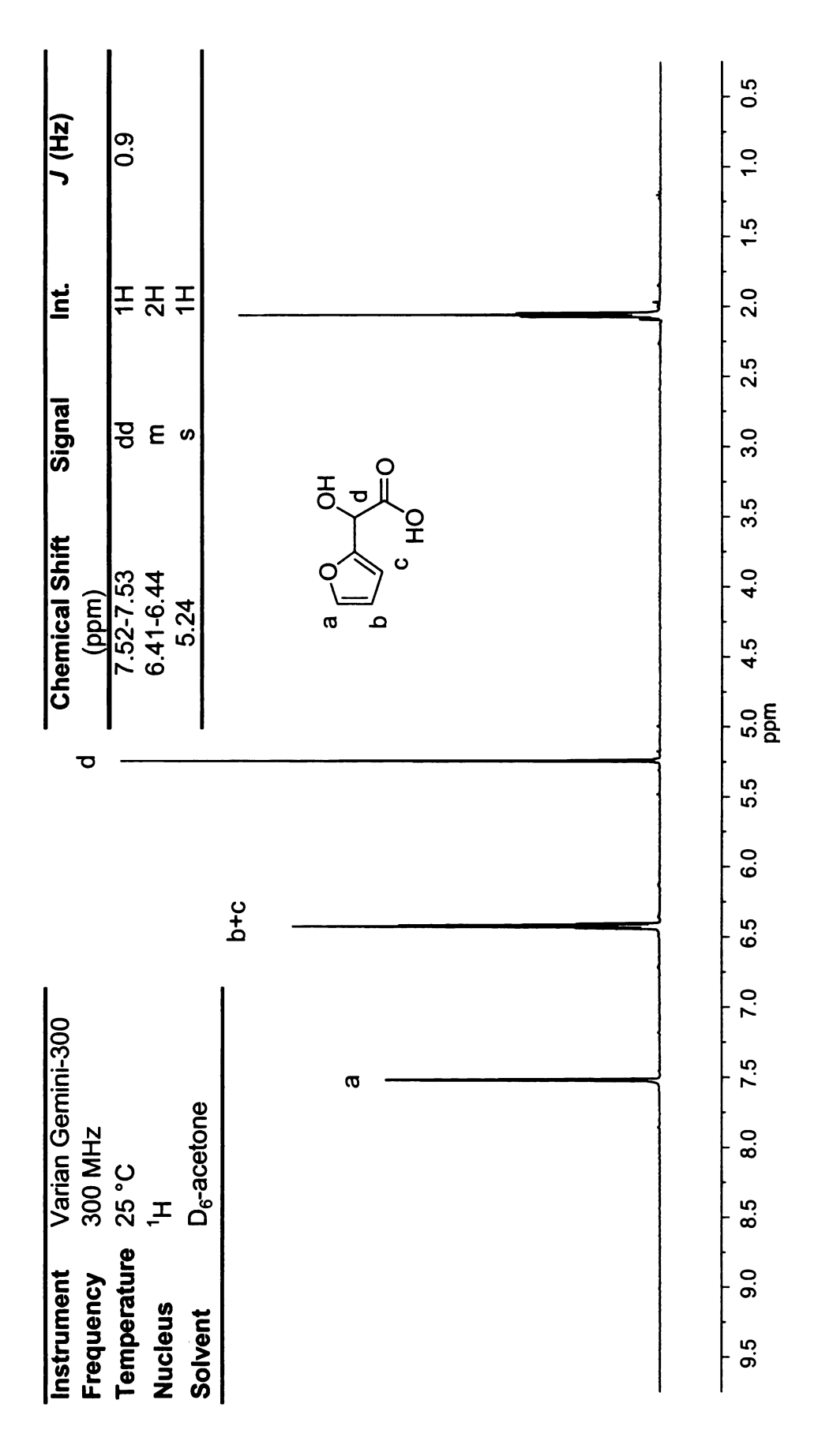


Figure A-5. ¹H NMR spectrum of 2-(furan-2-yl)-2-hydroxyacetic acid

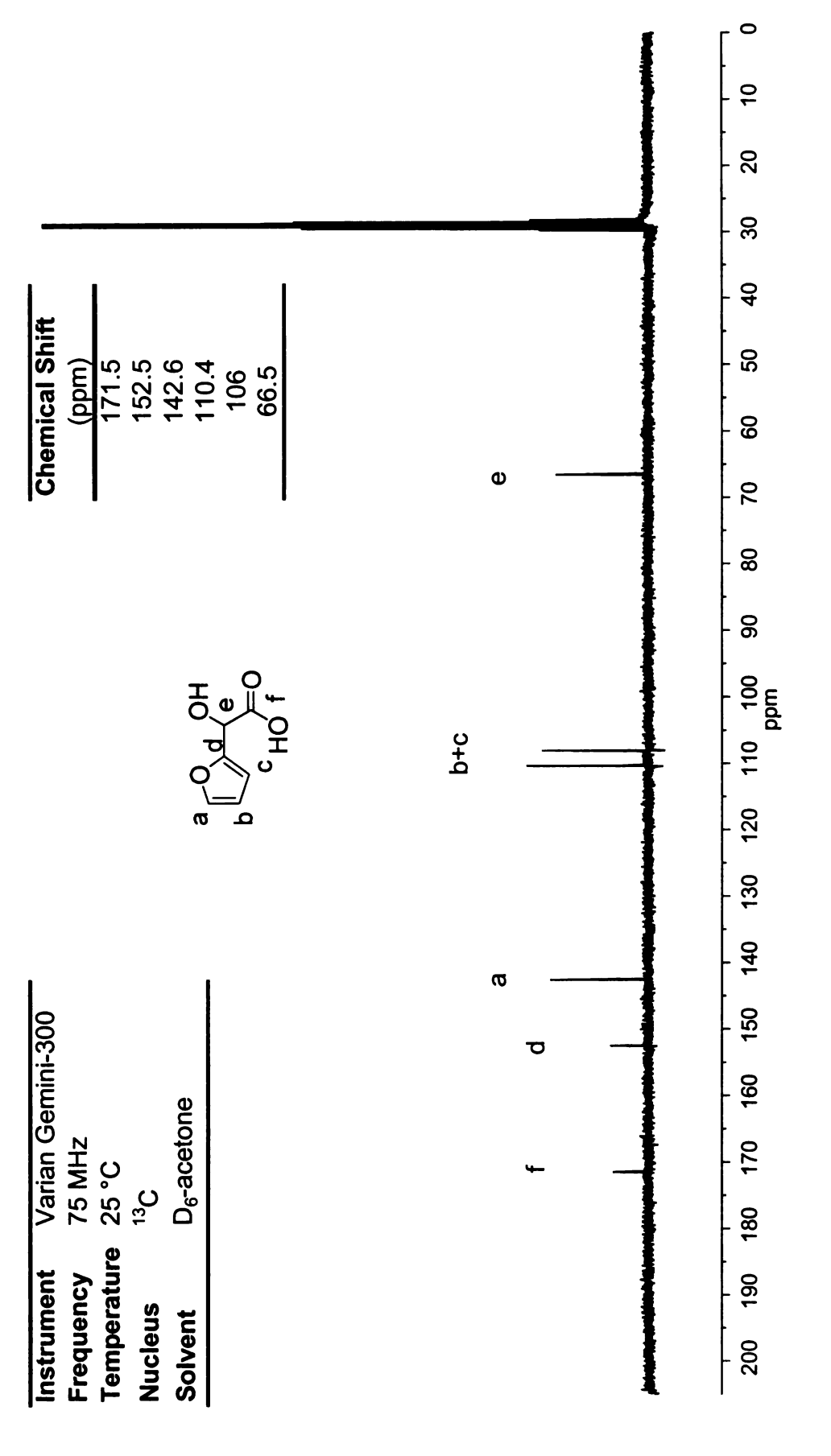


Figure A-6. ¹³C NMR spectrum of 2-(furan-2-yl)-2-hydroxyacetic acid

-

R,S/S,	a Od OH		5+q	,						*	
Φ -			<u>m</u>	-							
			J (Hz)		$^{1}J=6.9,^{2}J=2.4$	2.4					
Varian Gemini-300 300 MHz	25°C 'H	D ₆ -acetone	Signal Int.		dt 1H	d H	m H	m H	m 4H		
	Temperature		Chemical Shift	(mdd)	4.18-4.27	4.03-4.09	3.75-3.84	3.61-3.69	1.75-2.08		

Figure A-7. ¹H NMR spectrum of R,S/S,R-2-hydroxy-2-(tetrahydrofuran-2-yl)-acetic acid (* residual solvent ethyl acetate) 2.0 1.5 1.0 0.5 2.5 3.0 4.5 4.0 3.5 5.0 ppm 5.5 0.9 6.5 7.0 7.5 8.0 8.5 9.5

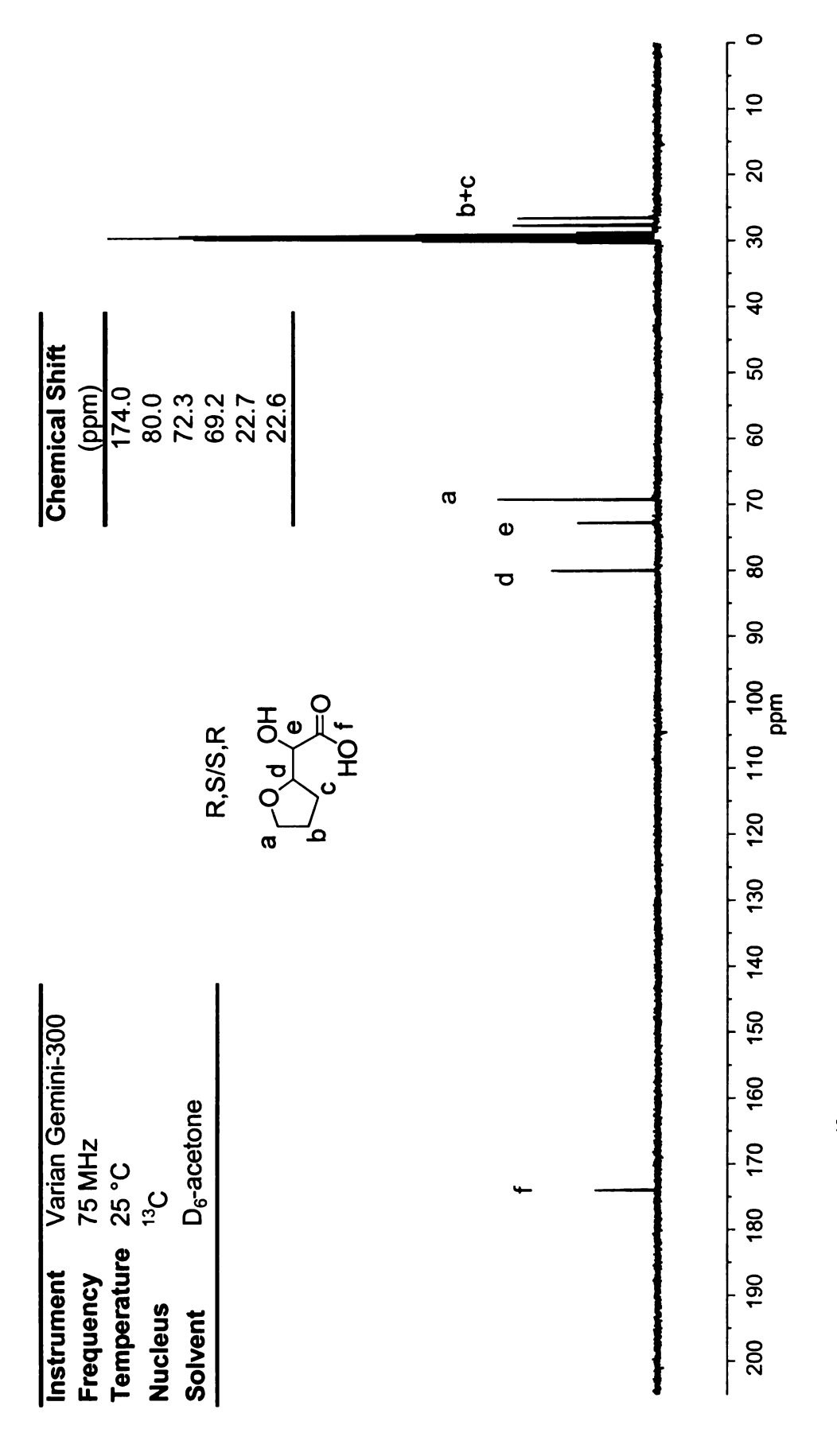


Figure A-8. ¹³C NMR spectrum spectrum of R,S/S,R-2-hydroxy-2-(tetrahydrofuran-2-yl)-acetic acid

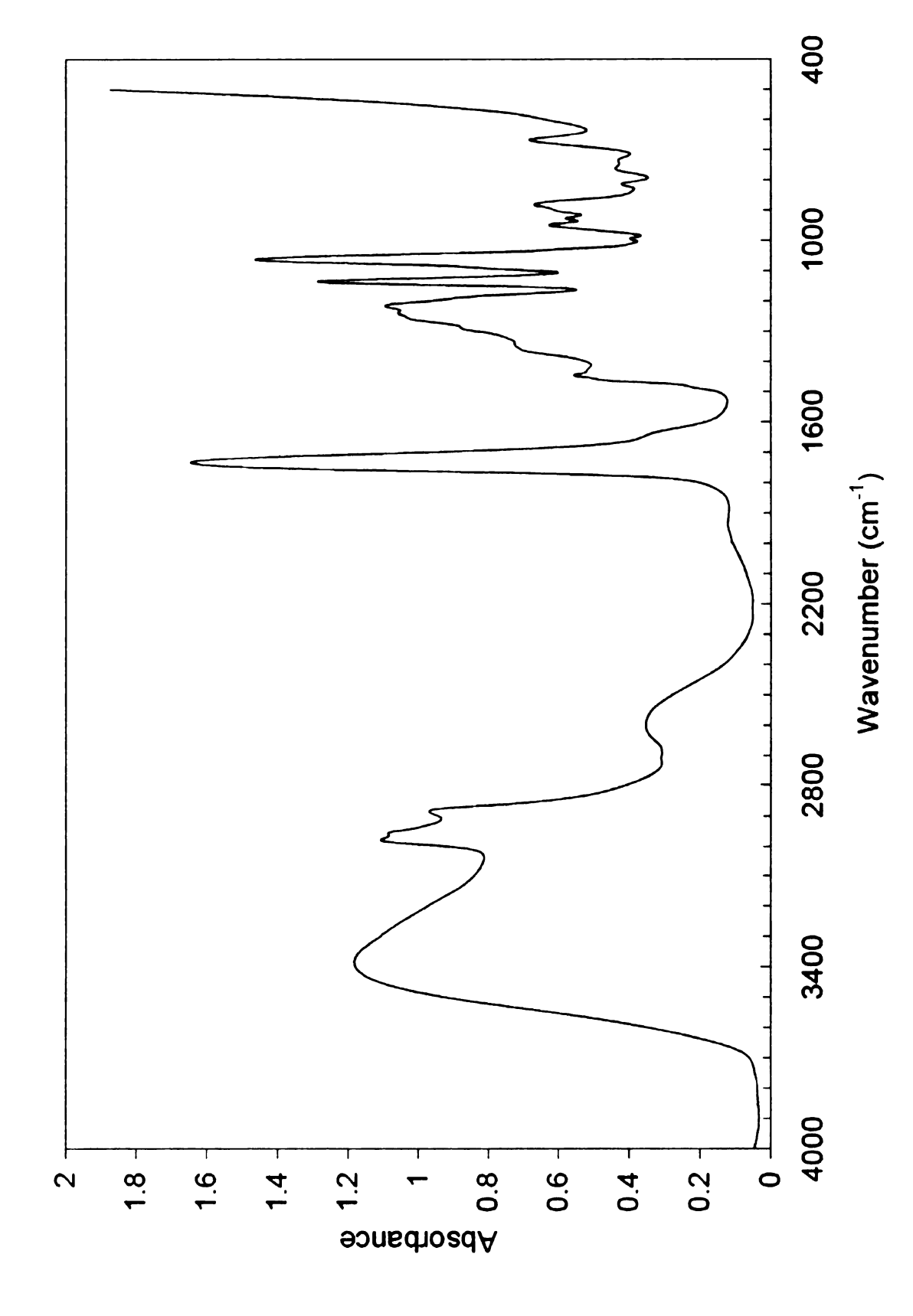


Figure A-9. IR spectrum R, S/S, R-2-hydroxy-2-(tetrahydrofuran-2-yl)-acetic acid

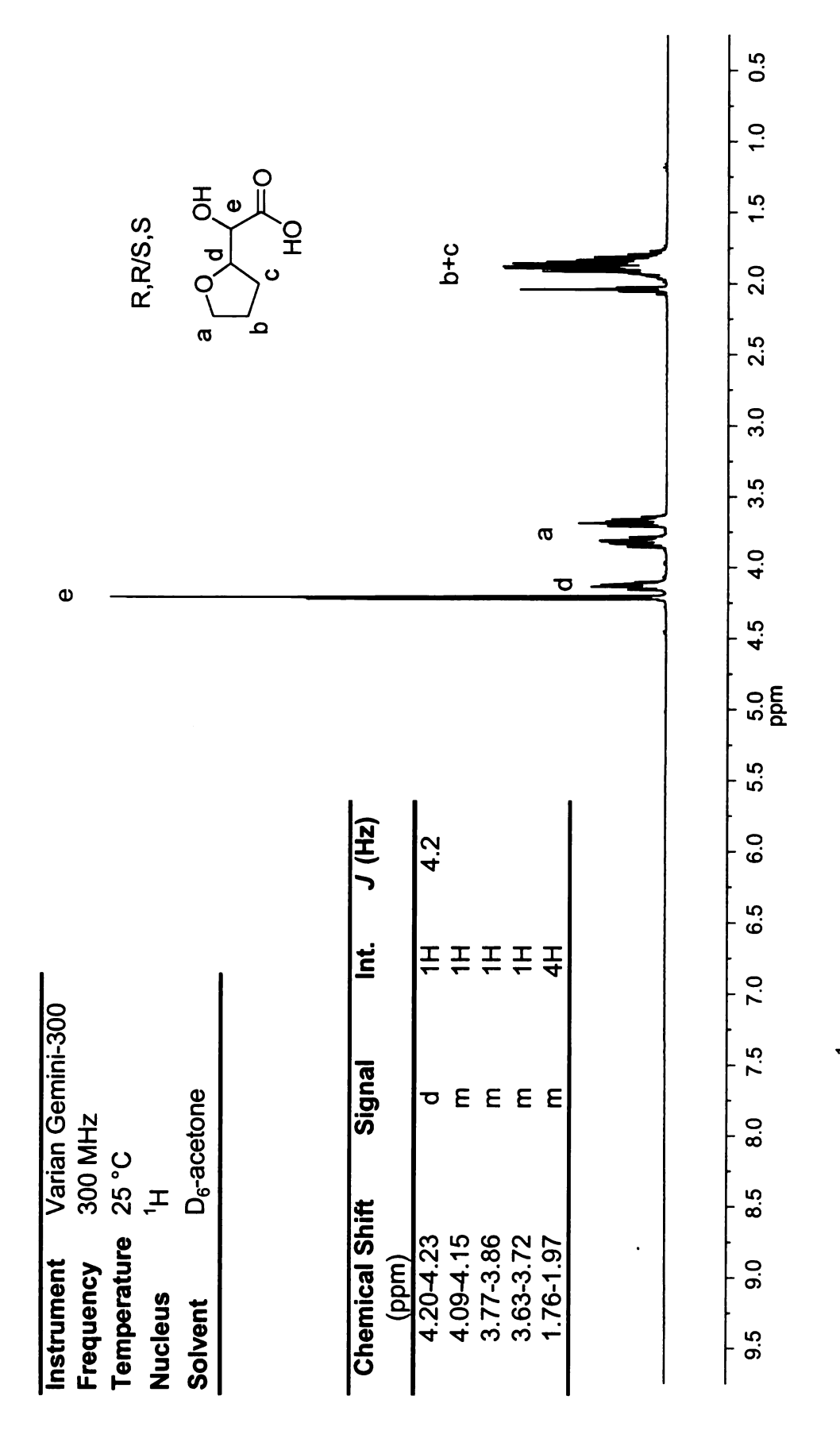


Figure A-10. ¹H NMR spectrum of R,R/S,S-2-hydroxy-2-(tetrahydrofuran-2-yl)-acetic acid

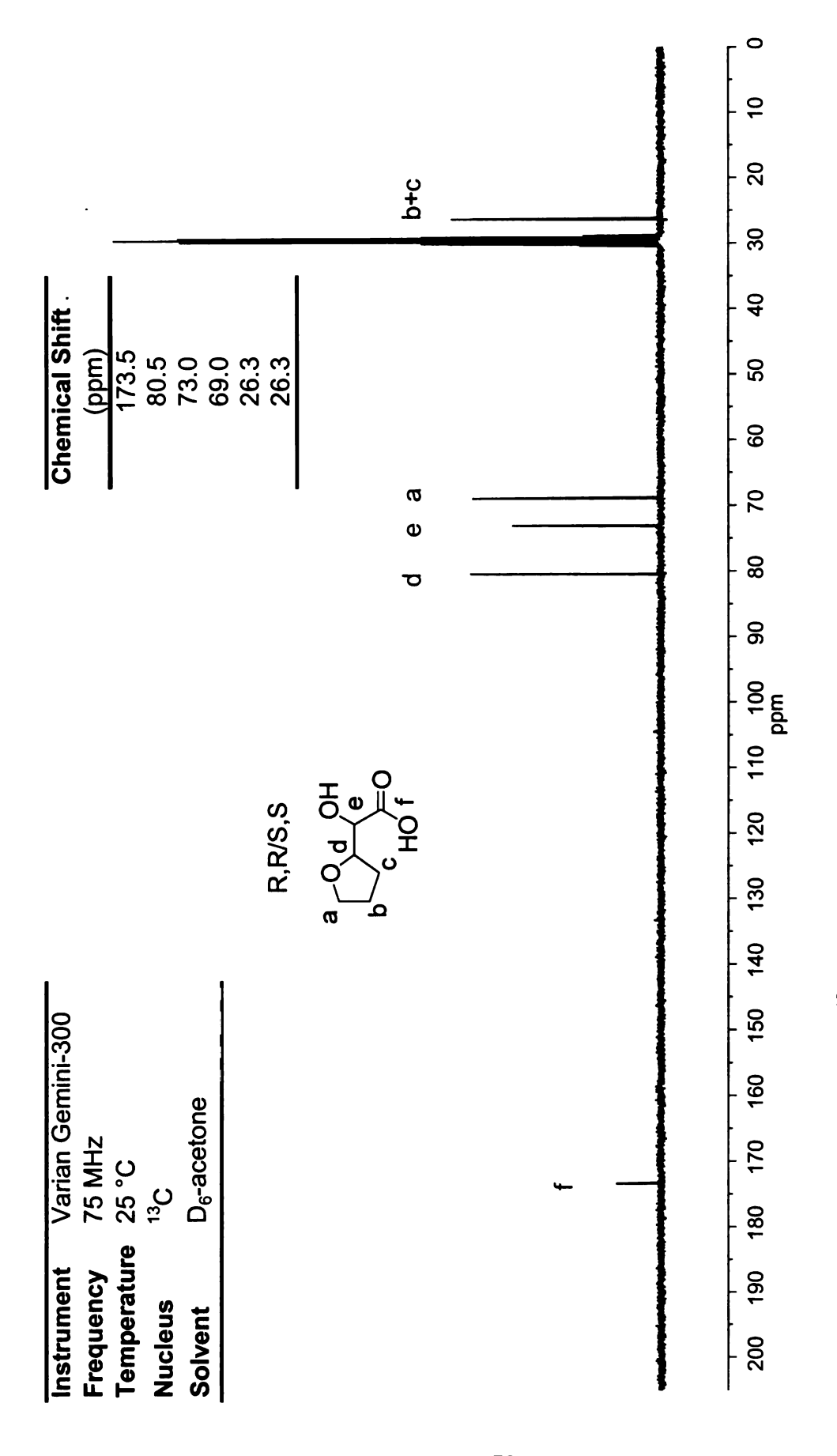


Figure A-11. ¹³C NMR of R,R/S,S-2-hydroxy-2-(tetrahydrofuran-2-yl)-acetic acid

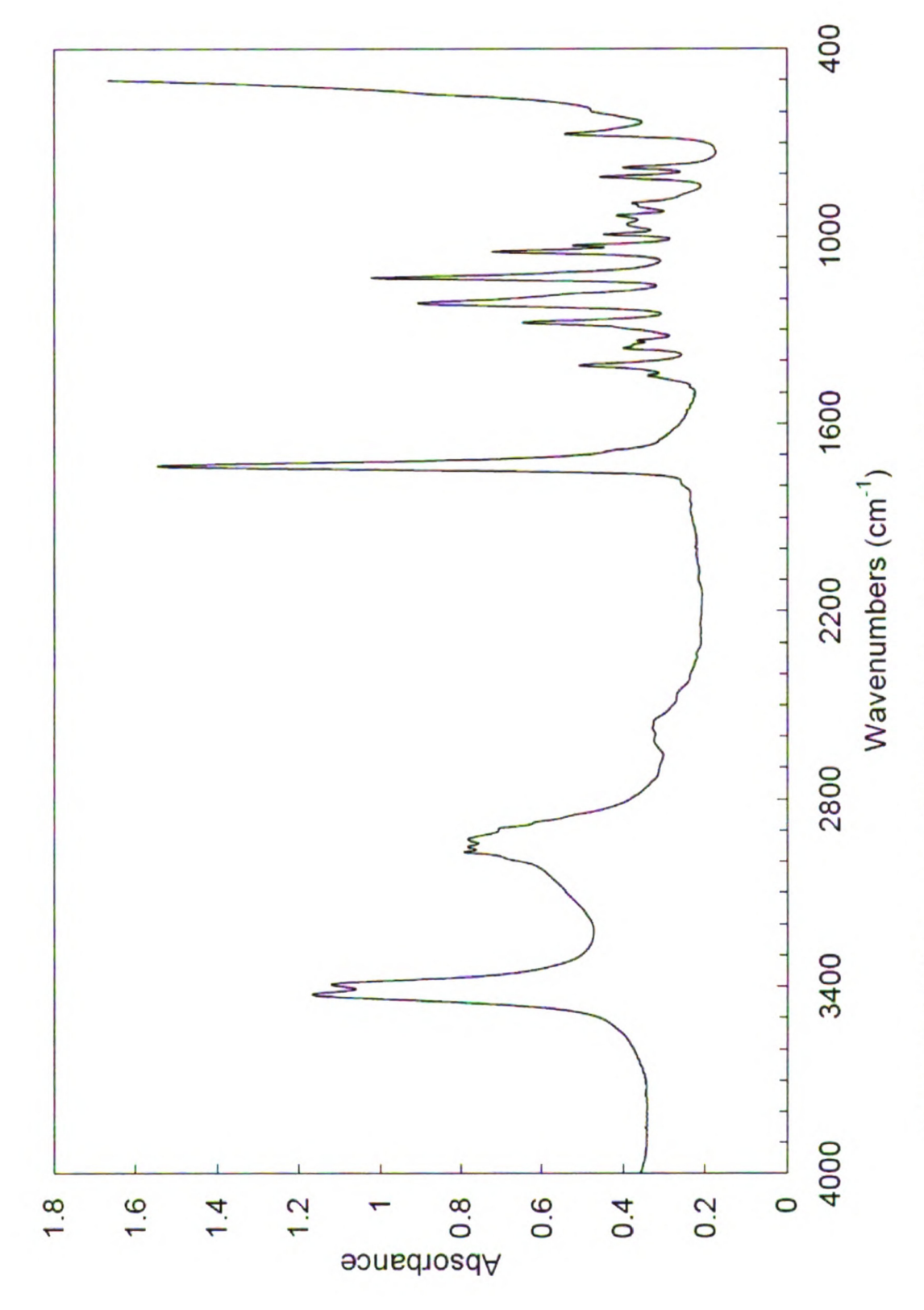


Figure A-12. IR spectrum R,R/S,S-2-hydroxy-2-(tetrahydrofuran-2-yl)-acetic acid

Frequency	300 MHz	(mdd)			(7.1.)
9	25 °C	4.84-4.88	Р	#	¹ J=3.6
Nucleus	<u>+</u>	4.48-4.56	đ	Ŧ	$^{1}J=6.9, ^{2}J=2.4$
Solvent	CDCI	3.77-3.91	Ε	2H	
		1.82-2.16	٤	4H	
		Φ			
Č	e ⟨				
				4	
	— —	œ)	
O P		ס		_	H ₂ 0
o		-			
ത				-	

Figure A-13. ¹H NMR spectrum of RSSR/SRRS, RSRS-3,6-bis(tetrahydrofuran-2-yl)-1,4-dioxane-2,5-dione (monomer 1) 9.5 9.0 8.5 8.0 7.5 7.0 6.5 6.0 5.5 5.0 4.5 4.0 3.5 3.0 2.5 2.0 1.5 1.0 0.5 f1 (ppm)



Figure A-14. ¹³C NMR spectrum of RSSR/SRRS,RSRS-3,6-bis(tetrahydrofuran-2-yl)-1,4-dioxane-2,5-dione (monomer 1)

ppm

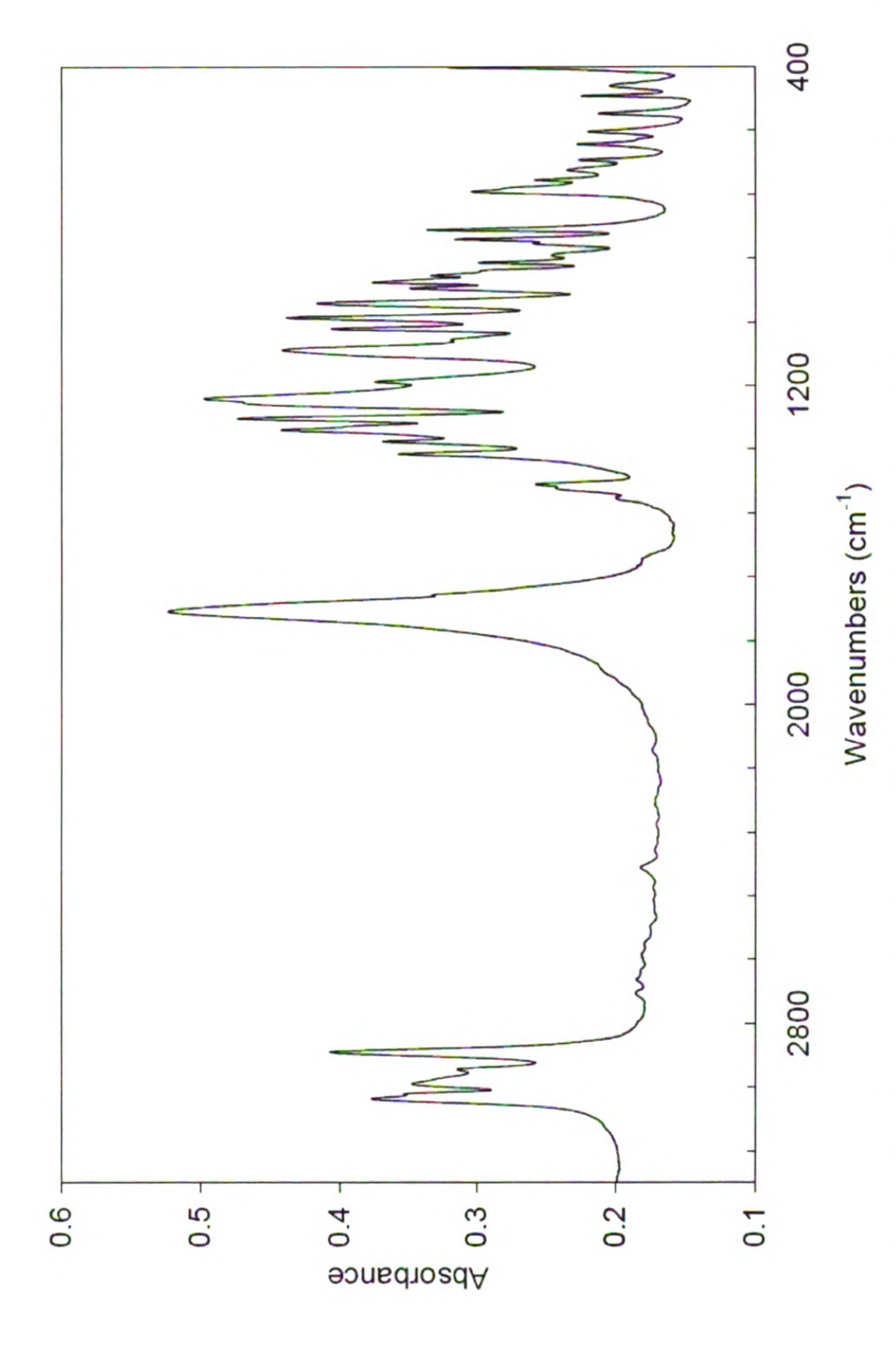


Figure A-15 IR spectrum of RSSR/SRRS/RSRS-3,6-bis(tetrahydrofuran-2-yl)-1,4-dioxane-2,5-dione (monomer 1)

							ľ									
Instrument	Vanal	Varian Gemini-300	300				ਹ	nemic:	Chemical Shift	_	Signal	=	ij) (HZ)	(2
Frequency	300 N	/Hz						(mdd)	m)							
Temperature 25 °C	e 25 °C							4.94-4.97	4.97		р		1H		1,7=3.0	0.0
Nucleus	Ŧ,							4.47~	4.54		Ħ		Ŧ		$J=9.0, ^2J=3.0$	=3.0
Solvent	CDCI	~						3.73-3.89	3.89		Ε		3 H			
								1.81-2.14	2.14		٤		4H			
	a 🚫	9							с							
0		o o					<u> </u>	ъ -					p+c	ပု		
) ~ O															
a																
							*							H_2O		
												,				
9.5 9.0	8.5 8	8.0 7.5	7.0	6.5	6.0	5.5	5.0 f1 (ppm)	4.5	4.0	3.5	3.0	2.5	2.0	1.5	1.0	0.5

Figure A-16. ¹H NMR spectrum of RSSR/SRRS, RSRS-3,6-bis(tetrahydrofuran-2-yl)-1,4-dioxane-2,5-dione (monomer 2,

	10
	50
	- 8
Shift -	40
(ppm) (ppm) 165.1 79.1 77.9 69.8 27.1 26.1	- 20
Chen	- 09
	- 88
	- 06
	110 100 f1 (ppm)
	10 1
	120
	130
	140
300	150
emini-	170 160 150
Varian Gemini-300 75 MHz 25 °C 1 ³ C CDCl ₃	170
Val 75 13 C CD	180
nent rature t t	200 190 180
Instrument Varian Ge Frequency 75 MHz Temperature 25 °C Nucleus 13 C Solvent CDCl ₃	200
- 	

Figure A-17. ¹³C NMR spectrum of RSSR/SRRS, RSRS-3,6-bis(tetrahydrofuran-2-yl)-1,4-dioxane-2,5-dione (monomer 2, 1, 1, 1, 1, 1, 2, unlabeled peaks are monomer 1 impurity)

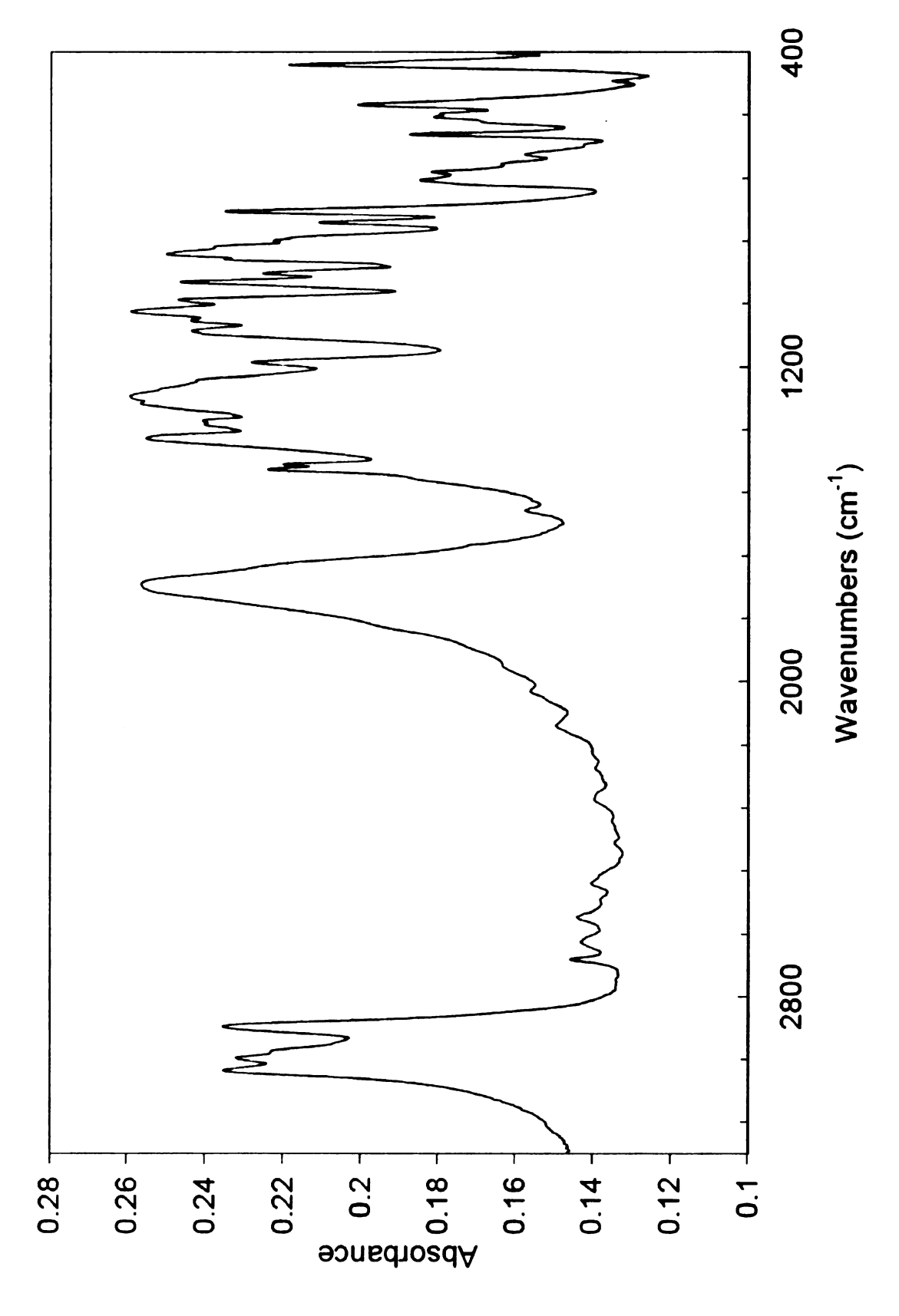


Figure A-18. IR spectrum of RSSR/SRRS/RSRS-3,6-bis(tetrahydrofuran-2-yl)-1,4-dioxane-2,5-dione (monomer 2)

Instrument	Varian Gemini-300		Chemical Shift	Signal	Int.) (Hz)
Frequency	300 MHz		(mdd)			
Temperature 25 °C	25 °C		5.17-5.21	P	Ħ,	3.0
Nucleus	<u>_</u>		5.04-5.08	P	Ŧ	3.0
Solvent	CDCl		4.52-4.59	đ	Ŧ	$^{1}J=3.0, ^{2}J=6.0$
			4.40-4.57	ŧ	Ŧ	$^{1}J=3.0, ^{2}J=6.0$
			3.73-3.99	Ε	4 H	
			1.80-2.20	٤	8H	
	a O O	Φ	ø		p+c	
	٥٥	_			-=	
Y 0	10		ъ		=	
U			_		=	
Д						
i						
					<u> </u>	
				İ		•
9.5 9.0	8.5 8.0 7.5 7.0	6.5 6.0 5.5	5.0 4.5 4.0 3.5	3.0 2.5	2.0	1.5 1.0 0.5

Figure A-19. ¹H NMR spectrum of RRRR/SSSS,RRSS-3,6-bis(tetrahydrofuran-2-yl)-1,4-dioxane-2,5-dione (monomer 3)

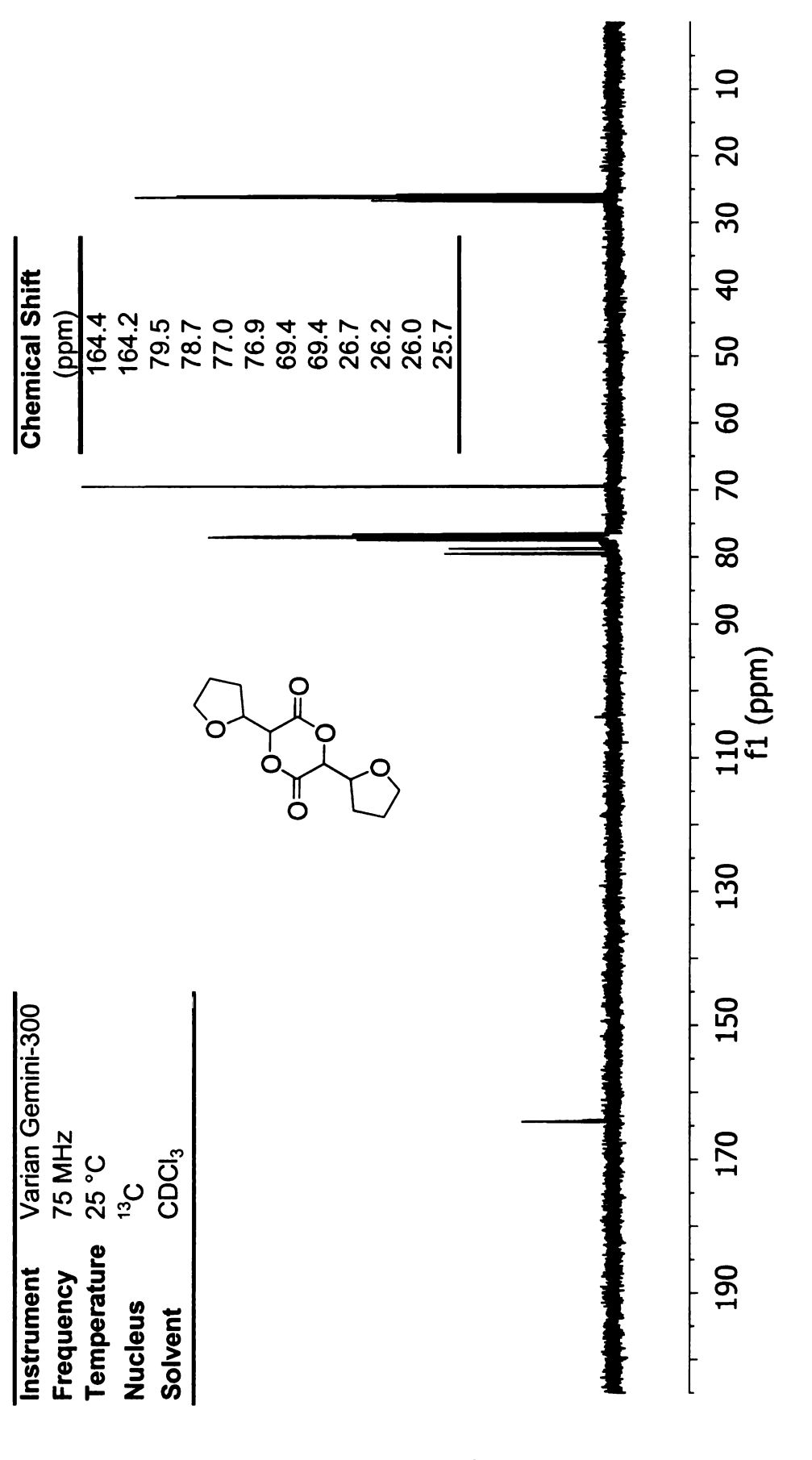


Figure A-20. ¹³C NMR spectrum of RRRR/SSSS, RRSS-3,6-bis(tetrahydrofuran-2-yl)-1,4-dioxane-2,5-dione (monomer

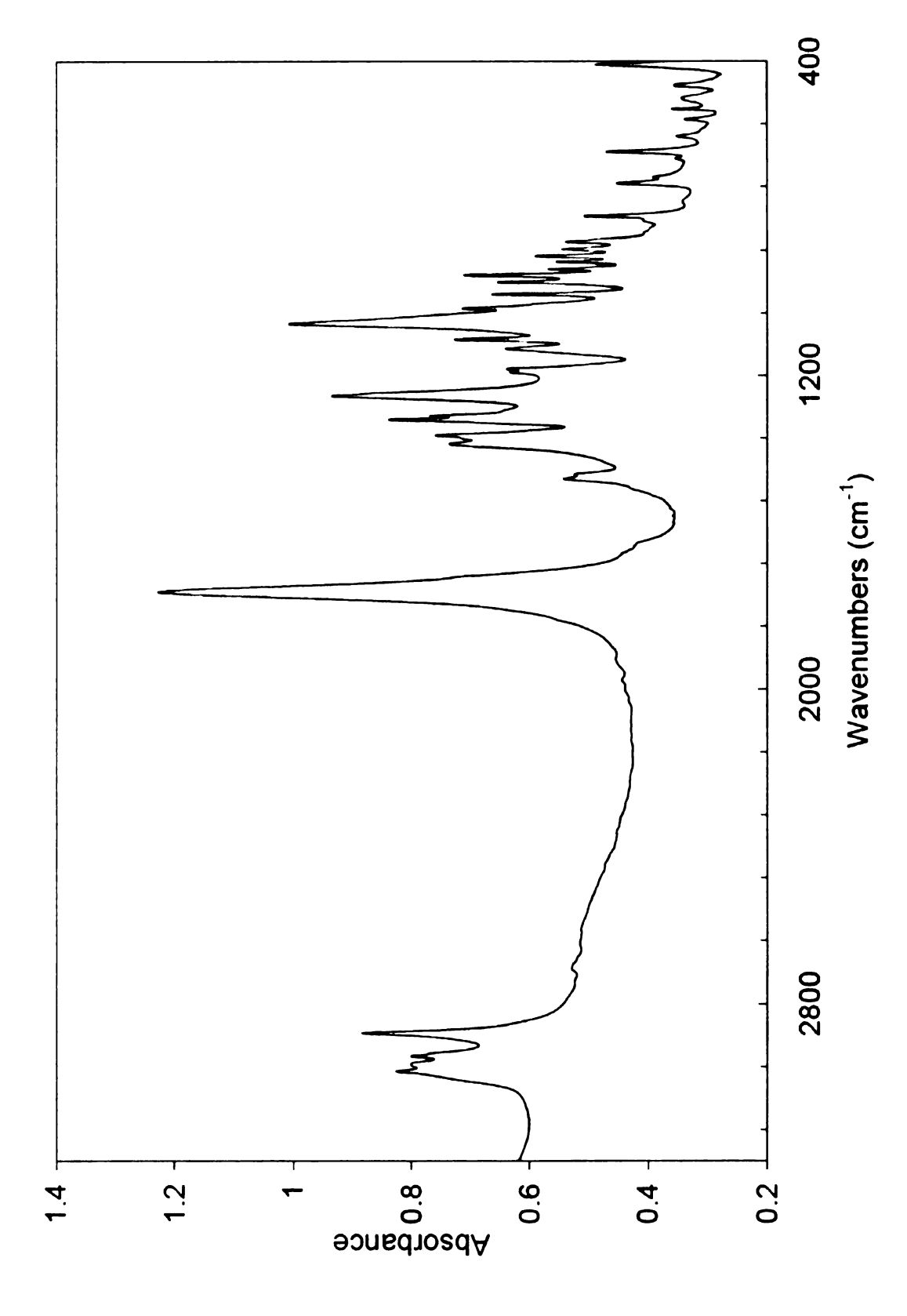


Figure A-21. IR spectrum of RRRK/SSSS/RRSS-3,6-bis(tetrahydrofuran-2-yl)-1,4-dioxane-2,5-dione (monomer 3)

1	Varia	Varian Gemini-300	ini-300										נט	Chemical Shift	al Shif		Int.
Frequency	300 MHz	JHz												(mdd)	٤		
Temperature	25 °C													4.82-5.55	5.55		Ŧ
Nichola N	Ļ													3.99-4.62	4.62	•	Ī
	ر د د						_	`	(3.57-3.95	3.95	`	Ŧ
Solvent	CDC13	3						0) }-	.,				2.72-3.03	3.03	•	Ī
								ø 	√	_				1.10-2.55	2.55	7	Ŧ
							_\ <u>`</u>		=0	, c				p+c			
									p	a							
							Φ			\(\begin{align*} \) \\ \\ \\ \\ \\ \\ \\ \\ \\ \\ \\ \\ \\ 		a .					
			\dashv			}	3		\geq			\leq	5	\rightarrow	3		
	-		ŀ	}			}	}	ļ		ŀ	}	}	}	-	}	
9.5 9.0	8.5	8.0	7.5	7.0	6.5	0.9	5.5 f1	5.0 f1 (ppm)	5.5	4.0	3.5	3.0	2.5	5.0	- 1 .	- 1.0	0.5

Figure A-22. ¹H NMR spectrum of poly(RSSR/SRRS, RSRS-ditetrahydrofurfurylglycolide) (monomer M1M2)

Chemical Shift (ppm) 166.0-169.0 79.0-80.0 75.5-76.5 74.0-75.5 68.5-70 66.5-67 64.5-65.6 38.5-39.5 27.0-29.0 22.5-26.5 20.0-21.0 19.0-20.0	70 60 50 40 30 20 10 0
	- 06
	140 130 120 110 100 f1 (ppm)
008:-	150
S 2	160
Varian Gemini-300 125 MHz 25 °C ¹³ C CDCl ₃	200 190 180 170 160
φ	180
Instrument Frequency Temperature Nucleus Solvent	190
Instrument Frequency Temperatu Nucleus Solvent	200

Figure A-23. ¹³C NMR spectrum of poly(RSSR/SRRS,RSRS-ditetrahydrofurfurylglycolide) (poly(M1M2))

Instrument	Varian Gemini-300		Chemical Shift	nt.
Frequency 300 MHz	300 MHz		(mdd)	
Temperature	25 °C		5.29-5.54	1H
Nichis	Ţ		4.58-4.98	Ŧ
	<u> </u>	, o, , , ,	3.66-3.96	2H
Solvent	CDCI3)= (1.43-2.13	4 H
		1 0/		
		b a		
	-			
			p+c	
		œ	<	
	•	- D		
9.5 9.0	8.5 8.0 7.5 7.0 6	6.5 6.0 5.5 5.0 4.5 4.0 3.5 3.0 f1 (ppm)	2.5 2.0 1.5 1.0	0.5

Figure A-24. ¹H NMR spectrum of poly(RRRR/SSSS,RRSS-ditetrahydrofurfurylglycolide) (poly(M3))

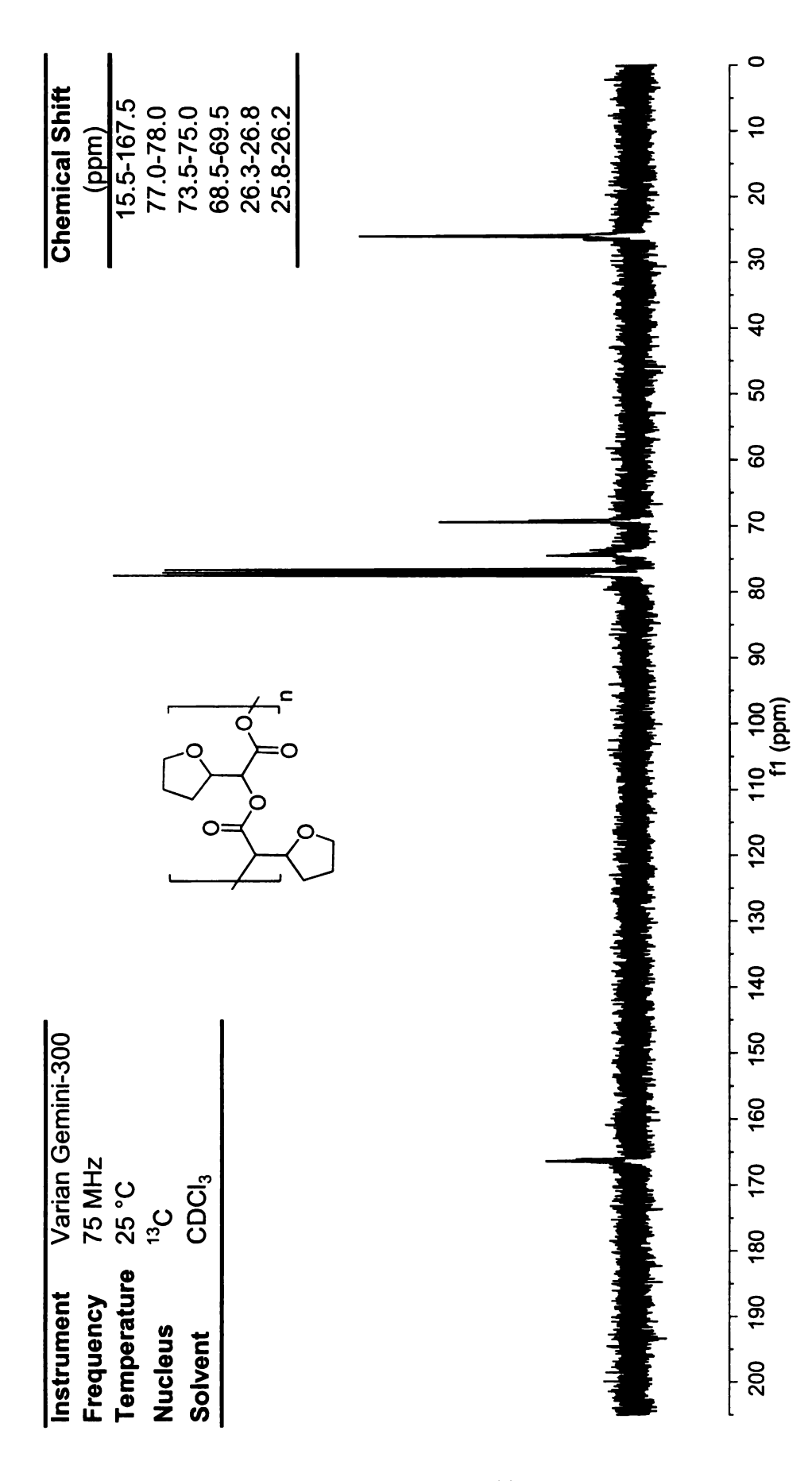


Figure A-25. ¹³C NMR spectrum of poly(RRRR/SSSS, RRSS-ditetrahydrofurfurylglycolide) (poly(M3))

REFERENCES

- (1) Auras, R. A.; Singh, S. P.; Singh, J. J. Packaging Technology and Science 2005, 18, 207-216.
- (2) Vink, E. T. H.; Rabago, K. R.; Glassner, D. A.; Gruber, P. R. Polymer Degradation and Stability 2003, 80, 403-419.
- (3) Sinclair, R. G. Journal of Macromolecular Science-Pure and Applied Chemistry 1996, A33, 585-597.
- (4) Simmons, T. L.; Baker, G. L. *Biomacromolecules* **2001**, *2*, 658-663.
- (5) Dechy-Cabaret, O.; Martin-Vaca, B.; Bourissou, D. Chemical Reviews 2004, 104, 6147-6176.
- (6) Drumright, R. E.; Gruber, P. R.; Henton, D. E. Advanced Materials 2000, 12, 1841-1846.
- (7) Purchasing **2009**, 138, 46-47.
- (8) Vert, M. Biomacromolecules **2005**, *6*, 538-546.
- (9) Bogaert, J. C.; Coszach, P. Macromolecular Symposia 2000, 153, 287-303.
- (10) John, R. P.; Nampoothiri, K. M.; Pandey, A. Applied Microbiology and Biotechnology 2007, 74, 524-534.
- (11) Fukushima, K.; Hirata, M.; Kimura, Y. Macromolecules 2007, 40, 3049-3055.
- (12) du Boullay, O. T.; Marchal, E.; Martin-Vaca, B.; Cossio, F. P.; Bourissou, D. Journal of the American Chemical Society 2006, 128, 16442-16443.
- (13) Baker, G. L.; Vogel, E. B.; Smith, M. R. *Polymer Reviews* **2008**, 48, 64-84.
- (14) Ryner, M.; Stridsberg, K.; Albertsson, A. C.; von Schenck, H.; Svensson, M. *Macromolecules* **2001**, *34*, 3877-3881.
- (15) Trimaille, T.; Moller, M.; Gurny, R. Journal of Polymer Science Part a-Polymer Chemistry 2004, 42, 4379-4391.
- (16) Kowalski, A.; Duda, A.; Penczek, S. Macromolecular Rapid Communications 1998, 19, 567-572.

- (17) Kricheldorf, H. R.; Kreiser-Saunders, I.; Stricker, A. Macromolecules 2000, 33, 702-709.
- (18) Nederberg, F.; Connor, E. F.; Moller, M.; Glauser, T.; Hedrick, J. L. Angewandte Chemie-International Edition 2001, 40, 2712-2715.
- (19) Bonduelle, C.; Martin-Vaca, B.; Cossio, F. P.; Bourissou, D. Chemistry-a European Journal 2008, 14, 5304-5312.
- (20) Fried, J. R. 2003, 2nd Ed, 155-156.
- (21) Yin, M.; Baker, G. L. Macromolecules 1999, 32, 7711-7718.
- (22) Jing, F.; Smith, M. R.; Baker, G. L. Macromolecules 2007, 40, 9304-9312.
- (23) Joziasse, C. A. P.; Veenstra, H.; Grijpma, D. W.; Pennings, A. J. Macromolecular Chemistry and Physics 1996, 197, 2219-2229.
- (24) Zhang, L.; Nederberg, F.; Messman, J. M.; Pratt, R. C.; Hedrick, J. L.; Wade, C. G. Journal of the American Chemical Society 2007, 129, 12610-+.
- (25) Ovitt, T. M.; Coates, G. W. Journal of the American Chemical Society 1999, 121, 4072-4073.
- (26) Cheng, M.; Attygalle, A. B.; Lobkovsky, E. B.; Coates, G. W. Journal of the American Chemical Society 1999, 121, 11583-11584.
- (27) Gupta, B.; Revagade, N.; Anjum, N.; Atthoff, B.; Hilborn, J. Journal of Applied Polymer Science 2006, 100, 1239-1246.
- (28) Urayama, H.; Moon, S. I.; Kimura, Y. Macromolecular Materials and Engineering 2003, 288, 137-143.
- (29) Odelius, K.; Finne, A.; Albertsson, A. C. Journal of Polymer Science Part a-Polymer Chemistry 2006, 44, 596-605.
- (30) Karikari, A. S.; Edwards, W. F.; Mecham, J. B.; Long, T. E. *Biomacromolecules* **2005**, *6*, 2866-2874.
- (31) Tasaka, F.; Ohya, Y.; Ouchi, T. Macromolecular Rapid Communications 2001, 22, 820-824.
- (32) Ouchi, T.; Ichimura, S.; Ohya, Y. *Polymer* **2006**, *47*, 429-434.
- (33) Breitenbach, A.; Kissel, T. *Polymer* **1998**, *39*, 3261-3271.

- (34) Ouchi, T.; Kontani, T.; Ohya, Y. Journal of Polymer Science Part a-Polymer Chemistry 2003, 41, 2462-2468.
- (35) Ouchi, T.; Kontani, T.; Ohya, Y. Polymer 2003, 44, 3927-3933.
- (36) Fox, T. G. Bulletin of the American Physical Society 1956, 1, 123.
- (37) Kumar, R.; Gao, W.; Gross, R. A. Macromolecules 2002, 35, 6835-6844.
- (38) Benabdillah, K. M.; Coudane, J.; Boustta, M.; Engel, R.; Vert, M. *Macromolecules* 1999, 32, 8774-8780.
- (39) Lee, R. S.; Yang, J. M. Journal of Polymer Science Part a-Polymer Chemistry 2001, 39, 724-731.
- (40) Chen, X. H.; Gross, R. A. Macromolecules 1999, 32, 308-314.
- (41) Trimaille, T.; Gurny, R.; Moller, M. Journal of Biomedical Materials Research Part A 2007, 80A, 55-65.
- (42) Glans, J. H.; Turner, D. T. *Polymer* **1981**, *22*, 1540-1543.
- (43) Sasaki, T.; Uchida, T.; Sakurai, K. Journal of Polymer Science Part B-Polymer Physics 2006, 44, 1958-1966.
- (44) Du, F. S.; Ye, W. P.; Gu, Z. W.; Yang, J. Y. Journal of Applied Polymer Science 1997, 63, 643-650.
- (45) Feng, Y.; Klee, D.; Hocker, H. Macromolecular Bioscience 2004, 4, 587-590.
- (46) Feng, Y.; Klee, D.; Hocker, H. Macromolecular Chemistry and Physics 2002, 203, 819-824.
- (47) Jiang, X. W.; Smith, M. R.; Baker, G. L. Macromolecules 2008, 41, 318-324.
- (48) Karbowiak, T.; Debeaufort, F.; Voilley, A. Critical Reviews in Food Science and Nutrition 2006, 46, 391-407.
- (49) Young, T. Philosophical Transactions of the Royal Society 1805, 95, 65-67.
- (50) Vogler, E. A. Advances in Colloid and Interface Science 1998, 74, 69-117.
- (51) Pepin, X.; Blanchon, S.; Couarraze, G. Pharmaceutical Science & Technology Today 1999, 2, 111-118.

- (52) Paragkumar, N. T.; Dellacherie, E.; Six, J. L. Applied Surface Science 2006, 253, 2758-2764.
- (53) Yang, J. Y.; Yu, J.; Li, M.; Pan, H. Z.; Gu, Z. W.; Cao, W. X.; Feng, X. D. Acta Chimica Sinica 2001, 59, 1809-1812.
- (54) Gandini, A.; Belgacem, M. N. Progress in Polymer Science 1997, 22, 1203-1379.
- (55) Theander, O.; Nelson, D. A. Advances in Carbohydrate Chemistry and Biochemistry 1988, 46, 273-326.
- (56) Win, D. T. Assumption University Journal of Technology 2005, 8, 185-90.
- (57) Roquemalherbe, R.; Deonatemartinez, J.; Navarro, E. Journal of Materials Science Letters 1993, 12, 1037-1038.
- (58) Galego, N.; Gandini, A. Revista Cenic 1975, 6, 163.
- (59) Galego, N.; Gandini, A. Revista Cenic 1984, 15, 143.
- (60) Zaldivar, D.; Peniche, C.; Bulay, A.; Roman, J. S. Journal of Polymer Science Part a-Polymer Chemistry 1993, 31, 625-631.
- (61) Amri, H.; Belgacem, M. N.; Gandini, A. Polymer 1996, 37, 4815-4821.
- (62) Fox, T. G.; Flory, P. J. Journal of Applied Physics 1950, 21, 581-591.
- (63) Mealares, C.; Hui, Z.; Gandini, A. *Polymer* **1996**, *37*, 2273-2279.
- (64) Moreau, C.; Belgacem, M. N.; Gandini, A. Topics in Catalysis **2004**, 27, 11-30.
- (65) Mitiakoudis, A.; Gandini, A. *Macromolecules* **1991**, *24*, 830-835.
- (66) Degering, E. F.; Boatright, L. G. Journal of the American Chemical Society 1950, 72, 5137-5139.
- (67) Normant, H. Comptes Rendus Hebdomadaires Des Seances De L Academie Des Sciences 1947, 225, 580-581.
- (68) Farmahini-Farahani, M.; Jafari, S. H.; Khonakdar, H. A.; Yavari, A.; Bakhshi, R.; Tarameshlou, M. *Macromolecular Materials and Engineering* **2007**, *292*, 1103-1110.
- (69) Lucht, B. L.; Collum, D. B. Accounts of Chemical Research 1999, 32, 1035-1042.

- (70) Purkarthofer, T.; Pabst, T.; van den Broek, C.; Griengl, H.; Maurer, O.; Skranc, W. Organic Process Research & Development 2006, 10, 618-621.
- (71) Raucher, S.; Lui, A. S. T.; Macdonald, J. E. Journal of Organic Chemistry 1979, 44, 1885-1887.
- (72) Felfer, U.; Strauss, U. T.; Kroutil, W.; Fabian, W. M. F.; Faber, K. Journal of Molecular Catalysis B-Enzymatic 2001, 15, 213-222.

